

50280

50280/1133

ACTA UNIVERSITATIS SZEGEDIENSIS

ACTA PHYSICA ET CHEMICA

NO. ~~1~~

TOMUS XXIX

FASCICULI 1-2

AUSHAF 29 (1-2) (1-102) (1983)

**HU ISSN 0324-6523 Acta Univ. Szeged
HU ISSN 0001-6721 Acta Phys. et Chem.**

**SZEGED, HUNGARIA
1983**



ACTA UNIVERSITATIS SZEGEDIENSIS

ACTA PHYSICA ET CHEMICA

NOVA SERIES

TOMUS XXIX

FASCICULI 1—2

AUSHAF 29 (1—2) (1983)

HU ISSN 0324—6523 Acta Univ. Szeged

HU ISSN 0001—6721 Acta Phys. et Chem.

SZEGED, HUNGARIA

1983

Adiuvantibus

M. BARTÓK, M. BÁN, L. CSÁNYI, J. CSÁSZÁR, P. FEJES, F. GILDE, P. HUHN,
I. KETSKEMÉTY, F. SOLYMOSI, L. SZALAY et F. SZÁNTÓ

Redigit

PÁL FEJES

Edit

Facultas Scientiarum Universitatis Szegediensis de
Attila József nominatae

Editionem curant

J. ANDOR, I. BÁRDI, Á. MOLNÁR, B. NÉMET et Á. SÜLI

Nota

Acta Phys. et Chem. Szeged

Szerkeszti

FEJES PÁL

A szerkesztő bizottság tagjai:

BARTÓK M., BÁN M., CSÁNYI L., CSÁSZÁR J., FEJES P., GILDE F., HUHN P.,
KETSKEMÉTY I., SOLYMOSI F., SZALAY L. és SZÁNTÓ F.

Kiadja

a József Attila Tudományegyetem Természettudományi Kara
(Szeged, Aradi vértanúk tere 1.)

Szerkesztő bizottsági titkárok:

ANDOR J., BÁRDI I., MOLNÁR Á., NÉMET B. és SÜLI Á.

Kiadványunk rövidítése:

Acta Phys. et Chem. Szeged

CHANGING IN THE DENSITY OF STATES CAUSED BY VACANCY IN GaP AND InP

By

G. PAPP* and F. BELEZNAV

Research Institute for Technical Physics, Budapest

(Received October 28, 1982)

A study of ideal-vacancy induced deep levels and changing in the density of states in two III—V compound semiconductors (GaP and InP) is presented. The Koster-Slater Green's-function technique is used in conjunction with a linear combination of atomic orbitals description of the electronic structure of the perfect solid.

Introduction

The electronic structure of localized defects in pure and III—V compound semiconductors is of crucial interest in the understanding of optical and electrical properties of a class of materials of major importance in most field of pure and applied solid-state physics. Excellent review of the various methods for the study of deep-level impurities and defects has been published by PANTELIDES [1].

In this paper the Green's-function method has been used to study the ideal-vacancy-induced deep levels and the change in the density of states in GaP and InP for both cation and anion vacancy.

In the calculation Koster and Slater method has been applied. They showed [2] that the electronic energy levels introduced in the band gaps by a localized perturbation could be calculated from a knowledge of the Green's function for the perfect crystal and the matrix elements of the potential, both calculated in the Wannier representation.

The method was developed further by CALLAWAY [3] and calculations of the electronic states in the band gap have been performed for the vacancy [4] and divacancy [5] of Si in the Wannier representation. The numerical determination of Wannier function turned out to be very tedious and difficult and for this reason only a few subsequent calculations have been made [6].

LANOO AND LENGART [7] observed that the Koster—Slater method can be applied using a conveniently chosen localized basis set. They performed a semiempirical tight binding band structure calculation for Si. The ideal vacancy was defined by removing all the Hamiltonian matrix elements between orbitals localized about the central atom with all basis states describing the system.

* Permanent adress: Institute of Theoretical Physics, Attila József University, Szeged

This method has been extended by BERNHOLC and PANTELIDES [8], and our calculation is based on this technique.

The outline of the development is as follows. In section A the tight binding formalism is described. Section B contains the Green's function in LCAO-basis. In section C the ideal vacancy potential is defined and section D contains the numerical results.

A. Tight binding formalism

A brief review of the Linear Combination of Atomic Orbitals (LCAO) Tight Binding Method will be given because the bulk solid electronic structure is calculated within the framework of this approximation [9].

Atomic orbitals are symbolized by $\varphi_\mu(\vec{r} - \vec{R}_n^\alpha)$ where μ signifies both angular and spin angular momentum quantum numbers of the atomic wave function and \vec{R}_n^α is the position of the α th atom in the n th primitive cell. Bloch sums, $\Phi_\mu^\alpha(\vec{k}, \vec{r})$ are formed by taking combinations of each of these atomic orbitals in each primitive cell, with the coefficients being fixed by the periodicity of the lattice:

$$\Phi_\mu^\alpha(\vec{k}, \vec{r}) = N^{-1/2} \sum_{n=1}^N e^{i\vec{k}\cdot\vec{R}_n^\alpha} \varphi_\mu(\vec{r} - \vec{R}_n^\alpha), \quad (1)$$

where the summation is over primitive cells. The perfect crystal wave functions, $\Psi_j^0(\vec{k}, \vec{r})$ are then linear combinations of the above Bloch functions:

$$\Psi_j^0(\vec{k}, \vec{r}) = \sum_{\mu, \alpha} C_\mu^\alpha(j, \vec{k}) \Phi_\mu^\alpha(\vec{k}, \vec{r}), \quad (2)$$

where j signifies the band index and $C_\mu^\alpha(j, \vec{k})$ are determined by minimizing the expectation value of the Hamiltonian. Solving the resulting secular equations,

$$\sum_{\mu, \alpha} \left(\sum_n e^{-i\vec{k}(\vec{R}_n^\alpha - \vec{R}_1^\beta)} \langle \varphi_\mu(\vec{r} - \vec{R}_n^\alpha) | H^0 | \varphi_\nu(\vec{r} - \vec{R}_1^\beta) \rangle - E_j(\vec{k}) \delta_{\alpha\beta} \delta_{\mu\nu} \right) C_\mu^\alpha(j, \vec{k}) = 0 \quad (3)$$

we get the j th band energy at wave vector \vec{k} , $E_j(\vec{k})$ and the expansion coefficients, $C_\mu^\alpha(j, \vec{k})$.

B. Green's function

Let H^0 be the perfect crystal Hamiltonian and V the vacancy potential, then the Hamiltonian of the crystal consisting of the vacancy can be written as

$$H = H^0 + V. \quad (4)$$

The Green operator of the perfect crystal's Schrödinger equation is:

$$G^0(E) = \lim_{\epsilon \rightarrow 0^+} (E - H^0 + i\epsilon)^{-1}. \quad (5)$$

The Schrödinger equation for the imperfect crystal can then be replaced by the Lippmann—Schwinger [10] equation

$$\Psi_j(\vec{k}, \vec{r}) = \Psi_j^0(\vec{k}, \vec{r}) + G^0(E)V\Psi_j(\vec{k}, \vec{r}), \quad (6)$$

or equivalently

$$[1 - G^0(E)V]\Psi_j(\vec{k}, \vec{r}) = \Psi_j^0(\vec{k}, \vec{r}). \quad (7)$$

In the band gap $\Psi_j^0(\vec{k}, \vec{r}) \equiv 0$, therefore the condition for the existence of a bound state becomes

$$D = \det \|1 - G^0(E)V\| = 0. \quad (8)$$

Within the energy bands of the perfect crystal D is nonzero and a phase shift [3] can be defined as follows:

$$\delta(E) = -\tan^{-1} \frac{\text{Im } D(E)}{\text{Re } D(E)}. \quad (9)$$

It can be shown [3] that the change in the density of states is given by

$$\Delta N(E) = \pi^{-1} \frac{d\delta(E)}{dE}. \quad (10)$$

$G^0(E)$ can also be expanded in the $\Psi_j^0(\vec{k}, \vec{r})$ basis set:

$$G^0(E) = \sum_{j, \vec{k}} \frac{|j, \vec{k}\rangle \langle j, \vec{k}|}{E - E_j(\vec{k}) + i\epsilon}. \quad (11)$$

Using Eq. (2) an expansion in the (μ, α) basis set is

$$G_{\mu\alpha n, \nu\beta m}^0 = N^{-1} \sum_{j, \vec{k}} \frac{C_{\mu}^{\alpha}(j, \vec{k}) C_{\nu}^{\beta*}(j, \vec{k}) e^{-ik(R_m^{\beta} - R_n^{\alpha})}}{E - E_j(\vec{k}) + i\epsilon}, \quad (12)$$

where N is the number of the unit cells.

C. The Ideal Vacancy Potential

The ideal vacancy is viewed as the absence of the appropriate atom in the n th unit cell leaving all other atoms at the same positions, the atomic-like orbitals are retained on all other atoms, and their interactions are assumed unaltered. As we have seen in part B Eq. (8) is the condition that must be satisfied for a bound state to exist. In the (μ, α) LCAO basis it becomes

$$\det \|\delta_{\mu\alpha, \nu\beta} - \sum_{\mu'\alpha'} G_{\mu\alpha, \mu'\alpha'}^0 V_{\mu'\alpha', \nu\beta}\| = 0 \quad (13)$$

If the functions φ_{μ}^{α} are localized about atomic site and the perturbation potential V has a finite range the matrix element $V_{\mu'\alpha', \nu\beta}$ will be nonzero if both φ_{μ}^{α} and φ_{ν}^{β} overlap with the potential and the size of the determinant reduces to the size of the nonzero part of the potential matrix [2]. The V for ideal vacancy within the tight-binding description using large cluster [11] represents a matrix which annuls all the interaction between the atom placed at vacancy site and all other atoms of the solid. In this method the perfect crystal Hamiltonian's matrix form is sheared four blocks (Fig. 1.a) where the vacancy site is taken to be X and \mathbf{H}_X^0 is the $m * m$ submatrix and m is the number of orbitals chosen for atom removed to form vacancy, and the imperfect crystal Hamiltonian is $\mathbf{H} = \mathbf{H}_1$. To achieve that let \mathbf{H} and \mathbf{H}^0 be of the same size,

\mathbf{H} is rewritten in the form of Fig 1b, where E_0 is arbitrary chosen outside the range of interest and since $\mathbf{V}=\mathbf{H}-\mathbf{H}^0$, \mathbf{V} has the form of Fig. 1c. An equivalent way to obtain a matrix representation of \mathbf{V} is to take the limit $E_0 \rightarrow \infty$ and use arbitrary matrices in the off-diagonal blocks. This can't change the eigenvalues of \mathbf{H} [8]. Choosing \mathbf{H} in the form of Fig. 1.d where $\mathbf{M}=\mathbf{H}_x^0+E_0\mathbf{1}$ with $E_0 \rightarrow \infty$, we obtain for \mathbf{V} (Fig. 1.e.)

$$\begin{array}{ccc} \mathbf{H}^0 = \begin{pmatrix} \mathbf{H}_x^0 & \mathbf{H}_A^0 \\ \mathbf{H}_A^0 & \mathbf{H}_1^0 \end{pmatrix} & \mathbf{H} = \begin{pmatrix} E_0\mathbf{1} & 0 \\ 0 & \mathbf{H}_1 \end{pmatrix} & \mathbf{V} = \begin{pmatrix} -\mathbf{H}+E_0\mathbf{1} & -\mathbf{H}_A^0 \\ -\mathbf{H}_A^0 & 0 \end{pmatrix} \\ a & b & c \end{array}$$

$$\begin{array}{cc} \mathbf{H} = \begin{pmatrix} \mathbf{M} & \mathbf{H}_A^0 \\ \mathbf{H}_A^0 & \mathbf{H}_1 \end{pmatrix} & \mathbf{V} = \begin{pmatrix} E_0\mathbf{1} & 0 \\ 0 & 0 \end{pmatrix} \\ d & e \end{array}$$

Fig. 1.

The net result is that no electron is allowed to reach the site of this atom. Since the perturbation matrix has the above form and the matrix of the Green's operator is

$$\mathbf{G}^0 = \begin{pmatrix} \mathbf{G}_x^0 & \mathbf{G}_A^0 \\ \mathbf{G}_A^0 & \mathbf{G}_1^0 \end{pmatrix},$$

the matrix of the operator $\mathbf{1}-\mathbf{G}^0\mathbf{V}$ becomes

$$\mathbf{1}-\mathbf{G}^0\mathbf{V} = \begin{pmatrix} \mathbf{1}-\mathbf{G}_x^0E_0 & 0 \\ \mathbf{G}_A^0E_0 & \mathbf{1} \end{pmatrix}$$

From this it follows that

$$\det \|\mathbf{1}-\mathbf{G}^0\mathbf{V}\| = \det \|\mathbf{1}-\mathbf{G}_x^0E_0\|, \quad (14)$$

so that the size of the determinant reduces to the size of the nonzero part of the potential matrix.

D. Calculations and results

In the present study s , p_x , p_y , p_z atomic orbitals were used, which, combined with the fact that GaP and InP have two atoms in the unit cell, yield an 8×8 secular matrix for the calculation of the band structure for the ideal crystal (Four valence and the four lowest conduction bands can be obtained).

For numerical calculations of the energy levels of the ideal vacancy we need to compute the Green's-function matrix elements $G_{\mu\mu}^0(E)$ on the atom X where $\mu=s$ or p and

$$G_{\mu\mu}^0(E) = \lim_{\epsilon \rightarrow 0^+} \sum_{j,\bar{k}} \frac{C_\mu(j,\bar{k})C_\mu^*(j,\bar{k})}{E-E_j(\bar{k})+i\epsilon}. \quad (15)$$

This expression can also be written as follows

$$G_{\mu\mu}^0(E) = \lim_{\varepsilon \rightarrow 0^+} \int \frac{dE'}{E - E' + i\varepsilon} C_{\mu\mu}(E'), \quad (16)$$

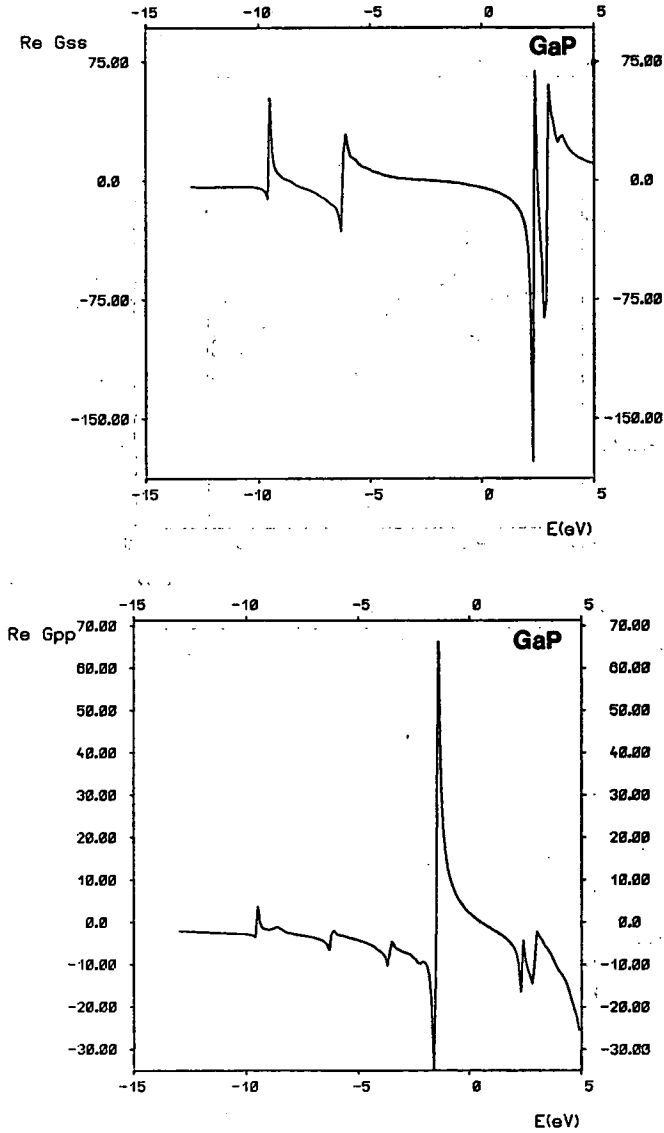


Fig. 2. Real parts of $G_{ss}^0(E)$ and $G_{pp}^0(E)$ of GaP in the case of cation vacancy.

where the quantity $C_{\mu\mu}(E')$ is given by

$$C_{\mu\mu}(E') = \sum_{j,\vec{k}} C_{\mu}(j, \vec{k}) C_{\mu}^*(j, \vec{k}) \delta(E' - E(j, \vec{k})). \quad (17)$$

Using the Dirac identity (15) becomes

$$G_{\mu\mu}^0(E) = P \int \frac{C_{\mu\mu}(E')}{E - E'} dE' - i\pi C_{\mu\mu}(E). \quad (18)$$

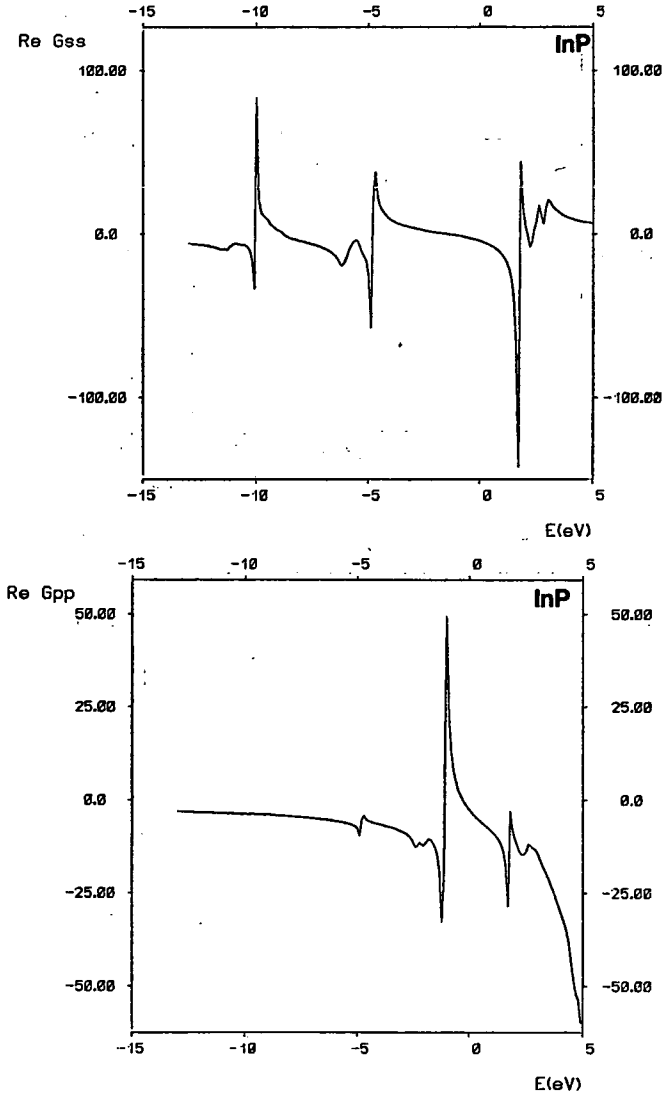


Fig. 3. Real parts of $G_{ss}^0(E)$ and $G_{pp}^0(E)$ of InP in the case of cation vacancy.

For our present calculations we have used the method of GILAT and RAUBENHEIMER [12] to evaluate the integral (17) for $C_{\mu\mu}(E')$. Principal value integrals were evaluated using the identity [13]

$$P \int_a^b \frac{g(E')}{E-E'} dE' = \int_a^b \frac{g(E')-g(E)}{E-E'} dE' - g(E) \ln \frac{b-E}{E-a}. \quad (19)$$

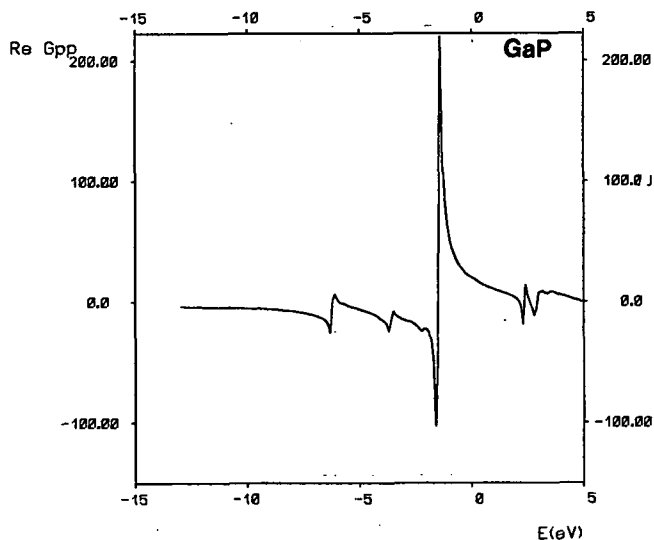
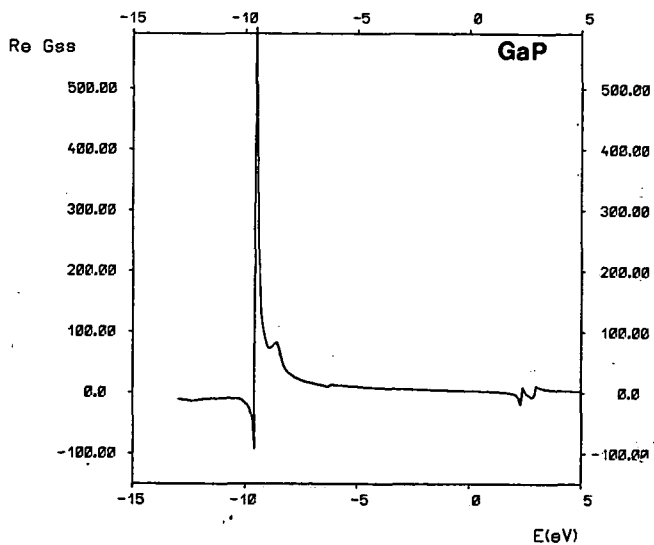


Fig. 4. Real parts of $G_{ss}^0(E)$ and $G_{pp}^0(E)$ of GaP in the case of anion vacancy.

Having evaluated the real parts of $G_{\mu\mu}^0(E)$, their zeros within the band gaps were located and identified as bound states. The changes in the densities of states within the energy bands were then evaluated using Eq. (10).

Calculations have been carried out for the ideal vacancy in GaP and InP. The parameterization of the energy bands of these materials is that of das SARMA and MADHUKAR [14] which retains the first and second nearest-neighbor interactions.

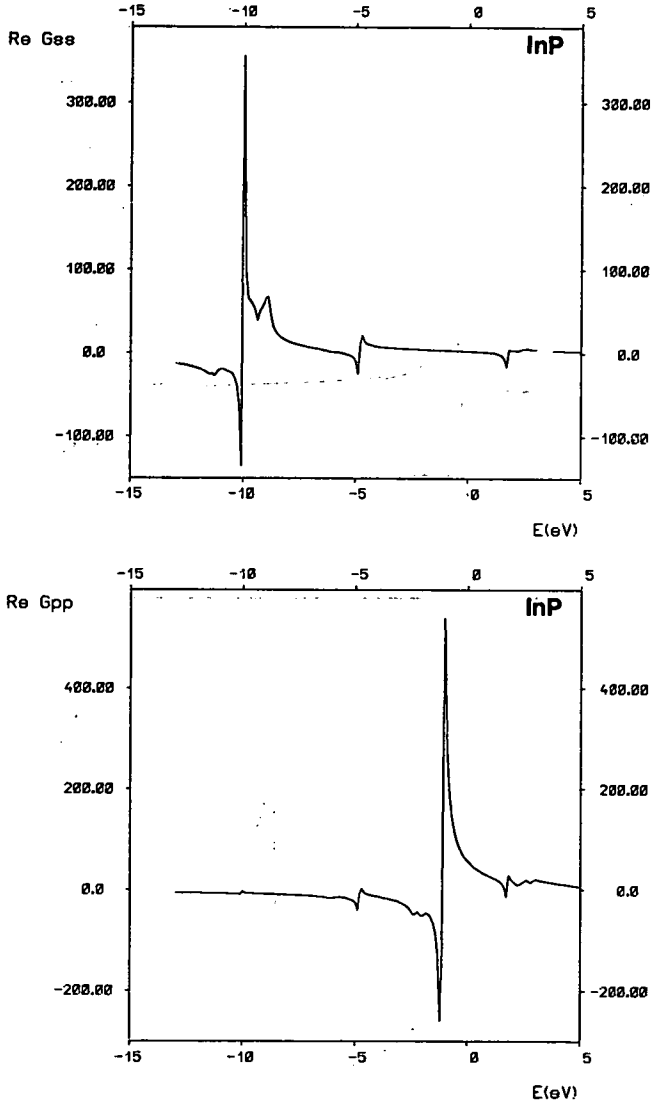


Fig. 5. Real parts of $G_{ss}^0(E)$ and $G_{pp}^0(E)$ of InP in the case of anion vacancy.

This parameterization were used to describe only the vacancy bound states of the same materials.

Figs. 2—3 show the real parts of Green's functions for GaP and for InP in the case of Ga and In vacancies, respectively. Figs. 4—5 show the real parts of Green's functions for GaP and for InP in the case of anion vacancies, respectively. The zeros

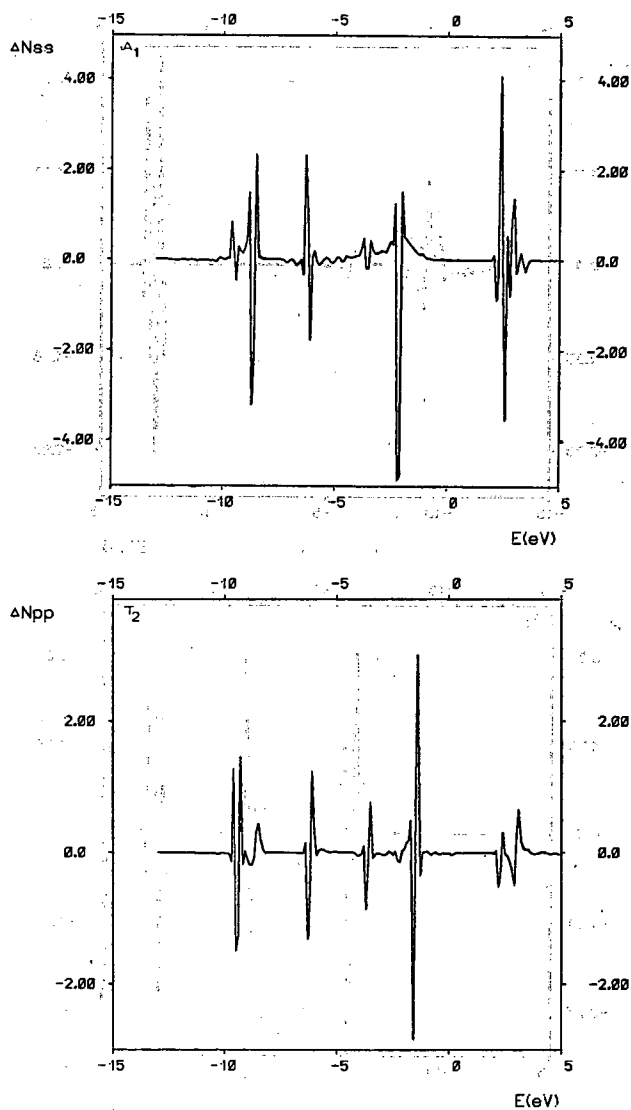


Fig. 6. A_1 and T_2 contributions to the change in density of states induced by an Ga vacancy in GaP.

of G_{ss}^0 in the regions of band gaps correspond to bound states of A_1 symmetry and the zeros of G_{pp}^0 in the regions of the band gaps correspond to bound states of T_2 symmetry.

The positions of the bound states within the gaps of materials are given in Table I. The changes in the densities of states are given in Figs. 6—9.

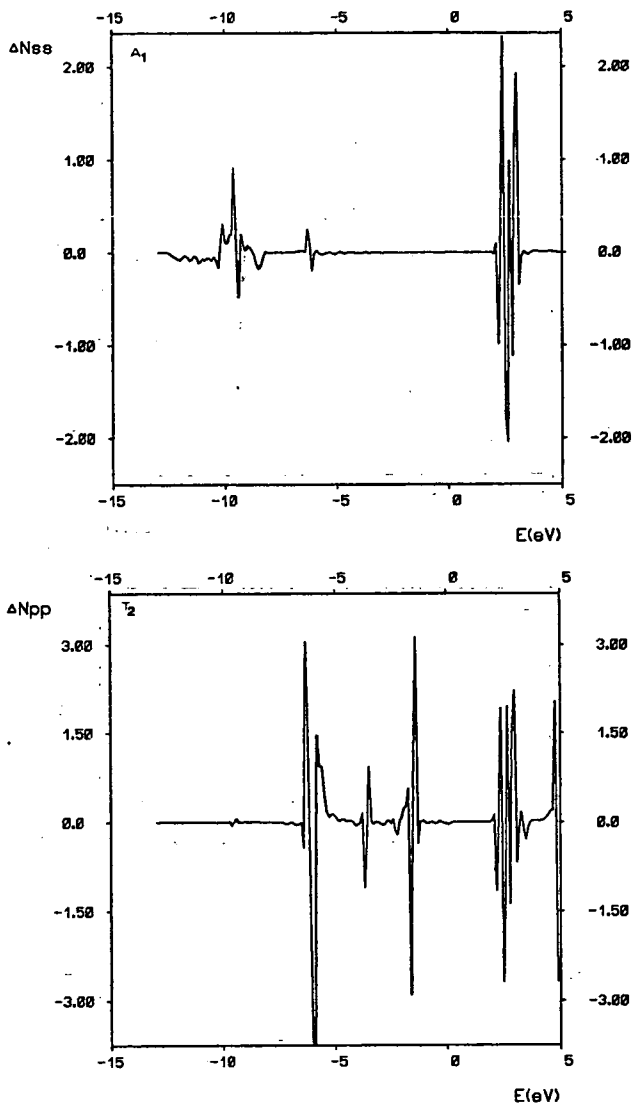


Fig. 7. A_1 and T_2 contributions to the change in density of states induced by an P vacancy in GaP.

Conclusion

The modified Koster-Slater technique has recently been widely used to calculate localized deep levels in semiconductors. A related quantity, the change in the density of states is investigated in this paper. The optical properties of the deep levels, which are of most important in many measurements and applications do depend on the

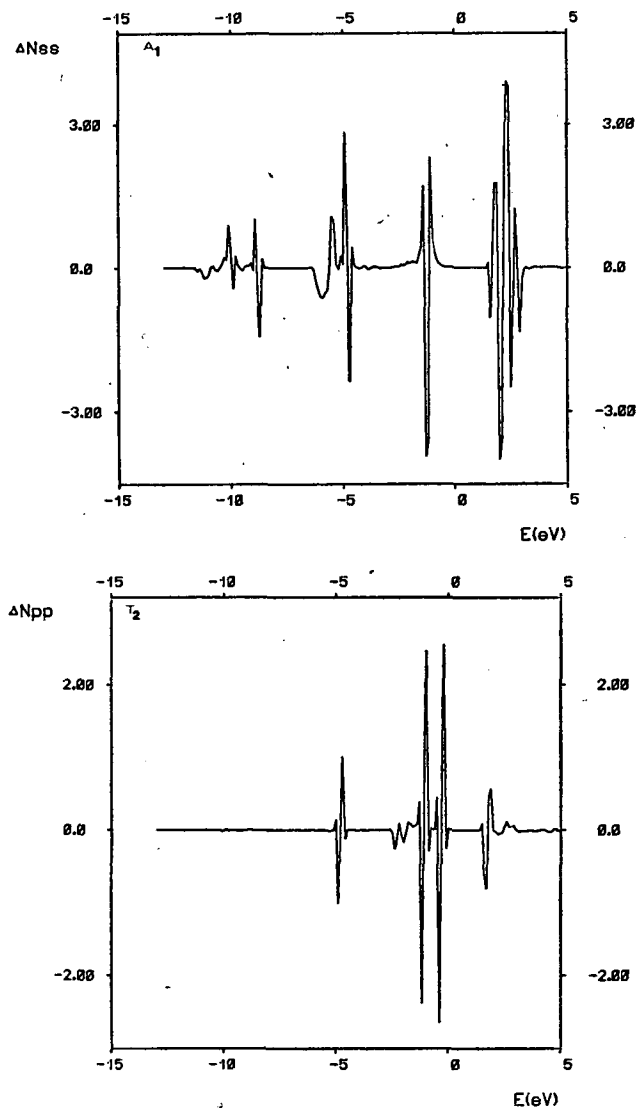


Fig. 8. A_1 and T_2 contributions to the change in density of states induced by an In vacancy in InP.

band states too from where transition takes place. From our calculations it is seen that in case of a reasonable "localized" transition significant structure can occur due to the sharp peaks in the change of the density of states. This, similarly to the "internal" transitions of the d-electrons in the crystal field for transition metal impurities might rise to unexpected structures even in case of an ordinary deep level if this energy difference is smaller than the forbidden gap. It remains to find an appropriate system where this effect should be seen experimentally.

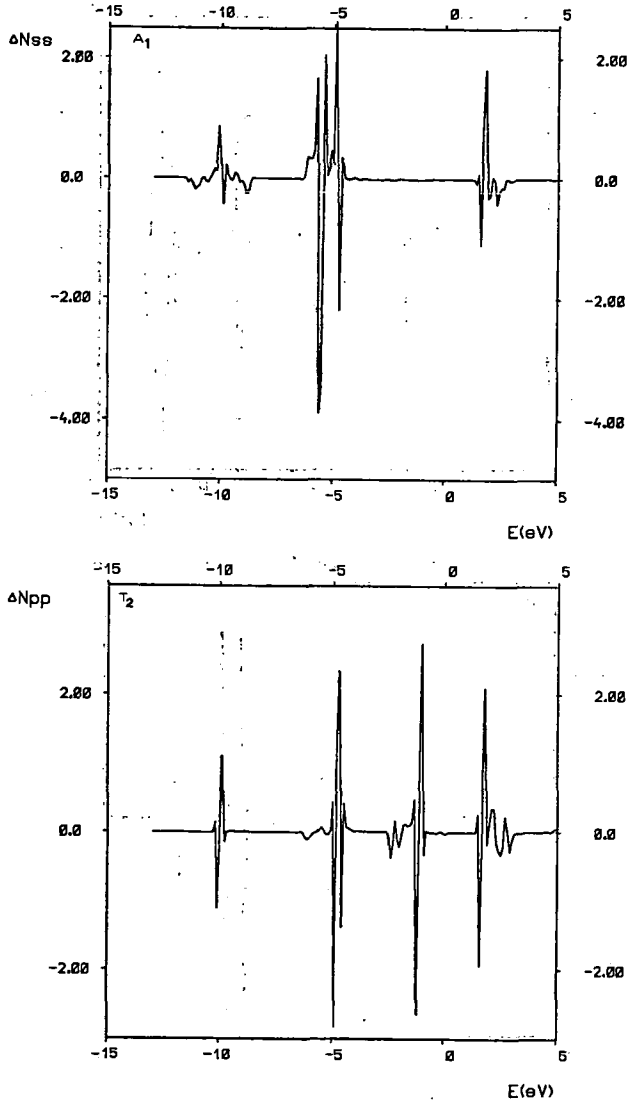


Fig. 9. A_1 and T_2 contributions to the change in density of states induced by an P vacancy in InP.

Table I

A_1 and T_2 levels obtained in this work. Energy in eV.
(The energy zero is at the top of the valence band)

	GaP		InP	
	A_1	T_2	A_1	T_2
V_{anion}	1.70	2.0	1.36	1.66
V_{cation}	—	0.5	—	—

References

- [1] Pantelides, S. T.: Rev. Mod. Phys. **50**, 797 (1978).
- [2] Koster, G. F., J. C. Slater: Phys. Rev. **95**, 1167 (1954). Phys. Rev. **96**, 1208 (1954).
- [3] Callaway, J.: J. Math. Phys. **5**, 783 (1964). Phys. Rev. **154**, 515 (1967).
- [4] Callaway, J., A. J. Hughes: Phys. Rev. **156**, 860 (1967).
- [5] Callaway, J., A. J. Hughes: Phys. Rev. **164**, 1043 (1967).
- [6] Parada, N. J.: Phys. Rev. B **3**, 2042 (1971). Callaway, J.: Phys. Rev. B **3**, 2556 (1971). Singhal, S. P.: Phys. Rev. B **4**, 2497 (1971). Phys. Rev. B **5**, 4203 (1972).
- [7] Lanoo, M., P. Lengart: J. Phys. Chem. Solids **30**, 2409 (1969).
- [8] Bernholc, J., S. T. Pantelides: Phys. Rev. B **18**, 1780 (1978).
- [9] Slater, J. C., G. F. Koster: Phys. Rev. **94**, 1498 (1954).
- [10] Lippman, B. A., J. Schwinger: Phys. Rev. **79**, 469 (1963).
- [11] Kauffer, E., P. Pecheur, M. Gerl: J. Phys. C **9**, 2913 (1976). Phys. Rev. B **15**, 4107 (1977).
- [12] Gilat, G., L. J. Raubenheimer: Phys. Rev. **144**, 390 (1966).
- [13] David, P. J., P. Rabinowitz: Numerical Integration, (Blaisdell, Waltham, Mass. 1967).
- [14] Das Sarma S., A. Madhukar: Phys. Rev. B **24**, 2051 (1981).

ИЗМЕНЕНИЯ В ПЛОТНОСТИ СОСТОЯНИЙ ВСЛЕДСТВИЕ ВАКАНСИЙ В GaP и InP

Г. Пани и Ф. Белезнаи

Исследуются глубокие уровни, созданные идеальной вакансией и изменения в плотности состояний в двух III—V полупроводниках (GaP и InP). Используется техника гриновских функций Костера—Слетера вместе с ЛКАО для электронной структуры идеального твердого тела.



DISTRIBUTED FEEDBACK DYE LASER TUNING BY DIVERGENT PUMPING BEAMS

By

ZS. BOR, S. SZATMÁRI, G. SZABÓ and B. RÁCZ

Institute of Experimental Physics, Attila József University, Szeged, Hungary

(Received 10th November, 1982)

A simple tuning method of distributed feedback dye lasers based on divergent beam pumping is presented. The tuning mechanism is described theoretically. The calculated and measured values of tuning sensitivity and maximum tuning are in good agreement. Continuous tuning of 5 Å was demonstrated experimentally.

Introduction

It has been shown recently that the N_2 laser pumped distributed feedback dye laser (DFDL) is capable of generating short transform-limited pulses. DFDL's are simple in construction, they produce stable, single picosecond pulses [1—3] without the use of expensive pulse selectors. Their operation range covers the visible and near UV part of the spectrum [4]. Amplification of the pulses by a few amplifier stages pumped by the same [5] N_2 laser is quite simple. It was found that the DFDL's have much lower amplified spontaneous emission (ASE) background level, and besides the efficiency and tuning range is about twice as large as that of the grating tuned lasers [6].

The pumping arrangements described in [4, 6, 7] allowed us to create a perfect pumping interference pattern even with superradiant (N_2 , Cu-vapor, excimer *etc.*) lasers with low temporal and spatial coherence.

The pumping arrangement incorporating the quartz parallelepiped described in [4, 6] is very simple in construction and it can be easily aligned. However, it is a disadvantage that the simple tuning method, based on the rotation of mirrors [7], cannot be applied to this case.

In this paper, we are proposing a very simple tuning method, based on pumping the DFDL by divergent beams allowing a change of a few Å in the laser wavelength.

Theoretical considerations

DFDL's are usually pumped by an interference pattern created by two beams of very low divergency [9]. Thus the points of maximum intensities form parallel and equidistant planes. In this case the period of the interference pattern at the surface of the dye cell (and consequently, the lasing wavelength) is unchanged against the

translations of the dye cell. A pumping interference pattern with tailored spatial dependent period allows a very straightforward tuning method, based on the shift of the dye cell. This principle was applied for tuning a DFDL in [10], where two slightly divergent pump beams were used to form the interference pattern. Similarly, we have also used divergent pump beams to pump the DFDL (Fig. 1). The pump source was a TEA-TE N_2 laser oscillator-amplifier system, similar to the one described in

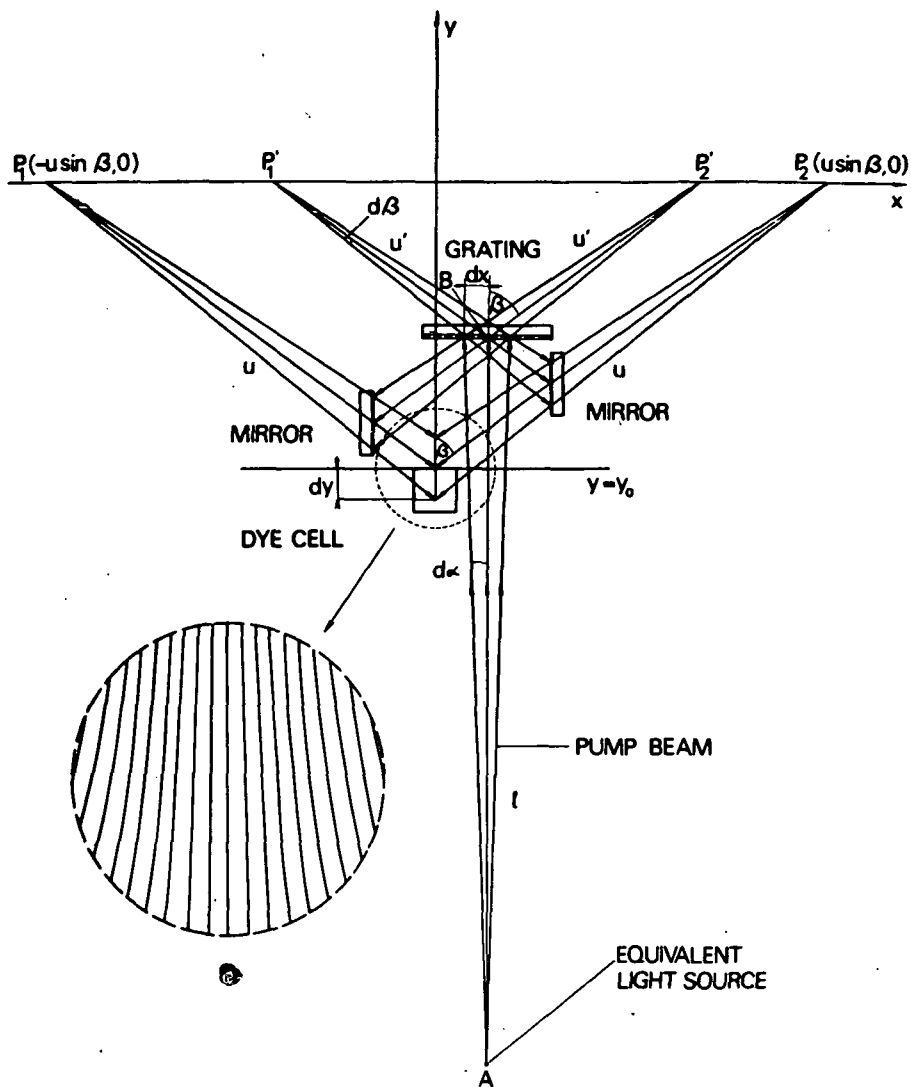


Fig. 1. The equivalent interference scheme of a DFDL pumped by divergent beams. P_1P_2 and A are the points where the two diffracted beams causing the interference and the pumping beam are emerging from, respectively.

[8] with a divergence of 0.4 mrad. The pump beam was sent through a telescope focussed almost to infinite. In this way, a pump beam was obtained which could be considered as to emerge from an equivalent point light source A. The position of point A was set by proper focussing the telescope. It can easily be shown (see Appendix 1) that the beams, diffracted by the grating, into the +1 and -1 orders are propagating as if they had emerged from points P'_1 and P'_2 respectively (see Fig. 1). The distance of P'_1 and P'_2 from the point B of the grating (u') can be calculated by $u' = l \cos^2 \beta$ (see Appendix 1), where $l = \overline{AB}$, and β is the angle of diffraction. The beams, after being reflected from the two mirrors, produce the same interference as if they had emerged from points P_1 and P_2 , thus the points of maximum intensities of the interference pattern form a set of hyperbolas. The distance of P_1 and P_2 from the dye cell (u) approximately equal to u' in our experiments. In Fig. 1, the co-ordinate system is chosen so that the co-ordinates of points P_1 and P_2 are $(-u \sin \beta, 0)$ and $(u \sin \beta, 0)$, respectively. Therefore, the equation of the curves of maximum intensities is:

$$\frac{x^2}{\left(\frac{n\lambda_p}{2}\right)^2} - \frac{y^2}{u^2 \sin^2 \beta - \left(\frac{n\lambda_p}{2}\right)^2} = 1, \quad (1)$$

where: λ_p is the wavelength of pumping and, n is an integer (the order of the interference).

It is easy to show that the x co-ordinates of the maximum intensities at the surface of the dye cell ($y = y_0 \equiv -u \cos \beta$) are given by

$$x_n = \pm \frac{n\lambda_p}{2 \sin \beta} \sqrt{1 + \frac{n^2 \lambda_p^2 \cos^2 \beta}{4u^2 \sin^2 \beta - n^2 \lambda_p^2}}. \quad (2)$$

The quasi-period of the DFDL structure is defined by

$$A = (x_{n+1} - x_n). \quad (3)$$

It can easily be shown that A varies along the axis of y . This effect can be used as a tuning method by shifting the active medium (or the grating) along axis y . There is also a small dependence of A on x which may spoil the periodicity of the DFDL structure. This effect can cause an unwanted line broadening. It can be proved easily by a geometrical consideration (Appendix 2) that the tangents of $y = y_0$ of the hyperbolas intersect at a point on axis y at a distance of $v = l \cos \beta$ from the $y = y_0$ line. Therefore the value of tuning sensitivity with respect to the shift of the dye cell:

$$\frac{dA}{A} = -\frac{dy}{l \cos \beta}. \quad (4)$$

Using the proportionality between A and the lasing wavelength (λ) we get:

$$\frac{d\lambda}{dA} = \frac{\lambda}{l \cos \beta}. \quad (5)$$

Equation (5) was verified experimentally. Fig. 2 shows the tuning sensitivity $\left(\frac{d\lambda}{dA}\right)$ versus the reciprocal distance of A from the grating $\left(\frac{1}{l}\right)$. The tuning sensitivity

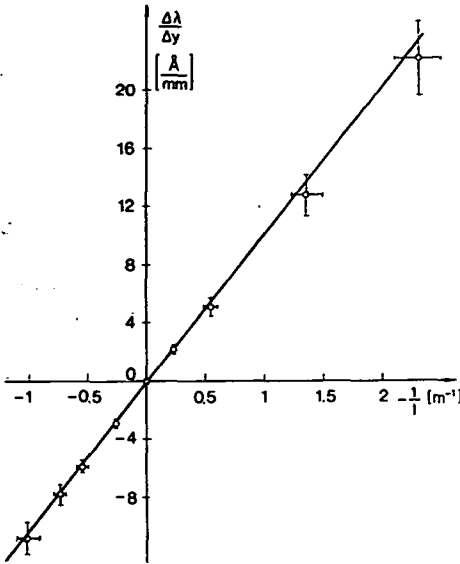


Fig. 2. The tuning sensitivity of DFDL based on the shift of the dye cell versus the reciprocal distance of A from the grating. The solid line is the theoretical curve, the points are the measured values.

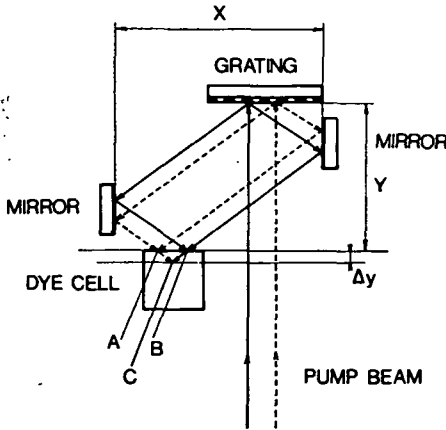


Fig. 3. The pumping arrangement produces an interference pattern with high visibility because the two beams coming from the same part of the pump beam (see points A and B in Fig. 3) will interfere at the surface of the dye cell. When the dye cell is shifted (Δy), different parts of the beam interfere (at point C).

was determined by measuring the change in the wavelength and the corresponding shift of the grating. The wavelength tuning was measured by a Fabry—Perot interferometer ($FSR=0.42 \text{ \AA}$ $F=20$). The value of l was calculated from the setting of the above mentioned telescope. The positive and negative values of l correspond to the divergent and convergent pump beams, respectively. In Fig. 2 the solid line is the theoretical curve, the points are the measured values. It can be seen that the agreement is very good.

Estimation of the tuning range

From equation (5), we obtain for the tuning range ($\Delta\lambda$) that

$$\Delta\lambda = \frac{\lambda}{l \cos \beta} \Delta y, \tag{6}$$

where Δy is the possible maximum shift of the active medium.

Let us look for those physical effects which determine the maximum value of Δy and the minimum value of l . The pumping arrangement described in [7] has the advantage that, if the geometrical relation

$$\frac{Y}{X} = \sqrt{\left(\frac{d}{\lambda_p}\right)^2 - 1} \tag{7}$$

holds (d is the grating constant), then two beams coming from the same part of the pump beam (see points A and B in Fig. 3) will interfere at the surface of the dye cell. Therefore there are no strict requirements for the spatial coherence of the pump beam. When the dye cell is shifted along axis y , the more distant parts of the pump beam produce interference (point C in Fig. 3). In this case, the visibility of the interference pattern decreases because of the finite spatial coherence of the N_2 laser beam. This effect

limits the maximum value of Δy . Δy can be obtained by using the threshold characteristics of DF DL. The measured threshold of DF DL versus the shift of the grating is shown in Fig. 4. Parameter M is the magnification of the telescope placed between the DF DL and the N_2 laser system. In this experiment, the telescope was focussed to infinite. The intensity of pumping was varied by a variable liquid filter. In Fig. 4. it can be seen that by increasing Δy the threshold is also increased. Furthermore, the spatial coherence of pumping is proportional to the magnification of the telescope, because the curves can be transformed into each other by a magnification of $\frac{1}{M}$ along axis x . Earlier investigations have shown that, for pump pulse duration of 1.5 ns, the DF DL generates a single pulse only when the pump intensity does not exceed by more than 1.3 times the threshold pump intensity. This pump energy range of the single pulse generation was regarded as the maximum movement of the grating or different values of magnification M (see Fig. 4).

It was mentioned before that the periodic structure of the DF DL was not strictly equidistant for a finite value of l , i.e. in the middle of the excited volume was different from that at the ends (see (2) and (3)). Let us calculate the minimum value of l determined by the allowable maximum non-periodicity of the DF DL structure. Let the difference in l caused by the above-mentioned effect be denoted by Δl . Where:

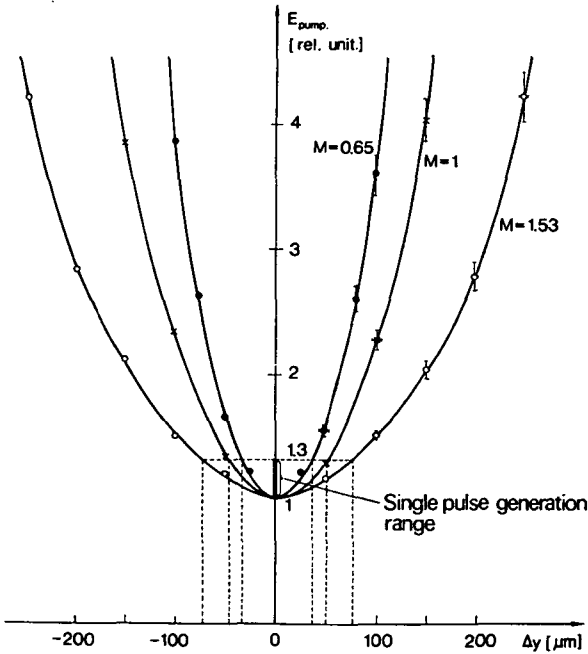


Fig. 4. The measured threshold pump energy versus the shift of the grating. Parameter M is the magnification of the telescope placed between the DF DL and the pumping N_2 laser system. All of the three curves are normalized at $x=0$ to unit.

Λ_0 is the quasi period belonging to $n=0$. Using equations (2) and (3), we get

$$\frac{\Lambda_n}{\Lambda_0} = \sqrt{1 + \frac{n^2 \lambda_p \cos^2 \beta}{4l^2 \cos^4 \beta \sin^2 \beta - n^2 \lambda_p}} \quad (8)$$

Using the $\lambda = d \sin \beta$ relation, and introducing the $\varphi = \frac{nd}{l}$ notation Eq. (8) becomes simpler:

$$\frac{\Lambda_n}{\Lambda_0} = \sqrt{1 + \frac{\varphi^2 \cos \beta}{4 \cos^2 \beta - \varphi^2}} \quad (9)$$

Notice that φ is the half angle of the pump beam illuminating the DFDL consisting of $2n$ periods. Using the proportionality between Λ and λ from equation (7) and (8) for small values of φ , we can obtain

$$\frac{\Delta\lambda}{\lambda} \sim \frac{\varphi^2}{8 \cos^2 \beta}, \quad (10)$$

where $\Delta\lambda$ is the passive bandwidth caused by the non-periodicity of the DFDL structure. $\Delta\lambda$ is supposed not to exceed the expected bandwidth of the DFDL ($\Delta\lambda^*$). A DFDL operating under our experimental conditions (pump pulse duration is 1.6 ns) is expected to generate 40 ps long pulses, as described in [11]. The bandwidth corresponding to this pulse duration for transform limited pulses is approximately 0.1 Å. Using this value for $\Delta\lambda$, one can get for $l=0.5$ m. With this value of l , and the highest magnification ($M=1.53$) of the telescope (see Fig. 4), a tuning range of 5 Å was achieved experimentally, as seen in Fig. 5. Fig. 5 shows the tuned DFDL output monitored by a Fabry-Perot interferometer (FSR = 0.84 Å, $F=20$). The curve was obtained from a signal of a Laser Photometer (Molelectron LP 20), which formed the ratio of the power of the beam light having passed through the Fabry-Perot interferometer to the power of the beam entering the interferometer as the reference.

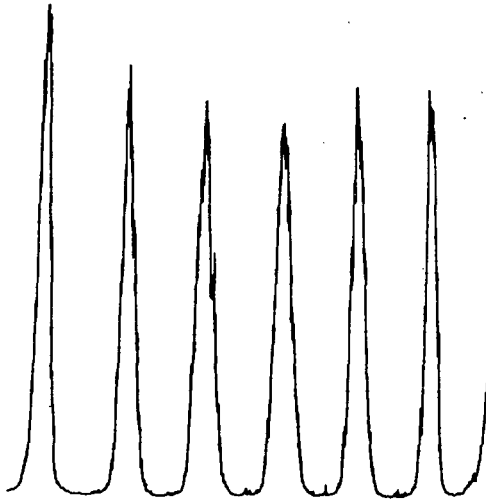


Fig. 5. The experimental tuning curve of the DFDL. Tuning was measured by a Fabry-Perot interferometer (FSR=0.84 Å, $F=20$) and a Laser Photometer (Molelectron LP 20).

The tuning method described above is based on dependence of Λ on y . Since the size of the active volume in this direction is in the order of hundredths of microns, the change in Λ can be considerable so as to lead to the broadening of the linewidth.

This effect can be avoided, if

$$(\Delta\lambda)^* < \left(\frac{d\lambda}{dy}\right)^* \cdot h, \quad (11)$$

where $\frac{d\lambda^*}{dy}$ is the dependence of λ on y inside the excited volume $\frac{d\lambda^*}{dy} = \frac{d\lambda}{dy} \frac{\cos \beta}{\cos \alpha} \frac{1}{n}$ (see Appendix 3), and h is the penetration depth of pumping. Condition (11) can be fulfilled by increasing the concentration of the dye solution, but this is limited by diffraction losses. Under our experimental conditions the the $6 \cdot 10^{-3}$ M Rhodamine 6G solution provided the best performance. It should be mentioned that by increasing the value of φ not only the bandwidth of the DF DL is increased, but also the divergence of the DF DL. This effect is caused by the non-parallelism of the interference lines. The value of the divergence can be estimated knowing the rise of the tangents of the hyperbolas and taking into consideration the law of their refraction (Appendix 3).

We have observed an increase in the divergence of the DF DL experimentally, as well.

Conclusion

We have described theoretically and studied experimentally a tuning method based on pumping the DF DL by divergent beams. The method is capable of a tuning of a few Å, and can be applied also when the pump arrangement incorporating a quartz parallelepiped is used [4, 6]. It is very likely that the reason for the tuning effect observed in [7] is the same as described above.

Appendix

1. From the grating equation, we can obtain:

$$\cos \alpha d\alpha = \cos \beta d\beta, \quad (A1)$$

where: α is the angle of incidence, (in our case $\alpha=0$), and β is the angle of diffraction. It can be read from Fig. 1 that

$$d\alpha = \frac{dx}{l}, \quad (A2)$$

and

$$d\beta = \frac{dx \cos \beta}{u'}, \quad (A3)$$

Therefore starting from (A1)—(A3)

$$u' = l \cos^2 \beta \quad (A4)$$

It can easily be calculated by simple geometrical considerations that

$$u = u' + X^2 + Y^2. \quad (A5)$$

2. Let point P be an arbitrary point of the excited volume belonging to the optical path difference of $n\lambda_p$ (Fig. 5). It is well known from geometry that the tangent of the hyperbolic curve at P is the bisector of $\overline{PP_1}$ and $\overline{PP_2}$. Applying the sine-formula for the triangle of P_1P_2P , we get for a small value of $d\beta$ that

$$\frac{\sin(\gamma + d\beta)}{\sin(\gamma - d\beta)} = \frac{u + \frac{n\lambda_p}{2}}{u - \frac{n\lambda_p}{2}} \tag{A6}$$

In our experiments $\frac{n\lambda_p}{2} \ll u$. In this case, (A6) is simplified to

$$d\beta = \frac{n\lambda_p \operatorname{ctg} \beta}{2u} \tag{A7}$$

It can be read from Fig. 5 that

$$d\beta = \frac{\overline{OP}}{v} = \frac{n\lambda_p}{2v \sin \beta} \tag{A8}$$

Comparing (A7) and (A8) we can obtain:

$$v = \frac{u}{\cos \beta} = l \cos \beta \tag{A9}$$

Since v is independent of n , it means that all the tangents of a hyperbola intersect at the same point C .

3. Let us look for the refraction law of the maximum intensity curves of the interference pattern formed by two beams intersecting at an angle of 2β , when they

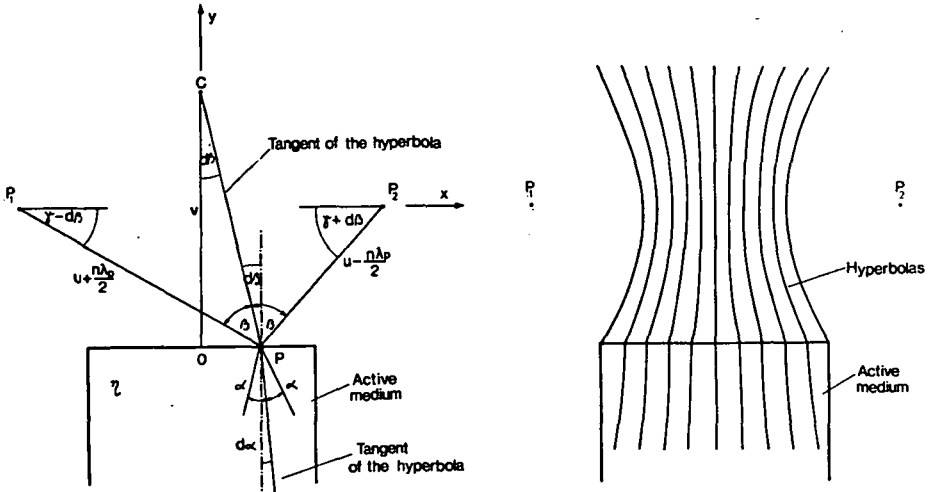


Fig. 6. Geometry for the calculation of tangents of the hyperbolas and their law of refraction.

are at the surface of a medium with a refractive index of η . Let $d\beta$ be the angle between the tangent of the maximum intensity curve (\overline{PC}) and the normal of the surface (indicated by a broken line in Fig. 6). In terms of the Snell's law we can obtain:

$$d\alpha = \frac{1}{2} \left\{ \arcsin \frac{\sin(\beta + d\beta)}{\eta} - \arcsin \frac{\sin(\beta - d\beta)}{\eta} \right\}.$$

Assuming a low value for $d\beta$:

$$d\alpha \approx \frac{\cos \beta}{\cos \alpha} \frac{1}{\eta} d\beta,$$

which can be regarded as the refraction law of the interference fringes.

References

- [1] Bor, Zs.: IEEE J. Quant. Electron. QE—16, 517 (1980).
- [2] Bor, Zs., A. Müller, B. Rácz, F. P. Schäfer: Appl. Phys. B27, 9 (1982).
- [3] Bor, Zs., A. Müller, B. Rácz, F. P. Schäfer: Appl. Phys. B27, 77 (1982).
- [4] Bor, Zs., A. Müller, B. Rácz: Opt. Commun. 40, 294 (1982).
- [5] Bor, Zs., B. Rácz, F. P. Schäfer: accepted by Sov. J. Quant. Electron.
- [6] Bor, Zs.: Opt. Commun. 39, 383 (1981).
- [7] Bor, Zs.: Opt. Commun. 29, 103 (1979).
- [8] Sánta, I., S. Szatmári, B. Németh, J. Hebling: Opt. Commun. 41, 59 (1982).
- [9] Shank, C. V., J. E. Bjorkholm, H. Kogelnik: Appl. Phys. Lett. 18, 395 (1971).
- [10] Gorot, K. F., V. I. Vashchuk, E. I. Zabello, N. M. Malykhina, E. A. Tikhonov: Sov. J. Quant. Electron. 7, 385 (1977).
- [11] Bor, Zs., B. Rácz, G. Szabó, S. Szatmári: 4th Conference on Luminescence, Szeged, 1982 Conference Digest p. 263.

ПЕРЕСТРАИВАНИЕ РОС ЛАЗЕРОВ, ВОЗБУЖДЕННЫХ РАСХОДЯЩИМ ПУЧКОМ

Ж. Бор, Ш. Сатмари, Г. Сабо и Б. Рац

Описан способ простого перестраивания по длине волны РОС лазеров, возбужденных расходящим пучком. Теоретически изучен способ перестраивания. Расчетные и экспериментальные данные характеристики перестраивания и максимальной области перестраивания находятся в хорошей соответствии. Экспериментально продемонстрировано непрерывное перестраивание в области 5 ангстремов.



FLUORESCENCE NONLINEARITY OF WATER DISSOLVED FLUORESCEIN UNDER THE ACTION OF LASER RADIATION OF HIGH POWER DENSITY

By

B. NÉMET, I. SÁNTA and L. KOZMA

Institute of Experimental Physics, Attila József University, Szeged

(Received 15th July, 1982)

The nonlinear dependence of the fluorescence of water dissolved fluorescein on a high power density of laser radiation (Φ) with a dye concentration of 10^{-6} – 10^{-9} M has been investigated by a pulsed laser microfluorimeter. When measuring the saturation factor Γ as a function of (Φ), one of the methods employed is the determination of true fluorescence intensity (I_t) from the intensity measured (I_m) by a microfluorimeter, and another method is proposed for calculating the excited state lifetime from the function $I_m(\Phi)$.

Introduction

Although lasers of high power and their application in the field of nonlinear optics is well known, the aim of these applications (high resolution laser spectroscopy, SHG, induced Raman scattering, *etc.*) have been first and foremost to investigate atoms and simple molecules and not complicated compounds.

The combined organic compounds (*e.g.* dyes, with broad and strong absorption bands in the visible region — $\sigma_a = 10^{-16}$ cm² — and having the short lifetime of the excited state in solution — $\tau = 2$ – 6 ns), require very high photon flux density (Φ) for fluorescence nonlinearity, a phenomenon mentioned in the theory of saturation of the excited electronic state of a fast three-level system, where the saturation photon irradiance (Φ_s) is defined as [1, 2]:

$$\Phi_s = \frac{1}{\sigma_a} \cdot \frac{1}{\tau} \quad (1)$$

The putting of dye lasers pumped by solid state or gas lasers (*e.g.* second or third harmonic of Nd and Rb lasers, or N_2 and excimer lasers) to practical use has not stimulated as yet the investigation into the nonlinear behaviour of the fluorescence of dyes depending on photon irradiance, because Φ of the pumping lasers is quite near the saturation limit, at every exciting wavelength.

But recently fluorescence microscopy in biology and medicine (*i.e.* laser microscopy — laser microfluorimetry [3, 4]) has used tunable pulsed dye lasers as pumping sources. In these experimental cases, when dyes are using several biological macromolecules for labelling, the power density exciting these dyes can change from

10 MW/cm² to 1 GW/cm² — *i.e.* 10²⁵—10²⁷ photon/cm s¹. (*E.g.* if the power of the pulse is not more than 5 kW, and the laser beam divergence is 1 mrad, when using a lens of 100 mm focal length (f_1), the diameter of the beam waist (d_1) is 100 μ m and the power density (Φ_1) is 50 MW/cm², but when using a $f_2=10$ mm lens, $d_2=10$ μ m and $\Phi_2=5$ GW/cm²).

Investigation into the nonlinear behaviour of the fluorescence of combined organic molecules as a function of high power density has not made great headway yet far-reaching, either theoretically or experimentally [5, 6]. For this reason, we aimed at studying the fluorescence nonlinearity of water dissolved fluorescein using a pulsed laser microfluorimeter, when the power density of the exciting laser light was about Φ_s .

Material and methods

For the object of investigation fluorescein dye (pH=12) dissolved in water was decided upon. Our choice fell on this dye because the fluorescein had been investigated with conventional methods many times and even by a pulsed laser fluorimeter [7] a few times, and this dye is one of the most popular labelling dyes in biological and medical microscopic investigation [8].

Fluorescein was purified by chromatography, and the solvent was deionized water. The watering was made from a concentration of 10⁻⁴ M drawn on the tenth part in every case, and the concentrations used were 10⁻⁶, 10⁻⁷, 10⁻⁸, 10⁻⁹ M. We applied these low concentrations, because the optical density of the solutions (OD) was very low, and so the power density showed a negligible change through a pathlength of 1 cm. In terms of the Beer—Lambert law a less than 10 *p. c.* absorptivity is after 1 cm pathlength, if the concentration (c) with fluorescein at exciting wavelength of 480 nm (λ_e) is:

$$\text{OD} = \log \frac{I_0}{I} = \varepsilon(\lambda_e) \cdot c \cdot d = \log 1.1, \quad c = \frac{\log 1.1}{\varepsilon(\lambda_e) \cdot d} = 10^{-6} \text{ M} \quad (2)$$

The experimental set-up

The main parts of the pulsed laser microfluorimeter are shown in Fig. 1.: Nitrogen laser (NL) (built in our institute) with triggering pulse generator, dye laser (DL) (also built in our institute), delaying pulse generator (D), sample holder (S), monochromator (M) with stepping motor, photomultiplier (Ph) with high voltage supply, multichannel analyser (MA), computer (Comp.) x - y plotter (x - y), F_1 , F_2 neutral optical density filters and L_1 , L_2 lenses.

The advantages of this apparatus comes from the use of the pulse measurement technique. The pulse generator of NL triggers everything. This pulse switches the discharge of NL, makes step through D , the stepping motor of M (*i.e.* tunes the monochromator), and opens an electric gate its time-duration is 100—500 ns. The amplitude/digital converter A/D of MA integrates the photocurrent receiving it under measure time, and converting it into a digital signal, which will be accumulated in one of the 1024 channels. MA, after this process makes step on M and is ready to receive the following data, and the first channel follows the last one. So this apparatus

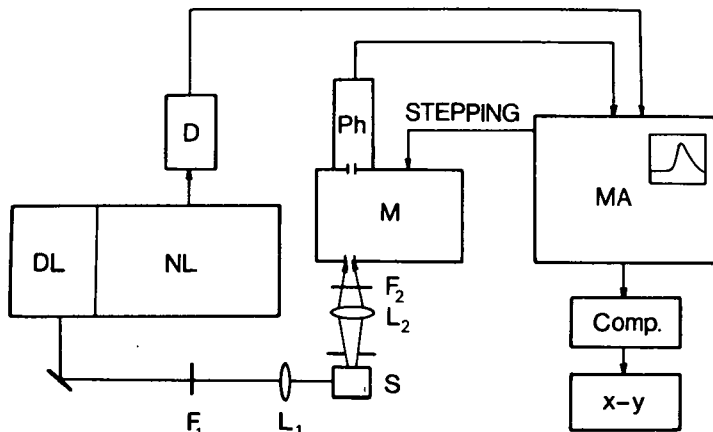


Fig. 1. Pulsed laser microfluorimeter design. NL — nitrogen laser, DL — dye laser, D — delaying pulsed generator, S — sample holder, M — monochromator, Ph — photomultiplier, MA — multichannel analyser, Comp. — computer, x-y — x-y plotter, F_1 , F_2 — neutral optical density filters, L_1 , L_2 — lenses.

— according to the programme — can measure many times the total spectrum (340 nm—640 nm), and therefore the signal to noise (S/N) ratio gets better. There is still a possibility to integrate the various parts of the full spectrum and to subtract the background signal from the total.

In the dye laser a 4-diethylamino-7-methylcoumarin dye was used. The energy and the duration of the pulses were 15 μ J and 3 ns, respectively, when the repetition rate was 25 Hz and the wavelength was 480 nm. The beam divergence was 1 mrad and the polarization degree on the horizontal plane was 0.99.

We determined the transmission function of the monochromator (Czerny—Turner construction), containing a grating of 600/mm and two concave mirrors of 25 cm, and of the photomultiplier (typed FEU—100), so we got corrected spectra by the x-y plotter.

The linearity of the Ph was studied with respect to the full spectrum of the fluorescein. There was such a concentration ($\sim 10^{-7}$ M) in the cuvette as it give a strong signal. We filtered the fluorescence signal by filters F_2 and we measured photocurrent (I) (I means the digital signal, the bit of the current), concerning unit gain one running. This characteristic can be seen in Fig. 2. in logarithmic scale (OD is the optical density of the filters F_2).

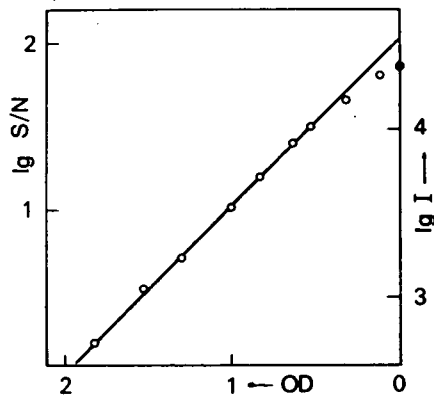


Fig. 2. The dependence of the measured photocurrent of the photomultiplier ($\lg I$) and the signal to noise ratio ($\lg S/N$) on the total fluorescence light intensity (OD).

It can be seen in Fig. 2. that if I is 10^4 bit, then undisturbance spectrum can be measured, and the S/N ratio is about 30.

The stereoscopic set-up of the sample holder is shown in Fig. 3.

We have decided on 140 mm for the focal length of lens L_1 . The product of this length and the beam divergence are $140 \mu\text{m}$, *i.e.* the diameter of the beam waist. In this case, the power density is 25 MW/cm^2 ($5 \cdot 10^{25}$ photon/cm 2 s $^{-1}$), since the average power of the laser pulse is 5 kW, and this value Φ is about 50 times higher, than the Φ_s producing saturation of the excited state ($\Phi_s = 0.5 \text{ MW/cm}^2$).

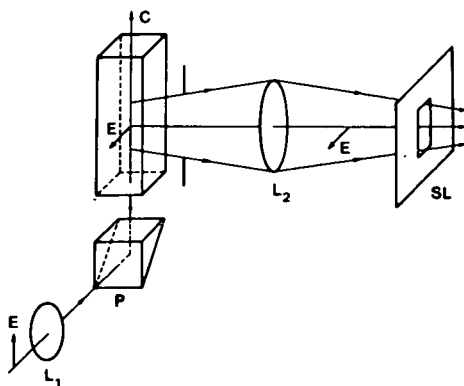


Fig. 3. The stereoscopic set-up of the sample holder. L_1 — lens of 140 mm, P — prism, C — cuvette.

The exciting, focused laser beam passes through prism (P) and goes vertically to the lower part of cuvette (C). The excited volume in the solution is a cylindrical shape, it is parallel to the slit of monochromator (SL), and it is projected in a ratio 1:1 by lens L_2 on to S. The width of the slit was 0.2 mm, so the spectral resolution of M was 2 nm. Vector E is the electric polarization vector of the laser beam, and its direction is unchanged — as compared to the direction of detection — to the set-ups of other investigations concerning the Raman scattering of water [8, 9]. The point, where the beam

goes to the cuvette, is not projected on to SL, so the scattered light on quartz is not disturbed.

We made choice of an exciting wavelength of 480 nm, because the fluorescein is highly absorbent at this wavelength, but the other organic traces in the water were less excited. This wavelength, as scattered light, has not disturbed the measurement of the fluorescence spectrum of fluorescein, and the band of the Raman scattering of water ($\sim 3400 \text{ cm}^{-1}$) arises at 745—750 nm, when $\lambda_e = 480 \text{ nm}$.

So the Raman band of the water and the maximum of the fluorescence of the fluorescein are at separated wavelength and the Raman scattering as a solvent blank is not much disturbed only at low concentrations, we measured the total spectra from 340 nm to 640 nm at every concentration and at every power density, five times. The blank signal from the total was subtracted and corrected with the transmission function of the apparatus. Then we calculated the integral of the corrected fluorescence spectra (I).

In every case we started the measurement of function $I_m(\Phi)$ without filters F_1 and we put before the monochromator filters F_2 of such optical density that the photomultiplier could get a light intensity corresponding to 10^4 bit. Then increasing the OD of F_1 we decreased the OD of F_2 at the same time.

Results

Fig. 4. shows the corrected spectra with the transmission function of the detector of 0.01 N water-dissolved fluorescein of 10^{-9} M ($\lambda_e=480$ nm and the observation of the radiation was perpendicular to the laser beam and as well as to E vector). The power density of the exciting laser light was filtered at various spectra what is shown in the Table I.

We can see from Fig. 4., when that we filter the power density, the maximum intensity of the Raman band of water is changing simultaneously with Φ , but the fluorescence intensity is not, and when the Φ is only 2—3% of the beginning power density — *i.e.* $\sim 10^{24}$ photon/cm²s⁻¹ — the fluorescence intensity compared to the intensity of Raman band shows no change.

As a second step, we also measured the dependence of the total fluorescence intensity (I) on the power density of the exciting light with other concentrations (10^{-8} , 10^{-7} , 10^{-6} M). This connection is shown in Fig. 5 in log-log scale.

In Fig. 5 small circles are the symbols of the experimental results. I depends linearly on Φ , if the photon flux density is lower than 10^{24} cm⁻²s⁻¹. So to most of the measured points at a 10^{-6} M concentration a straight line at angles up to 45° — expressive of the linear connection — can be fitted, and we lengthened this line to the vertical axis. We have drawn three further theoretical lines at 10^{-7} , 10^{-8} , 10^{-9} M parallel to the line concerning 10^{-6} M. These lines were shifted with one, two and three decades. One part of the measured points concerning 10^{-7} M was perfectly congruent with the

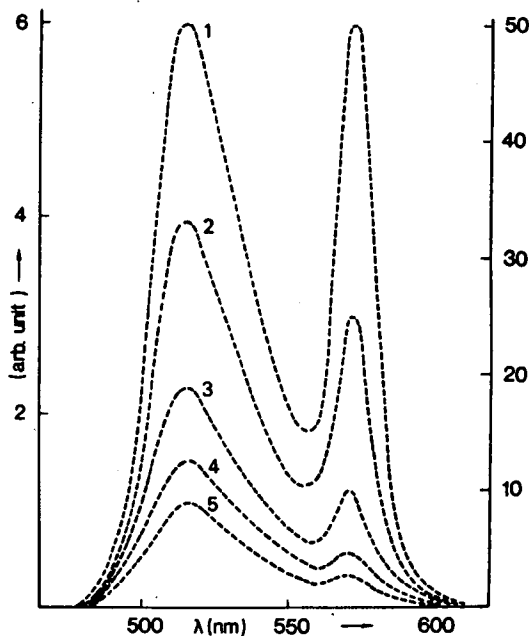


Fig. 4. The spectra of the total scattered light fluorescence, Raman scattering of the 10^{-9} M fluorescein in water (pH=12) as a function of the several exciting power density Φ . 1—25 MW/cm², 2—12.5 MW/cm², 3—4.16 MW/cm², 4—1.25 MW/cm², 5—0.8 MW/cm².

Table I

Curve number	1	2	3	4	5
OD of filters	0	0.3	0.8	1.3	1.5
Filtering (%)	100	50	16.6	5	3.3
Power density (MW/cm ²)	25	12.5	4.2	1.25	0.84
Photon flux density (photon/cm ² s ⁻¹)	$5 \cdot 10^{25}$	$2.5 \cdot 10^{25}$	$8 \cdot 10^{24}$	$2.5 \cdot 10^{24}$	$1.6 \cdot 10^{24}$

theoretical line, while the linear part, at lower concentrations could not be measured because of a significant decrease in the fluorescence detected.

The measured points concerning an Φ higher, than $10^{24} \text{ cm}^{-2} \text{ s}^{-1}$ can be found on the log-log scale, also along a straight line (broken line). The slope of these lines significantly deviates from the line angles to 45° , and the tangent of this angle is equal to 0.55, *i.e.* about 0.5. Such a kind of line on the log-log scale is a parabola on the linear-linear scale:

$$I_m \sim \sqrt{\Phi}, \quad \text{if } 3 \cdot 10^{24} \text{ cm}^{-2} \text{ s}^{-1} < \Phi < 50 \cdot 10^{24} \text{ cm}^{-2} \text{ s}^{-1} \quad (3)$$

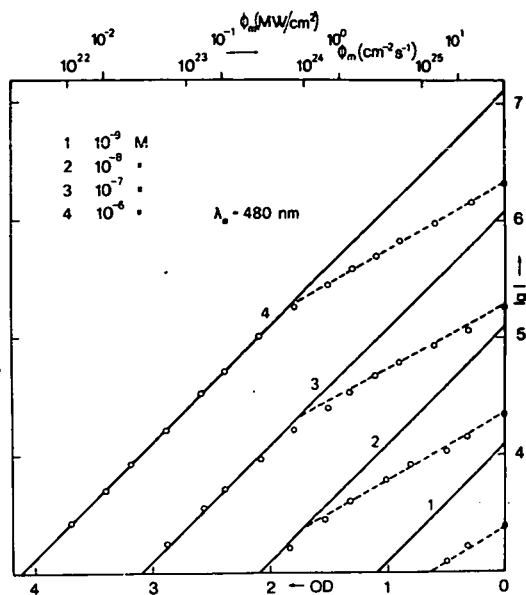


Fig. 5. The dependence of the fluorescence intensity (I) of the water dissolved fluorescein on the power density of the exciting light pulses Φ with 10^{-9} M (1), 10^{-8} M (2), 10^{-7} M (3), 10^{-6} M (4) concentrations. Exciting wavelength $\lambda_0 = 480$ nm. Continuous line — linear part, broken line — non-linear part.

We can draw some important conclusions from Fig. 5: The broken lines intersect the lines of 45° at the same Φ' ($\sim 10^{24} \text{ cm}^{-2} \text{ s}^{-1}$), their slope is also the same and they are equidistant (this separation is exactly 1.0). The nonlinear behaviour of the fluorescence of fluorescein in water solution at every concentration occurs at the same Φ' value, *i.e.* Φ' depends only on the molecular parameters corresponding to Eq. (1), so that *this phenomenon is the saturation of the excited state*.

But the approximation given in Eq. (3) does not show saturation. Equal to the former effect is that factor Γ (Γ is the ratio of I^0 — the number of fluorescent photons, which would have been detected in the absence of saturation, the value of the linear angles to 45° , — and of I_m — the measured number of fluorescent photons — at the same excitation) as the function of Φ is not linear.

Conclusions

Experimental results shown in Fig. 5 can be used in many respects: to several purposes.

1. One of the possibilities is the calculation of the true fluorescence intensity I^0 at a Φ value, from the measured intensity with the help of Γ , i.e. *the measured fluorescence intensity is needed for corrections made in terms of the saturation factor*. For the purposes of correction measuring function $I_m(\Phi)$ at an optional concentration is quite sufficient. (It is best to carry out at the concentration limited by Eq. (2), because the longest linear part of function $I_m(\Phi)$ can be observed in this case). E.g. in our measurements the photon flux density without filtering is $5 \cdot 10^{25} \text{ cm}^{-2} \text{ s}^{-1}$ and the $\lg \Gamma = 0.8$. It means that if is with the I_m produced with 6.3 that we obtain the true fluorescence intensity. It is an important factor which has to be taken into account, if we want quantitative analysis from fluorescence measurement under microscope.

2. The other possibility is *the determination of the lifetime of the excited state at very low concentrations* 10^{-6} — 10^{-8} M . This determination is based upon the observation that two straight lines, which are fitted to the measured points, intersect in the log-log scale about $10^{24} \text{ cm}^{-2} \text{ s}^{-1}$ with accuracy ± 0.1 . Using this value together with the value of the absorption cross-section at 480 nm $\sigma_a = 2.2 \cdot 10^{-16} \text{ cm}^2$ we can calculate from Eq. (1) τ , which is given as $4.5 \pm 1.0 \text{ ns}$. It is in good agreement with the results obtained by other methods at low concentrations [10—12].

3. The third possibility is *the calculation of the absorption cross-section* from Eq. (1), if we use a tunable dye laser, and if its power density is known at every wavelength, and if the lifetime of the excited state of the molecule studied is measured by an other method *at low concentrations* 10^{-6} — 10^{-8} M .

References

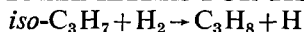
- [1] Herchher, M.: Appl. Opt. **6**, 947 (1967).
- [2] Smith, B. W., F. W. Plankey, N. Omenetto, L. P. Yart, J. D. Winefordner: Spectrochimica Acta **30A**, 1459 (1974).
- [3] Sacchi, C. A., O. Svelto, G. Prena: Histochem. J. **6**, 251 (1974).
- [4] White, J. G.: Electro-Opt. Syst. Des. **11**, 23 (1979).
- [5] Chekalyuk, A. M., V. V. Fadeev, G. M. Georgiev, Zh. S. Nicolov: Opt. Commun. **38**, 177 (1981).
- [6] Fadeev, V. V., A. M. Chekalyuk, V. V. Chubarov: Dokl. Acad. Sci. USSR **262**, 338 (1982).
- [7] Imasaka, T., H. Kadone, T. Ogawa, N. Ishibashi: Anal. Chem. **49**, 667 (1977); N. Ishibashi, T. Ogawa, T. Imasaka, M. Kunitake: Anal. Chem. **51**, 2096 (1979).
- [8] Taylor, D. L., Yu-Li Wang: Nature **284**, 405 (1980).
- [9] Slusher, R. B., V. E. Derr: Appl. Opt. **14**, 2116 (1975); N. P. Romanov, V. S. Shuklin: Opt. i. Spekt. **38**, 1120 (1975).
- [10] Ketskeméty, I., L. Gáti, A. Györi, L. Kozma: Acta Phys. Acad. Sci. Hung. **43**, 109 (1977).
- [11] Szűcs, K., B. Rácz, B. Németh, L. Kozma, I. Sánta, M. Hilbert: Acta Phys. et Chem. Szeged **24**, 437 (1978).
- [12] Imasaka, T., Y. Kawaba, N. Ishibashi: Rev. Sci. Instrum. **52**, 1473 (1981).

ФЛУОРЕСЦЕНТНАЯ НЕЛИНЕЙНОСТЬ ФЛУОРЕСЦЕИНА, РАСТВОРЕННОГО
В ВОДЕ, ПРИ ВОЗБУЖДЕНИИ ИМПУЛЬСАМИ ЛАЗЕРНОГО ИЗЛУЧЕНИЯ
ПРИ ВЫСОКОЙ ПЛОТНОСТИ МОЩНОСТИ

Б. Немет, И. Шанта и Л. Козма

Нелинейная зависимость флуоресценции флуоресцеина, растворенного в воде, исследована импульсным лазерным микрофлуориметром при высокой плотности мощности лазерного излучения (Φ), при малых концентрациях красителя 10^{-6} — 10^{-9} моль. На основании измерения зависимости фактора насыщения флуоресценции (Γ) от Φ , разработан метод для расчёта истинной интенсивности флуоресценции (I) из измеренной микрофлуориметром интенсивности (I_M), что является предложением нового метода для определения времени жизни возбуждённого состояния из функции $I_M(\Phi)$.

ARRHENIUS PARAMETERS FOR THE REACTION



By

L. SZIROVICZA

Institute of General and Physical Chemistry, Attila József University, Szeged, Hungary

(Received 29th September, 1982)

The kinetics of decomposition of 2,2-azobispropane was studied in the presence of excess molecular hydrogen at temperatures from 473 to 559 K. The initial rates of formation of the products were determined. The results are explained in terms of the proposed mechanism by evaluation of k_4 for the reaction:



Introduction

Hydropyrolysis is an industrial method in which hydrocarbons are pyrolyzed in the presence of molecular hydrogen. This method can be applied to modify the composition of the products in the pyrolysis of hydrocarbons. The basis of the influence of molecular hydrogen in the hydropyrolysis is a competition between two elementary reactions [1]: the abstraction of hydrogen by alkyl radicals from hydrocarbons, and the abstraction of hydrogen by alkyl radicals from molecular hydrogen.

In this work the aim was to provide kinetic parameters for the reaction of isopropyl radical with molecular hydrogen. For this reaction experimental and estimated kinetic data are available. BALDWIN and coworkers [2] suggested the rate constant shown below, obtained from results on the oxidation of isobutyraldehyde:

$$\log(k_4/\text{dm}^3 \text{ mol}^{-1} \text{ s}^{-1}) = 9.5 - 66.5 \text{ kJmol}^{-1}/2.3 \text{ RT}$$

For the activation energy of the title reaction Le Roy suggested 52.3 kJmol^{-1} [3].

Arrhenius parameters were estimated by means of thermochemical calculations, the following data being taken from the literature:

- a, The thermochemical data shown in Table I.
- b,

$$\log(k_{-4}/\text{dm}^3 \text{ mol}^{-1} \text{ s}^{-1}) = 10.8 \pm 0.4 - 32.6 \pm 3.3 \text{ kJmol}^{-1}/2.3 \text{ RT}$$

suggested by BALDWIN [4] for the reverse reaction.

The following equations were used [5]:

$$\ln \frac{A_4}{A_{-4}} = \frac{\Delta S^0}{R} \quad \text{and} \quad E_4 - E_{-4} = \Delta H^0$$

Table I

Thermochemical data [4, 6] for the reaction $iso-C_3H_7 + H_2 \xrightleftharpoons[k_4]{k_3} C_3H_8 + H$

	<i>iso-C₃H₇</i>	H ₂	C ₃ H ₈	H
$\frac{\Delta H^0}{\text{kJmol}^{-1}}$	73.6	0	-103.8	218
$\frac{S^0}{\text{JK}^{-1}\text{mol}^{-1}}$	279	130.5	269.9	114.6

where A and E are the Arrhenius A factor and activation energy, respectively; ΔS^0 and ΔH^0 are the standard entropy and enthalpy change of the reaction, respectively. The result of the estimation can be given as follows:

$$\log(k_4/\text{dm}^3 \text{mol}^{-1} \text{s}^{-1}) = 9.5 - 73.2 \text{ kmol}^{-1}/2.3 RT$$

As there are some differences between the calculated and estimated data, it seemed worth redetermining the Arrhenius parameters of the title reaction in a new system.

Experimental

The isopropyl radical was produced by thermal decomposition of 2,2-azobispropane (hereafter AIP) in the presence of excess molecular hydrogen. The ratio of the concentration of H₂ to the concentration of AIP was varied between 50 and 200 at 473–559 K. Experiments were carried out in a conventional static vacuum apparatus equipped with greaseless taps. Reactions were performed in a 108 cm³ cylindrical Pyrex vessel installed in an electric furnace. The reactions were started by measuring the pressure of the reactant in a 72 cm³ closed part of the vacuum line, thereafter shared with the reaction vessel. Reactions were quenched by admitting the products into an evacuated sampling bulb connected to the vacuum line by a high-vacuum joint. Products were analyzed by G. C. on a Perkin—Elmer F 11 gas chromatograph equipped with FID. Analyses were performed on the following columns: a 3 m column filled with 20 w% didecyl phthalate on Chromosorb PS at 343 K, and a 2 m column filled with 40/100 mesh alumina at programmed temperatures. Leads and analytical system, where necessary, were heated to 320 K by heating tape to avoid condensation and adsorption.

Reactions were performed under atmospheric pressure. Measurable reactions occurred only at high [H₂]/[AIP] ratios. To ensure high [H₂]/[AIP] ratios, the concentration of AIP in the reaction mixture was kept low. To increase the accuracy of the analyses of the products, an internal standard was used. Perfluoromethylcyclohexane (PFMCH) was selected as internal standard, as the peak of this compound did not interfere with those of the products of the reaction or the starting material. PFMCH proved to be stable under the conditions applied. In the experiments the concentration of AIP was seven times higher than that of PFMCH.

Results and Discussion

With regard to our earlier results [7, 8] the following reactions seemed worthy of consideration in this system:

- (1) $AIP \rightarrow N_2 + 2 iso-C_3H_7$
- (2) $2 iso-C_3H_7 \rightarrow 2,3\text{-dimethylbutane}$
- (3) $2 iso-C_3H_7 \rightarrow C_3H_8 + C_3H_6$
- (4) $iso-C_3H_7 + H_2 \rightarrow C_3H_8 + H$
- (5) $iso-C_3H_7 + AIP \rightarrow C_3H_8 + C_3H_6 \dots N \dots N \text{-} iso-C_3H_7$

In this short-form mechanism reaction (1) shows the formation of isopropyl radical, and reactions (2) and (3) its combination and disproportionation. Reaction (4) is the subject of our studies, and reaction (5) is another hydrogen-abstraction reaction in this system. Propane can be formed in reactions (4) and (5) as well as in reaction (3). From this mechanism it is to be expected that in the presence of H_2 the rate of formation of propane increases. Experiments have proved this expectation.

Kinetic data were derived from the initial rate of formation of propane by taking into account the roles of reactions (3) and (5). The concentration of isopropyl radical was calculated from the initial rate of formation of 2,3-dimethylbutane (DMB) and from the rate constant of reaction (2) taken from the literature [9].

In a closed system such as this, the rate of change of a compound ($W = \frac{dc}{dt}$) formed, transformed or decomposed by different elementary reactions can be given by vector equation I:

$$W = [v]R \quad (I)$$

where v is the stoichiometric number and R is the rate of the elementary reaction. On the basis of Eqn I, the rate of formation of any compound (W_i) can be given by

$$W_i = \sum_j v_{i,j} R_j \quad (II)$$

where $v_{i,j}$ is the stoichiometric number of component i in reaction j .

The elements of the matrix for all of the substances $i=1\dots 9$ and for all of the unidirectional reactions $j=1\dots 5$ in this system are given in Table II.

Table II

Transformed elements of $[v_{i,j}]$ matrix for substances $i = 1\dots 9$ and for reactions $j = 1\dots 5$

$j \backslash i$	1 AIP	2 N ₂	3 C ₃ H ₇ *	4 DMB	5 C ₃ H ₈ *	6 C ₃ H ₆	7 H	8 R**	9 H ₂
1	-1	1	2	0	0	0	0	0	0
2	0	0	-2	1	0	0	0	0	0
3	0	0	-2	0	1	1	0	0	0
4	0	0	-1	0	1	0	1	0	-1
5	-1	0	-1	0	1	0	0	1	0

* $C_3H_7 = iso-C_3H_7$

R** = $C_3H_6 \dots N \dots N \text{-} iso-C_3H_7$

In the experiments the initial rates of formation W_4 and W_5 were determined, *i.e.* the initial rates of formation of DMB and C_3H_8 , respectively. These are given below on the basis of the stoichiometric numbers of Table II.

$$W_4 = \frac{d[\text{DMB}]}{dt} = \sum_{j=1}^5 \nu_{4,j} R_j = \nu_{4,2} R_2 = 1 \cdot k_2 [\text{iso-C}_3\text{H}_7]^2 \quad (\text{III})$$

$$\begin{aligned} W_5 &= \frac{d[\text{C}_3\text{H}_8]}{dt} = \sum_{j=1}^5 \nu_{5,j} R_j = \nu_{5,3} R_3 + \nu_{5,4} R_4 + \\ &+ \nu_{5,5} R_5 = 1 \cdot R_3 + 1 \cdot R_4 + 1 \cdot R_5 = k_3 [\text{iso-C}_3\text{H}_7]^2 + \\ &+ k_4 [\text{iso-C}_3\text{H}_7][\text{H}_2] + k_5 [\text{iso-C}_3\text{H}_7][\text{AIP}] \end{aligned} \quad (\text{IV})$$

R_3 can be given from the ratio R_3/R_2 :

$$R_3 = \frac{k_3}{k_2} [R_2] = \frac{k_3}{k_2} \frac{d[\text{DMB}]}{dt} \quad (\text{V})$$

Taking R_3 from Eqn V and $[\text{iso-C}_3\text{H}_7] = (W_4/k_2)^{1/2}$ from Eqn III, we obtain:

$$\left(W_5 - \frac{k_3}{k_2} W_4 \right) (W_4)^{-1/2} = \frac{k_5}{k_2^{1/2}} [\text{AIP}] + \frac{k_4}{k_2^{1/2}} [\text{H}_2] \quad (\text{VI})$$

In Eqn VI, besides the measured quantities and literature data for k_2 , k_3 and k_5 , the only unknown is the value of k_4 . For the determination of k_4 , the left side of Eqn VI was plotted as a function of $[\text{H}_2]$. A straight line was found, from the slope of which $k_4/k_2^{1/2}$ was determined at seven different temperatures. Results are shown in Table III. Taking $k_2 = 10^{9.5} \text{ dm}^3 \text{ mol}^{-1} \text{ s}^{-1}$ from the results of Golden and coworkers [9], values of k_4 were calculated.

The Arrhenius parameters of reaction (4) were determined in the usual way

Table III
Experimental data for determination of the Arrhenius parameters of reaction (4)

T/K	$10^3 k_4/k_2^{1/2} *$	$10^{-2} k_4 **$	$\log k_4$	10^3 K/T
473	0.398	5.05	2.70	2.11
493	0.972	5.46	2.74	2.03
523	4.75	26.7	3.43	1.91
543	10.5	59.0	3.77	1.84
559	10.1	56.8	3.75	1.79
563	11.0	62.0	3.79	1.78
573	13.9	78.1	3.89	1.75

$$k_4/k_2^{1/2} * = k_4/k_2^{1/2} \text{ dm}^{3/2} \text{ mol}^{-1/2} \text{ s}^{-1/2}$$

$$k_4 ** = k_4/\text{dm}^3 \text{ mol}^{-1} \text{ s}^{-1}$$

from the temperature-dependence of k_4 . The graph of $\log k_4$ versus $1/T$ is shown in Figure 1.

From the slope and intercept of Fig. 1, the rate constant of reaction [4] is

$$\log(k_4/\text{dm}^3 \text{ mol}^{-1} \text{ s}^{-1}) = (10.3 \pm 0.7) - (69.4 \pm 6.7 \text{ kJmol}^{-1})/2.3 RT$$

where the errors in brackets are the standard deviations.

To check these data, Arrhenius parameters for the reverse reaction were calculated by means of thermochemical calculations, the results of which gave:

$$\log(k_{-4}/\text{dm}^3 \text{ mol}^{-1} \text{ s}^{-1}) = (11.6 \pm 0.7) - (28.8 \pm 6.7 \text{ kJmol}^{-1})/2.3 RT$$

This expression is similar to that obtained experimentally [4].

The Arrhenius parameters of reaction [4] were compared with those of similar

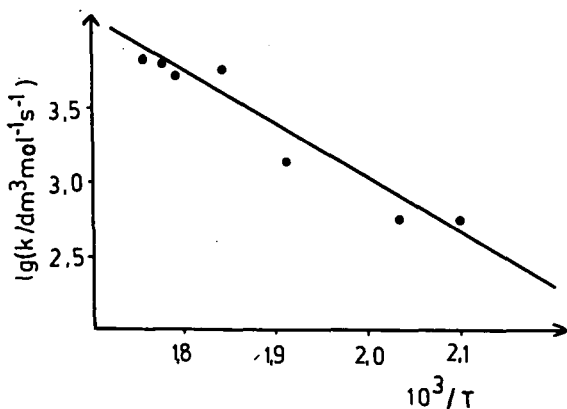


Figure 1. Temperature-dependence of k_4 .

Table IV

Arrhenius parameters of the reaction
 $R + H_2 \rightarrow RH + H$
 (from Reference [10])

Reaction	$\log A^*$	E^*	$\log k^*$	
			700 K	1000 K
$CH_3 + H_2 \rightarrow CH_4 + H$	9.2	47.3	5.7	6.7
$C_2H_5 + H_2 \rightarrow C_2H_6 + H$	9.6	58.6	5.2	6.5
$1-C_3H_7 + H_2 \rightarrow C_3H_8 + H$	9.2	64.4	4.4	5.8
$2-C_3H_7 + H_2 \rightarrow C_3H_8 + H$	10.3 ± 0.7	69.4 ± 6.7	5.1	6.7
$2-C_4H_9 + H_2 \rightarrow C_4H_{10} + H$	9.7	71.9	4.3	5.9

$\log A^* = \log A/\text{dm}^3 \text{ mol}^{-1} \text{ s}^{-1}$; $E^* = E/\text{kJmol}^{-1}$
 $\log k^* = \log k/\text{dm}^3 \text{ mol}^{-1} \text{ s}^{-1}$

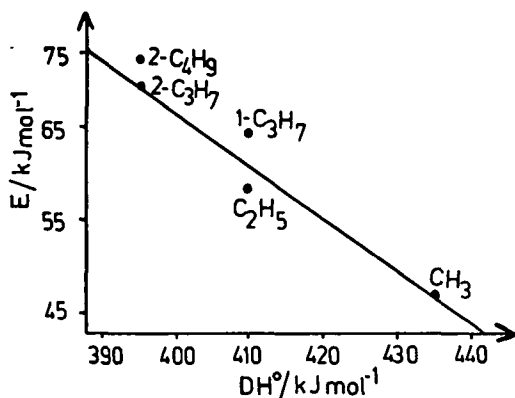


Figure 2. Application of Polanyi's rule for the reaction $R \cdot + \text{H}_2 \rightarrow \text{RH} + \text{H}$. E = activation energy, DH^0 = bond-dissociation energy.

reactions, compiled in Table IV together with rate constants at the usual temperature of hydrolysis. It can be seen from Table IV that the activation energies increase with increasing carbon number of the reacting radicals, and secondary radicals have higher activation energies than primary radicals. Such an increase in activation energies is in accordance with the Polanyi rule, as can be seen from Figure 2, where activation energies (E) are shown versus the bond-dissociation energies (DH^0) of the R-H bond. A comparison of the rate constants in Table IV proves that different hydrocarbon radicals behave similarly in their reactions with molecular hydro-

gen, especially at higher temperatures. This means that in the hydrolysis of hydrocarbons all of the radicals present need consideration.

Acknowledgement

The author is indebted to Professor T. Bérces for initiating this work.

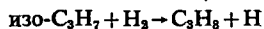
Literature

- [1] *Taniewski, M., A. Lachowicz, K. Skutil, D. Maciejko*: Ind. Eng. Chem. Prod. Res. Dev. **20**, 746 (1982).
- [2] *Baldwin, R. R., C. J. Cleugh, W. Walker*: J. C. S. Faraday I. **72**, 1715 (1976).
- [3] *Le Roy, D. J.*: Can. J. Chem. **33**, 580 (1955).
- [4] *Baldwin, R. R.*: Trans. Faraday Soc. **60**, 527 (1964).
- [5] *Benson, S. W.*: Thermochemical Kinetics, 2nd. Ed. John Wiley and Sons, (1976).
- [6] *Seres, L., L. Zalotai, F. Márta*: Acta Phys. et Chem. Szeged, **23**, 365 (1977).
- [7] *Szirovicza, L., F. Márta*: Int. J. Chem. Kinet. **8**, 897 (1976).
- [9] *Golden, D. M., L. W. Piskiewicz, M. J. Perona, P. C. Beadle*: J. Am. Chem. Soc., **96**, 1645 (1974).
- [10] *Allara, D. L., R. Show*: J. Phys. Chem. Ref. Data, **9**, 523 (1980).

АРРЕНИУСОВСКИЕ ПАРАМЕТРЫ ДЛЯ РЕАКЦИИ $\text{изо-C}_3\text{H}_7 + \text{H}_2 \rightarrow \text{C}_3\text{H}_8 + \text{H}$

Л. Сировица

Изучена кинетика распада 2,2-азобис-пропана в присутствии избытка молекулярного водорода в интервале температур от 343 до 559 К. Определены начальные скорости образования продуктов. Полученные результаты обсуждены с точки зрения предложенного механизма с расчетом k для реакции:





THERMAL DECOMPOSITION OF PROPANE IN A RECIRCULATION SYSTEM III. INVESTIGATIONS IN THE PRESENCE OF OLEFIN-ABSORBER

By

I. BÁRDI¹ and T. BÉRCES²

(Received 10th October, 1982)

The pyrolysis of propane was carried out in a circulation system, in the presence of olefin-absorber, at temperatures in the range 450–545 °C, at propane pressures of 30–470 Torr, in a wide conversion range (0.1–72%). Under the given experimental conditions the ratio of methane to hydrogen (α) does not change with conversion; α increases slightly with temperature. The dependence of α on the propane concentration is a function of temperature. A simple reaction mechanism was derived on the basis of data found in the literature and from the present experimental results. The α values calculated in accordance with this mechanism are in agreement with the experimental values.

We have previously reported [1] results on the thermal decomposition of propane in a recirculation system, using a stirred flow reactor. Under these circumstances the mechanism of thermal decomposition of propane is rather complicated. The complication (the self-inhibition character of the reaction) is caused by the reactions of the product olefins. In this work we investigate the thermal decomposition of propane under olefin-free circumstances, the product olefins being removed continuously from the recirculation system with an absorber. It is to be expected that a simple mechanism is valid under olefin-free circumstances and in this way an opportunity arises to determine more exact and reliable kinetic characteristics for the thermal decomposition of propane.

Experimental

The mercury perchlorate — perchloric acid system (MP—PA) showed the best olefin-absorption capacity, and was used in our experiments. The compound was absorbed in a g.c. support, which was filled into a glass U-tube. The absorber was used at room temperature (see [1]).

The apparatus, the experimental methods and the chemicals used were described in detail in [1, 2].

The experiments were conducted at 6 different temperatures (450, 475, 495, 515, 535 and 545 °C), at a total pressure of 1 atm, the partial pressure of propane varying

¹ Institute of General and Physical Chemistry, Attila József University, Szeged, Hungary.

² Central Research Institute for Chemistry of the Hungarian Academy of Sciences, Budapest, Hungary.

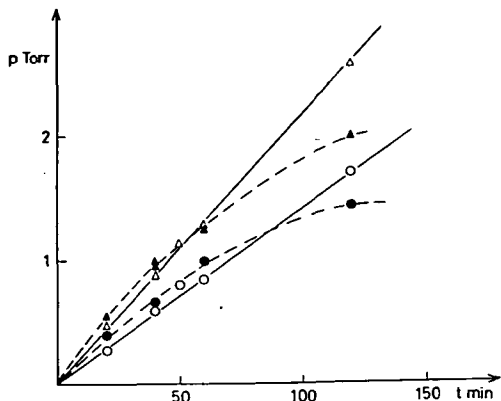


Fig. 1. Product vs. time plots at 515 °C, at a propane pressure of 61 Torr. Symbols: open triangles H_2 , open circles CH_4 (using olefin-absorber), filled triangles H_2 , filled circles CH_4 (without olefin-absorber).

pressure of 61 Torr. In the experiments in which absorber was used, the product vs. time plots give practically straight lines. As can be seen in Fig. 1, in absorber-free experiments the product vs. time plots exhibit curvature; this originates from the inhibiting effect of the product olefins.

We have earlier discussed [1] that, owing to the olefin-absorber used in the experiments, self-inhibition-free pyrolysis conditions were achieved only at 515 °C and lower temperatures, at low (<5%) conversions. At higher temperatures 535–545 °C) ethylene and propylene were detected in small amounts among the products. This was a consequence of the unsatisfactory functioning of our absorber. In the experiments conducted at temperatures higher than 515 °C, there is a definite residual olefin level; this level decreases slightly with conversion. In Fig. 2 we show the residual olefin level as a function of conversion at two temperatures. The decreasing tendency is readily observable. It is easy to explain the decrease in the concentration of olefins. The absorption of olefins in the absorber is relatively slow. For this reason, at low conversions, where as a consequence of the greater concentration of propane the rate of formation of olefins is higher, a higher stationary residual olefin level results. This level will decrease, the lower the rate of formation of olefins.

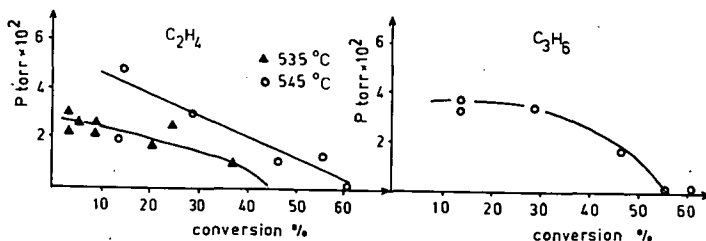


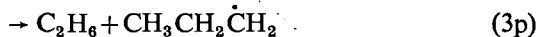
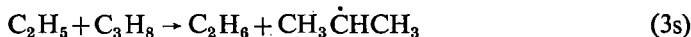
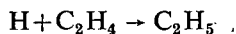
Fig. 2. Variation of residual olefin level with conversion

between 30 and 470 Torr. As diluent, carefully purified (deoxygenated) nitrogen was used. The circulation rate in every case was 12 dm³/hour. The conversion varied in the range 0.1–72%; it was calculated from the measured concentrations of products. Under the above experimental conditions, usually only three products were detected: methane, ethane and ethylene.

At 515 °C and lower temperatures the kinetics of the decomposition of propane was studied under practically olefin-free circumstances. This situation is shown in Fig. 1, which depicts the methane and hydrogen product distribution curves at 515 °C and at a propane

At 545 °C (the highest temperature in our study) it can easily be seen from the product distribution data that the amount of residual ethylene is about 0.1—1% of the methane formed, which corresponds to the concentrations formed at conversions of about 0.02—0.2% propane. In our experience, at such low conversions under our experimental conditions, self-inhibition is not yet significant. This is verified by the experimental finding that the shapes of the product formation curves for methane and hydrogen at 535 and 545 °C are similar to those obtained at lower temperatures (515, 495 °C) where there is practically no self-inhibition.

A significant difference was obtained in the ethane *vs.* conversion curves. In the olefin-absorber-free experiments, the concentration of ethane increases steeply with conversion, while in the experiments in which absorber was used, the amount of ethane changes only slightly in wide conversion and temperature ranges. At the same initial concentration of propane, more ethane is formed in the absorber-free experiments than in the presence of the absorber, and the difference increases with conversion (see Table I). This shows that in the experiments in the absence of absorber, an important ethane-producing process is the addition of an H atom to ethylene and, following this, the H atom abstraction reaction between ethyl radical and propane



Further, in the presence of olefin-absorber the nature of the chain rupture step probably changes too.

Table I

Partial pressure of ethane, measured during the
pyrolysis of propane
 $t = 535^\circ\text{C}$ $p_0 = 61$ Torr

No.	conversion %	ethane Torr
experiments with olefin-absorber		
189	3.40	0.0305
222	3.97	0.0113
190	6.09	0.0154
217	9.50	0.0144
191	9.70	0.0212
192	17.19	0.0289
193	25.25	0.0504
196	37.23	0.0333
olefin-absorber-free experiments		
194	3.20	0.0452
221	3.22	0.0216
186	5.92	0.0535
186	7.4	0.0780
187	10.61	0.1625
197	17.71	0.3582

Temperature-dependence of the main products

There is a slight temperature-dependence of the formation of methane and hydrogen in the presence of olefin-absorber, as can be seen in Fig. 3, where the pressures of CH_4 and H_2 are plotted against conversion at four different temperatures and at a propane pressure of 61 Torr. The experimental values fit a straight line, even at high conversions.

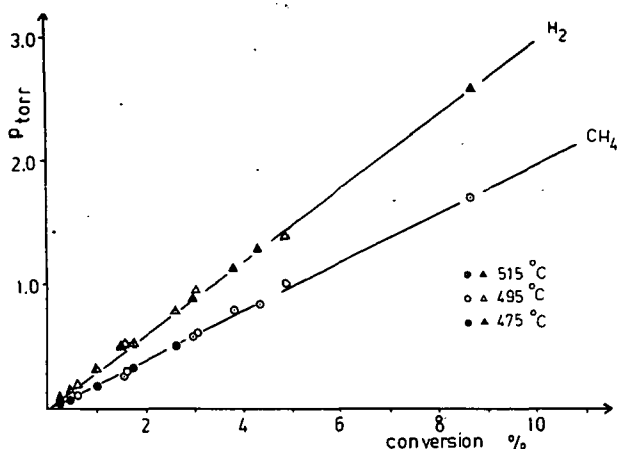


Fig. 3. Plots of hydrogen and methane yields against conversion at different temperatures (using olefin-absorber).

The ratio of methane to hydrogen

Plots of the methane pressure against the hydrogen pressure in experiments at five different temperatures and various conversions (0.01–77%) and at a propane concentration of 61 Torr yielded straight lines of slope 0.730 ± 0.0095 (Fig. 4). To simplify comparison, the same Figure gives the methane *vs.* hydrogen values obtained in olefin-absorber-free experiments under the same experimental conditions. It can be seen from Fig. 4 that at lower conversions (<10%) the two graphs coincide, but at higher conversions (>10%) the points for the absorber-free experiments deviate from linearity, the curve inclining towards the methane axis. This behaviour can be explained by the hydrogen consumption taking place as a consequence of self-inhibition. In the absorber-free experiments, the initial slope of the curve is 0.796. This value is in accordance with the slope in the presence of olefin-absorber.

The ratio of methane to hydrogen (α) shows no significant dependence on conversion, in contrast with the results of the absorber-free experiments. This can be seen in Fig. 5, where the α values obtained at 535 °C at a propane pressure of 61 Torr are plotted *vs.* conversion. For comparison, the α values obtained in absorber-free experiments are also plotted in the same Figure. It is important to note that values extrapolated to zero conversion (from experiments using olefin-absorber) are in good agreement with the α values determined directly by experiment.

Interesting behaviour was found in the dependence of α on the initial pressure of propane (see Table II and Fig. 6). In Fig. 6 the α values obtained in the presence of olefin-absorber are plotted as a function of propane pressure at 450 and 515 °C. There is a slight increase in α at 515 °C, while at 450 °C α increases significantly with increasing propane concentration. This behaviour is in agreement with literature experience [3]. For the concentration-dependence of α , the following simple expression

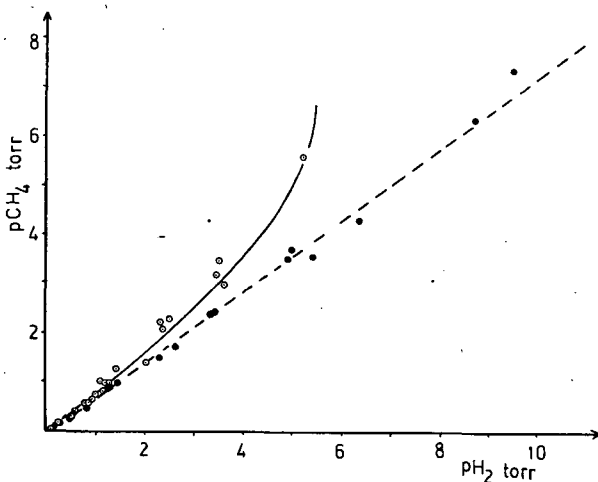


Fig. 4. Plots of methane yield against hydrogen yield in the pyrolysis of propane, at an initial pressure of 62 Torr and temperatures between 475 and 545 °C (the highest point was measured at 33.4% conversion) ● absorber-free experiments, ○ using olefin-absorber.

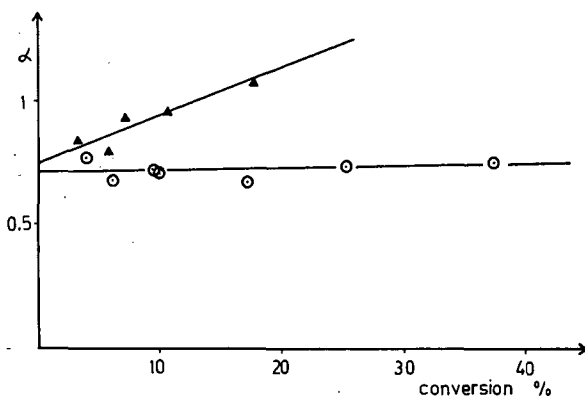


Fig. 5. Dependence of α on conversion, at an initial propane pressure of 61 Torr, at 535 °C. Open circles: using olefin-absorber, filled triangles: without olefin-absorber.

Table II
 Dependence of α on the propane pressure in the
 presence of olefin-absorber
 $t = 515^\circ\text{C}$

No.	propane Torr	conversion %	α
228	30.72	2.77	0.681
226	30.79	4.32	0.669
227	30.65	7.95	0.714
177	61.14	1.09	0.563
178	61.05	2.35	0.665
179	60.44	3.41	0.658
220	60.63	3.20	0.701
240	61.10	3.45	0.687
180	61.05	6.87	0.660
223	122.54	1.86	0.788
235	121.81	1.30	0.744
224	121.25	4.96	0.803
225	121.63	7.52	0.820
229	184.66	1.54	0.824
230	182.34	3.03	0.831
231	182.88	4.57	0.791
232	462.42	1.42	0.928
233	464.18	2.83	0.929
234	461.31	4.28	0.915

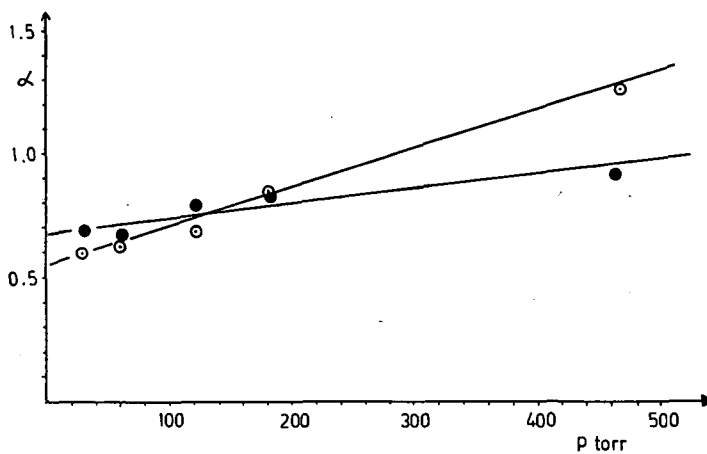


Fig. 6. Dependence of α on propane pressure at different temperatures. Filled circles: $t = 515^\circ\text{C}$, open circles: $t = 450^\circ\text{C}$.

was described by LEATHARD and PURNELL [3]:

$$\alpha = a + bp_i$$

where a and b are constants and p_i the initial pressure of propane.

From our experimental data it was possible to calculate the a and b values, which are as follows:

$$\begin{array}{ll} t = 450^\circ\text{C} & t = 515^\circ\text{C} \\ a = 0.539 \pm 0.020 & a = 0.683 \pm 0.029 \\ b = 0.0016 \pm 0.0001 & b = 0.0006 \pm 0.0001 \end{array}$$

These parameters are in approximate agreement with literature data [3].

The trend of the temperature-dependence of α is the same in the absorber-free experiments and in the experiments in the presence of olefin-absorber, *viz.* there is a slight increase in α as the temperature increases (see Table III). From our experimental

Table III

Temperature-dependence of α in the presence of olefin-absorber
 $p = 61$ Torr propane

t °C	450	475	495	515	535	545
$\bar{\alpha}$	0.631	0.619	0.657	0.671	0.720	0.728
α_0	—	0.578	0.618	0.688	0.711	0.716

$\bar{\alpha}$ = mean value of all α values measured in a system containing olefin-absorber
 α_0 = α values extrapolated to zero conversion using the α vs. conversion plots

results, the temperature-dependence of α (at a propane pressure of 61 Torr) can be described by the following expression:

$$\alpha = 10^{2.50 \pm 1.31} \exp(-2029 \pm 412/RT)$$

For comparison, PURNELL and LEATHARD [3] report that in the ranges 510—560 °C and 25—260 Torr propane the temperature-dependence of α can be described by the following expression:

$$\alpha = 10^{0.67 \pm 0.13} \exp(-2890/RT)$$

The order of reaction

From the $\log w_0$ vs. $\log p_0$ plots (where w_0 is the initial rate calculated from experiments in the presence of olefin-absorber, and p_0 is the initial pressure of propane), it was possible to determine the orders of formation of methane and hydrogen. As can be seen from Figs. 7a, 7b and 7c, similarly as for the results of LAIDLER ET AL. [4] and ZALOTAI, BÉRCES and MÁRTA [5], these plots do not give straight lines. At 515 °C the inflexion point can be found at a propane pressure of 120 Torr. The ini-

tial order of methane formation in the pressure range 120—460 Torr is 0.94, while in the range 30—120 Torr the order is 1.21. According to LAIDLER and his coworkers, first-order kinetics hold for the decomposition of propane above the inflexion point, while below the inflexion point the order is 1.5. Roughly the same order values were obtained for hydrogen formation. At 450 °C the $\log w_0$ vs. $\log p_0$ plots give practically straight lines and the initial order for methane formation is 1.21 in this case.

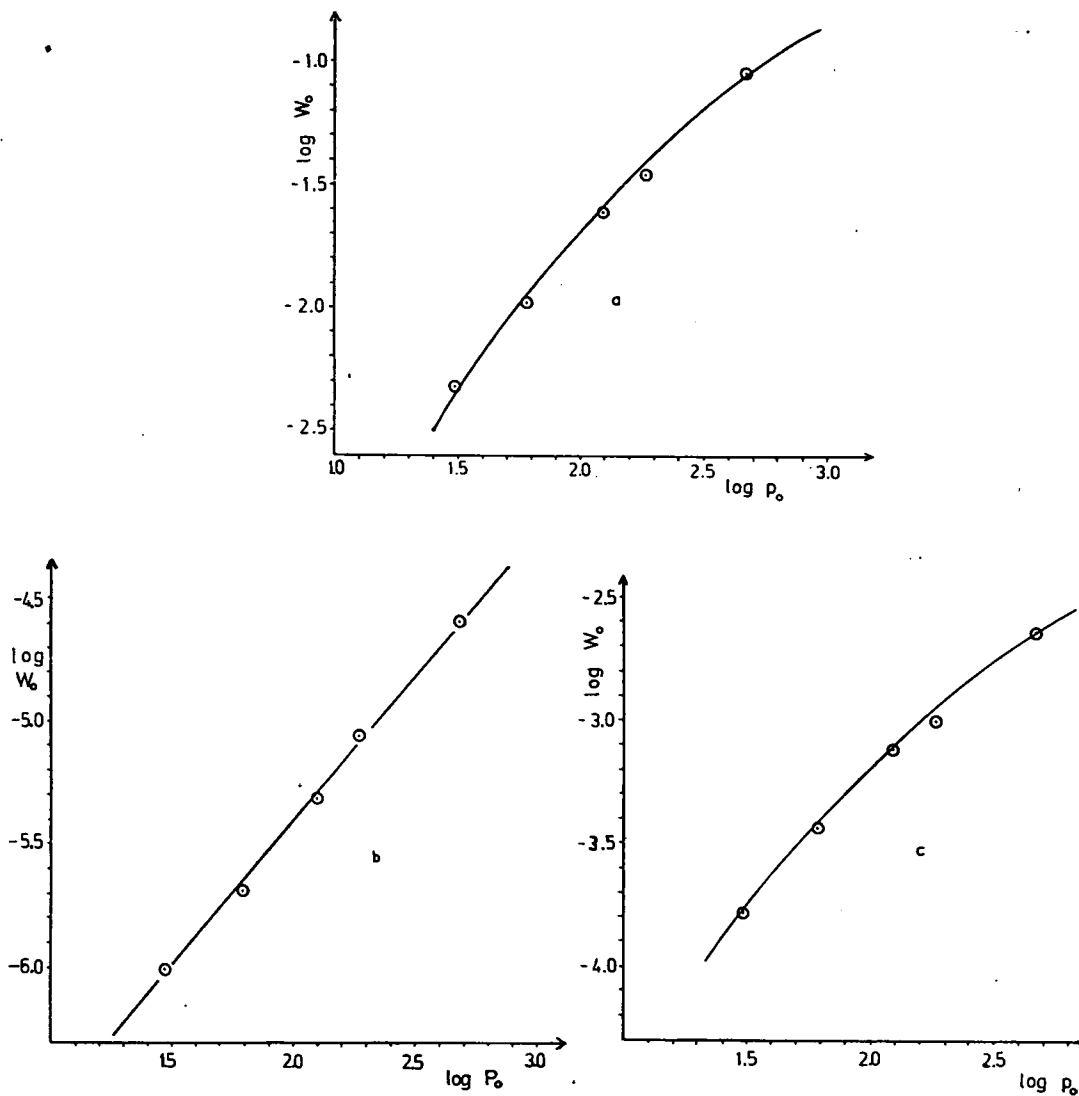


Fig. 7. $\log w_0$ vs. $\log p_0$ plots for methane and hydrogen at different temperatures. (a) $t = 515^\circ\text{C}$, CH_4 , (b) $t = 450^\circ\text{C}$, CH_4 , (c) $t = 515^\circ\text{C}$, hydrogen.

Energy of activation

From the temperature-dependence of the initial rate of formation of methane and hydrogen, the activation energy for the decomposition of propane can be determined (Fig. 8). From the $\log w_0$ vs. $1/T$ plots (using the experimental data calculated from the experiments in the presence of absorber), the following Arrhenius parameters were calculated:

$$E_a = 68.9 \pm 2.6 \text{ kcal/mol} \quad \log A = 17.2 \pm 0.7 \quad (\text{CH}_4)$$

$$E_a = 68.6 \pm 0.9 \text{ kcal/mol} \quad \log A = 16.7 \pm 0.2 \quad (\text{H}_2)$$

These values are in good agreement with data in the literature (68.0 kcal/mol in the pressure range 50—200 Torr).

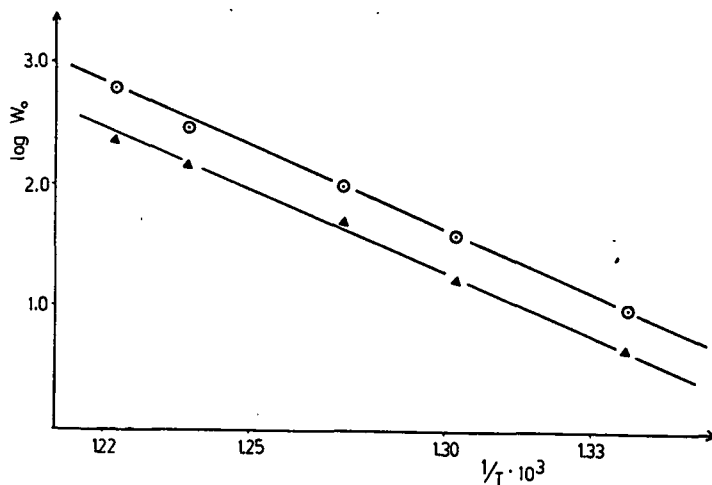


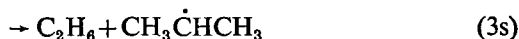
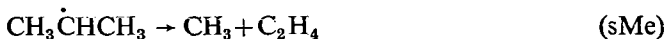
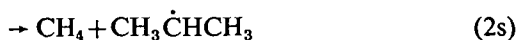
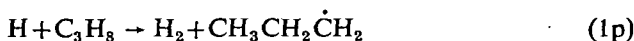
Fig. 8. $\log w_0$ vs. $1/T$ plots for hydrogen (Δ) and methane (\circ)

Discussion

In a preceding paper [2] a mechanism was set down which was able to describe the decomposition of propane to a good approximation in a recirculation system. When an olefin-absorber is used, the mechanism of the decomposition will be essentially simpler; with the continuous absorption of olefins formed during the decomposition, the reactions involving olefin participation are negligible. It is important to note that the absorption of olefins is practically complete at lower conversions and at temperatures below 535 °C.

From our experimental results when an olefin-absorber was used and from data to be found in the literature, the following simple mechanism can be given for the

thermal decomposition of propane



From this mechanism, the following expression can be given for the ratio $[\text{C}_4\text{H}]/[\text{H}_2]$:

$$\frac{[\text{CH}_4]}{[\text{H}_2]} = \frac{k_2}{k_1} \frac{[\text{CH}_3]}{[\text{H}]}$$

where

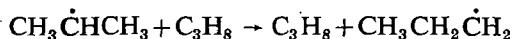
$$\frac{k_2}{k_1} = \frac{k_{2p} + k_{2s}}{k_1 + k_{1s}} \quad \text{and} \quad \frac{[\text{CH}_3]}{[\text{H}]} = \frac{k_1}{k_2} \frac{1}{\beta}$$

$$\beta = \frac{k_{sH} + \alpha' k_{pH}}{k_{sMe} + \alpha' k_{pMe}} \quad \alpha' = \frac{k_{sH} + k_{sMe}}{k_{pH} + k_{pMe}}$$

Hence

$$\alpha = \frac{[\text{CH}_4]}{[\text{H}_2]} = \frac{1}{\beta} \quad (\text{II})$$

This expression indicates that α is independent of the initial concentration of propane. This is in contradiction with our experimental results (see Fig. 6 and Table II). The difference probably originates from the insufficiency of the mechanism described. LEATHARD and PURNELL [3, 6] also observed the dependence of α on the propane concentration and conclude that this can be explained by the following bimolecular isomerization step



On the basis of our experimental results it is reasonable to suppose that the dependence of α on the propane concentration under self-inhibition-free conditions

is a consequence of the competition between the above bimolecular isomerization and the (sH) decomposition of *s*-propyl radicals. This assumption is supported by the observation that the extent of the concentration-dependence of α decreases with increasing temperature (see Fig. 4). With increasing temperature the decomposition reaction (sH), which has a higher activation energy, becomes of relatively greater importance, whereas the isomerization plays an ever smaller part and finally the competition of these two reactions gradually comes to an end.

Table IV

Experimental and calculated α values at propane pressure
 $p=61$ Torr (in the presence of olefin-absorber)

°C	No.	conversion %	α experimental	α calculated (ZBM I)	α calculated (ZBM II)	α calculated (LP)
450	236	0.0498	0.705	1.440	—	—
	237	0.0869	0.642	1.440	—	—
	238	0.1530	0.560	1.440	—	—
	239	0.2061	0.615	1.440	—	—
475	208	0.211	0.633	1.466	—	0.619
	204	0.3185	0.648	1.466	—	0.620
	205	0.7550	0.611	1.466	—	0.623
	207	1.3320	0.631	1.466	—	0.624
	209	2.1010	0.678	1.466	—	0.637
495	174	0.5154	0.696	1.368	—	0.668
	172	1.1945	0.614	1.368	—	0.675
	176	1.2114	0.612	1.368	—	0.674
	173	2.3867	0.637	1.368	—	0.686
	175	4.1128	0.739	1.368	—	0.744
515	177	1.0997	0.563	1.623	1.623	0.682
	178	2.3538	0.665	1.623	1.623	0.689
	220	3.1989	0.701	1.623	1.622	0.694
	179	3.4133	0.658	1.623	1.623	0.699
	180	6.8679	0.660	1.623	1.624	0.725
535	189	3.40	0.715	1.643	1.664	0.704
	222	3.97	0.773	1.643	1.664	0.707
	190	6.093	0.683	1.643	1.669	0.732
	191	9.70	0.708	1.643	1.717	0.766
	217	9.50	0.714	1.643	1.645	0.795
	192	17.19	0.674	1.643	1.645	0.861
	193	25.25	0.732	1.643	1.646	0.952
	196	37.23	0.747	1.643	1.644	1.143
545	218	14.08	0.721	1.653	1.669	—
	216	14.25	0.653	1.653	1.680	—
	202	15.09	0.752	1.653	1.647	—
	203	29.20	0.777	1.653	1.673	—
	193	47.31	0.772	1.653	1.665	—
	200	56.01	0.673	1.653	1.645	—
	201	61.17	0.752	1.653	1.643	—

(ZBM I) calculated *via* expression (II), see text

(ZBM II) calculated *via* expression in Ref. [12]

(LP) calculated *via* expression (III), see Ref. [6]

Table V
Kinetic parameters used in the calculations

Reaction	log A (dm ³ mol ⁻¹ s ⁻¹)	E _a Kcal/mol	References
H + C ₃ H ₈ → H ₂ + P	11.1	9.7	[7]
→ H ₂ + S	10.8	7.7	[7]
CH ₃ + C ₃ H ₈ → CH ₄ + P	9	11.5	[8]
→ CH ₄ + S	8.8	10.5	[7]
P → H + C ₃ H ₈	13.2	38.6	[7]
→ CH ₃ + C ₂ H ₄	13.1	32.5	[7]
S → H + C ₃ H ₈	13.9	40.4	[7]
→ CH ₃ + C ₂ H ₄	14.6	44	[9]
H + C ₃ H ₆ → P	9.9	2.9	[10]

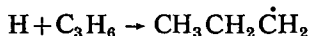
By means of expression (II), α values were calculated from the result, obtained in the presence of absorber; these data are collected in column 5 of Table IV. The experimentally determined α values can be found in column 4. The Arrhenius parameters used in these calculations are shown in Table V. Table IV reveals that α values calculated *via* expression (II) differ from the experimental α values by a factor of 2, similarly as in the absorber-free experiments (see [2]). This difference between the two sets of data may originate from the inaccuracy of the Arrhenius parameters used in the calculations.

If a more complicated expression (involving the concentrations of propane and olefins) is used for the calculation of α (see [2]), the α values in column 6 of Table IV are obtained. These values are in good agreement with the values calculated with expression (II).

According to LEATHARD and PURNELL [6], at low conversions (<2%) the following simple expression can be given for the ratio of methane to hydrogen

$$\alpha = \frac{[\text{CH}_4]}{[\text{H}_2]} = \frac{1 + k_{2p}/k_{2s}}{1 + k_{1s}/k_{1p}} = \left(1 + \frac{k_{p-H}[\text{H}_2]}{2k_{1s}[\text{C}_3\text{H}_8]} \right) \quad (\text{III})$$

where k_{p-H} is the rate constant for the reaction



The α values calculated using expression (III) are given in column 7 of Table IV. As can be seen from the data and from Figs. 9 and 10, in the temperature range 475–515 °C, at low conversions (<5%), similarly as in the absorber-free experiments there is a good agreement between the experimental and calculated α values. At 535 and 545 °C and at higher conversions (>5%), a significant positive error appears, and in addition the calculated α values increase significantly with the conversion (Fig. 10).

The results discussed above indicate that with the use of an olefin-absorber the self-inhibition taking place during the thermal decomposition of propane can easily be decreased or stopped completely, and consequently the kinetics of decomposition

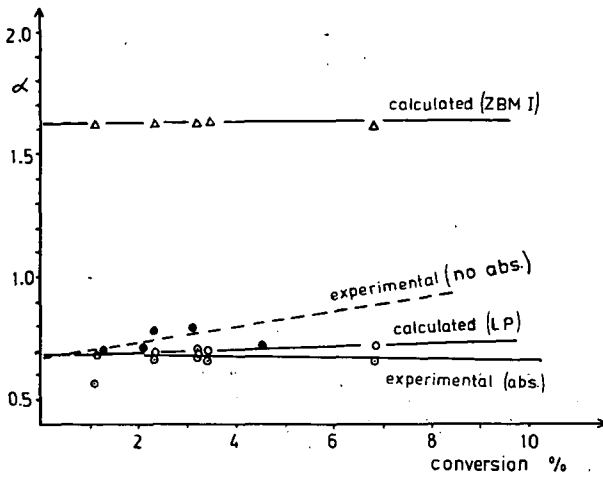


Fig. 9. Dependence of α on conversion (propane pressure, $p_0=61$ Torr, $t=515$ °C). experimental (abs.): experimental points (using olefin-absorber), calculated (LP): points calculated *via* the expression of Leathard and Purnell, experimental (no abs.): experimental points (without olefin-absorber), calculated (ZBMI): points calculated *via* the expression of Zalotai, Bérces and Márta

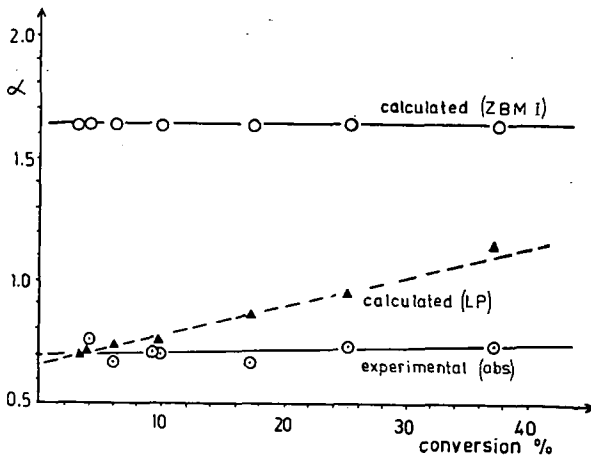


Fig. 10. Dependence of α on conversion (propane pressure, $p_0=61$ Torr, $t=535$ °C). experimental (abs.): experimental points (using olefin-absorber), calculated (LP): points calculated *via* the expression of Leathard and Purnell, calculated (ZBMI): points calculated *via* the expression of Zalotai, Bérces and Márta

will be significantly simpler. The mechanism described for the kinetics of decomposition is in accord with the experimental results. It is necessary, however, to complement this mechanism, with the bimolecular isomerization step proposed first, by LEATHARD and PURNELL.

Acknowledgements

The authors are grateful to Mrs. M. Tóth and T. P. Árnayas for technical assistance.

References

- [1] Bárdi, I., T. Bérces: *Acta Phys. et Chem. (Szeged)* **28**, 153 (1962).
- [2] Bárdi, I., T. Bérces: *Acta Phys. et Chem. (Szeged)* **28**, 161 (1982).
- [3] Leathard, D. A., J. H. Purnell: *Proc. Roy. Soc.* **A306**, 553 (1968).
- [4] Laidler, K. J., N. H. Sagert, B. W. Wojciechowski: *Proc. Roy. Soc.* **A270**, 242 (1962).
- [5] Zalotai, L., T. Bérces, F. Márta: *Magyar Kém. Folyóirat* **78**, 335 (1972).
- [6] Leathard, D. A., J. H. Purnell: *Proc. Roy. Soc.* **A305**, 517 (1968).
- [7] Allara, D. L., R. Shaw: *J. Phys. Chem. Ref. Data* **9**, 523 (1980).
- [8] Jackson, W. M., J. M. McNesby, B. de B. Darwent: *J. Chem. Phys.* **37**, 1610 (1962).
- [9] Szivovicza, L., I. Szilágyi: *Int. J. Chem. Kinetics* **12**, 113 (1980).
- [10] Kerr, J. A., M. J. Parsonage: *Evaluated Kinetic Data on Gas Phase Addition Reactions*, Butterworth, 1972.
- [11] Zalotai, L., F. Márta, T. Bérces, D. Halász: *Ox. Communications* **1**, 85 (1979).
- [12] Zalotai, L., T. Bérces, F. Márta: *Magy Kém. Folyóirat* **78**, 549 (1972).

ТЕРМИЧЕСКИЙ РАСПАД ПРОПАНА В РЕЦИРКУЛЯЦИОННОЙ СИСТЕМЕ III. ИССЛЕДОВАНИЕ В ПРИСУТСТВИИ АДСОРБЕНТА ОЛЕФИНОВ

И. Барди и Т. Берцеш

Проведен пиролиз пропана в рециркуляционной системе в присутствии адсорбента олефинов при температурах в области 450—545 °С, давлении пропана 30—470 Торр, в широком диапазоне конверсии (0,1—72%). В принятых экспериментальных условиях отношение метана к водороду (α) не изменяется с изменением конверсии, α несколько меняется с температурой. Зависимость α от концентрации пропана является функцией температуры. Предложен простой механизм реакции на основании литературных данных и полученных экспериментальных результатов. Значение величин α , рассчитанных на основании предложенного механизма, находятся в хорошем согласии с экспериментально найденными значениями.

ЭКСПРЕСС МЕТОД ДЛЯ ОПРЕДЕЛЕНИЯ СОДЕРЖАНИЯ ИЗОПРОПАНОЛА В СУСПЕНЗИЯХ КЕРОСИНО-СУЛЬФОНАТА

И. ШЕРЕЩ, М. БЕРКЕШ, и Г. АЧ

Кафедра неорганической химии университета им. Аттилы Йожефа Сегед

(Поступило в редакцию 20 октября 1982 г.)

Описана методика определения содержания изопропанола в водных керосино-сульфонатных суспензиях, применяемых при третичной добыче нефти. Анализ проводится непосредственным введением разбавленной пробы на колонку с носителем «Chromosorb 102», с использованием в качестве внутреннего стандарта этанола и (или) н-пропанола при пламенно-ионизационном детектировании. Точность метода лучше, чем $\pm 5\%$.

В процессах третичной добычи нефти в больших количествах используются водные суспензии керосино-сульфоната, в которых быстрое и точное определение содержания изопропанола является весьма важной задачей.

Для определения содержания летучих органических соединений в водных растворах обычно применяют методику, которая основана на принципе дестилляционного или экстракционного выделения определяемого соединения или его производного, с последующим количественным анализом каким-нибудь физическим методом. Обычно для определения изопропанола в водных растворах также применяют различные экстрагенты [1].

В последнее время Куо с сотрудниками [2] провели детальное изучение газо-хроматографического определения полярных водорастворимых органических соединений выделенных выпариванием с последующей абсорбцией и термической десорбцией.

Эти же авторы в другой своей работе [3] описывают дестилляционный газо-хроматографический метод определения содержания изопропанола с точностью ппб. Характерным примером для определения изопропанола в виде его производного может служить способ описанный в работе [4].

Нами разработан метод непосредственного газо-хроматографического определения содержания изопропанола в достаточно разбавленных керосино-сульфонатных суспензиях, с применением в качестве внутреннего стандарта этанола и (или) н-пропанола. Газо-хроматографический анализ проводили в стеклянной колонке длиной 1,2 м и внутренним диаметром 2 мм с носителем марки «CHROMOSORB 102», обладающим диаметром частиц в пределах 80—100 меш. Нами применялся хроматограф типа «CHROM 41» с пламенно-ионизационным детектором. Колонка термостатировалась на 120 °С, а детектор и место введения проб содержались при 150 °С. Скорости потока газов были следующими: азот — 30 см³/мин, водород — 25 см³/мин, воздух — 0,5 л/мин.

Описание проведения анализа для концентрированных суспензий (содержание изопропанола 10—20%).

В мерную колбу на 100 см³ вводят 50 см³ дистиллированной воды и затем взвешивают на аналитических весах. Примерно 1 см³ анализируемой суспензии добавляют в колбу и снова взвешивают и находят точную навеску (G). Объем смеси дополняют до 100 см³ дистиллированной водой, закрывают плотно пробкой и встряхиванием проводят гомогенизацию (раствор I).

В мерную колбу на 50 см³ с помощью пипеты вводят 5 см³ стандартного раствора, содержащего 1 г/100 мл этанола и 2 г/100 мл н-пропанола, затем объем доводят до метки раствором I. После гомогенизации смеси по 4 мл всprыскивают в приемник хроматографа (необходимо проведение трех параллельных измерений). Отсчитывают интегральные значения, соответствующие площадям, находящимся под пиками хроматограмм.

Расчет производится по формулам:

$$\% \text{ изопропанола} = \frac{I V_s C_s \cdot 100}{I_s f \frac{45}{100} G} = R \frac{A}{G}$$

$$R = \frac{I}{I_s} \quad A = \frac{V_s C_s 10^4}{f 45}$$

где I — интегральное значение соответствующее содержанию изопропанола.

I_s — интегральное значение стандарта.

V_s — объем стандартного раствора (5 см³).

C_s — концентрация стандартного раствора (г. см³).

G — навеска сульфонатной суспензии в 100 см³ (г).

f — фактор хроматографирования (в случае этанола 1,11, пропанола 0,93).

Описание проведения анализа (для суспензий с концентрацией изопропанола 0,05—0,2%).

Измерение проводят аналогично вышеописанному, только стандартный раствор дополняют до 50 см³ не раствором I, а непосредственно анализируемым раствором.

Расчет производится по формулам:

$$\% \text{ изопропанола} = R A^1 \quad A^1 = \frac{V_s C_s 100}{f 45}$$

Обозначения сохранены прежние. Точность определения лучше 5%-ов.

Замечания

При приготовлении и использовании растворов, стандартных растворов и проб, необходимо соблюдать условия наименьшего контактирования с воздухом, в связи с возможными довольно значительными потерями, в особенности при более высоких температурах этанола и даже н-пропанола.

При высоких концентрациях суспензии керосино-сульфоната, после гомогенизации, пробу необходимо отобрать по возможности быстро, чтобы избежать ошибки, возникающие вследствие неоднородности распределения.

Пробы вводились в хроматограф с помощью шприца с иглой достаточной длины для того, чтобы смесь непосредственно попала в колонку или закрывающую ее силионизированную стеклянную вату. (После многократного анализа необходимо произвести смену стеклянной ваты или носителя в колонке на глубину 1—2 см).

Обычно вводились пробы объемом в 4 мл, но можно варьировать объем проб в пределах 4—10 мл с целью получения наиболее удобных величин пиков хроматограмм. Необходимо отметить, что при низких концентрациях фактор хроматографирования в некоторой мере зависит от концентрации, поэтому не рекомендуется изменять те параметры (объем пробы, температура, скорость газа носителя, чувствительность прибора) при которых определялся фактор хроматографирования. Лучше варьировать концентрацию проб таким образом, чтобы отношение площадей под пиками изопропанола и стандарта было в пределах 0,1—10, но удобнее всего близко к 1. Расчеты были проведены относительно обоих стандартов и взяты средние значения.

В серии изменений рекомендуется приготовить относительно большое количество стандартного раствора (1 л), который необходимо сохранять на холоду. Для работы отбирали только то количество стандартного раствора, которое израсходуется за день.

При приготовлении нового стандартного раствора необходимо во избежание ошибок (например, из-за абсорбции воды растворами спиртов) произвести проверку фактора хроматографирования.

Работа была выполнена по заказу и финансированию Государственной корпорации нефти и газа.

Литература

- [1] *Snell, F. D., C. T. Snell: Colorimetric Methods of Analysis, 1961. Vol. IIIA, p. 32.*
- [2] *Kuo, P. P. K., E. S. K. Chian, F. B. DeWalle, J. K. Kim: Anal. Chem. 49, 1023 (1977).*
- [3] *Chian, E. S. K., P. P. K. Kuo, W. J. Cooper, W. F. Cowen, R. C. Fuentes: Env. Sci. Techn. 11, 282 (1977).*
- [4] *Etienne, H.: Ind. Chim. Belg. 17, 4555 (1952).*

RAPID METHOD FOR DETERMINATION OF *i*-PROPANOL IN PETROLEUM SULPHONATE SUSPENSIONS

I. Seres, M. Berkes and G. Ács

A gas chromatographic method for the determination of *i*-propanol in water-petroleum sulphate suspensions used in tertiary petroleum producing is described. After dilution with water the samples were injected directly onto the column (Chromosorb 102). Ethanol or/and propanol as internal standard(s) and a flame ionisation detector were used. The accuracy is better than $\pm 5\%$.



THE CHEMISTRY OF 1,3-BIFUNCTIONAL SYSTEMS, XXVIII* A NEW DIRECT SYNTHESIS OF 1,3-DIOXAN-2-YLIUM SALTS FROM 1,3-DIOLS

By

T. P. KOSULINA and V. G. KULNEVICH

Department of Organic Chemistry, Polytechnical Institute, Krasnodar, U. S. S. R.

and

J. APJOK, M. BARTÓK

Department of Organic Chemistry, Attila József University, Szeged

(Received 20th October, 1982)

2-Phenyl-1,3-dioxan-2-ylidium hexachloroantimonates (5—8) can be prepared in good yield from 1,3-diols (1—4) with the use of benzoyl chloride and antimony pentachloride (Scheme 1). Conclusions may be drawn with regard to the mechanism of the process.

Introduction

MEERWEIN et al. [1] were the first to prepare a 1,3-dioxan-2-ylidium cation as its tetrafluoroborate or hexachloroantimonate, well-defined crystalline compounds, by the cleavage of the ethoxy anion of a cyclic orthoester. The existence of this cation was confirmed by other authors, in studies of the Prins reaction [2,3] the solvolysis of 1,3-dioxane derivatives [4] and the reactions of 1,3-diols and acid chlorides [5]. The existence of the 1,3-dioxan-2-ylidium cation in the reaction between acetyl chloride and 1,3-butanediol could be confirmed by comparison of the rotations of the optically active starting 1,3-butanediol and the chloroacetate end-product [5].

Examples of the preparative separation of the 1,3-dioxan-2-ylidium cation are syntheses starting from the esters of 1,3-diols [6, 7] or other 1,3-diol derivatives [8—11], in the course of which the cation can be separated in the form of its hexachloroantimonate, perchlorate or tetrafluoroborate. The synthesis and properties of salts of this type have been reviewed [12].

In the literature examples of the synthesis of 1,3-dioxan-2-ylidium salts the corresponding diol derivative was prepared in every case in a separate reaction step, and the salts were then precipitated [2, 6—11].

* Part XXVII: Acta Phys. et Chem. Szeged 28, 225 (1982).

Results and discussion

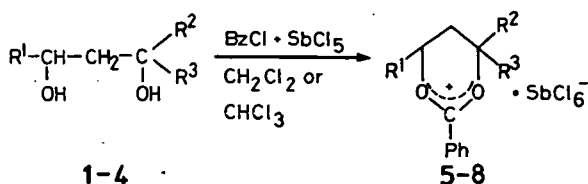
In the method we propose, a 1:2:1 mixture in chloroform or dichloromethane of antimony pentachloride, benzoyl chloride (BzCl) and 1,3-diols containing hydroxy groups of different orders (1—4) is allowed to stand or is boiled, when 2-phenyl-1,3-dioxan-2-ylum hexachloroantimonates (5—8) can be separated in crystalline form in one step after cooling of the mixture and its treatment with ether (Scheme 1).

1,5 $R^1, R^2, R^3=H$

2,6 $R^1, R^2=H, R^3=Me$

3,7 $R^1=H, R^2, R^3=Me$

4,8 $R^1, R^2, R^3=Me$



Scheme 1

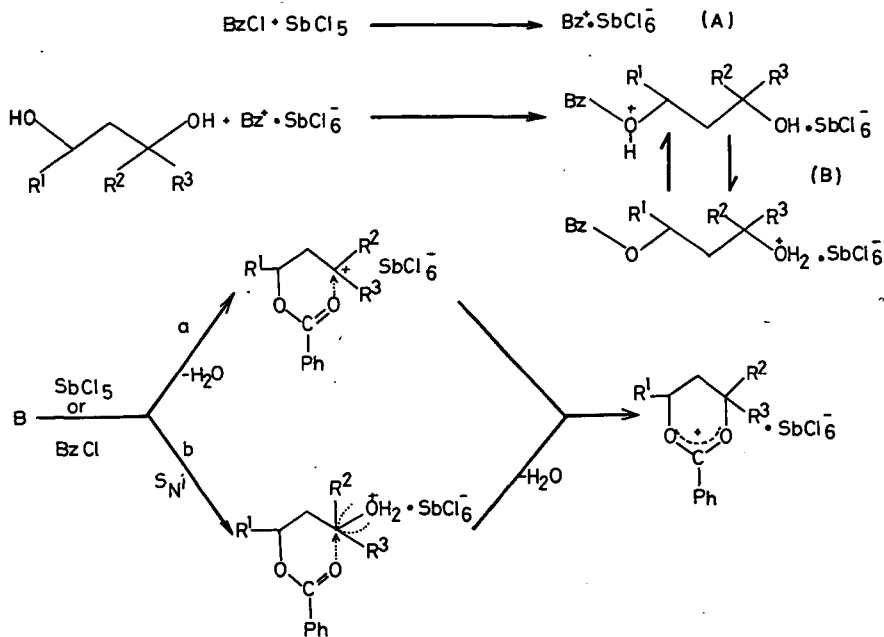
The yields of the 1,3-dioxan-2-ylum salts (5—8) and the reaction rates are influenced appreciably by the reaction conditions, *e.g.* the ratio of the components, the structure of the diol, and the temperature and duration of the reaction. In syntheses starting from 1,3-diols, a two-fold quantity of benzoyl chloride in all cases resulted in an increased yield of the salt. A few characteristic experimental results are to be seen in the following Table:

The yields of the salts (5—8) increase with increase of the order of the carbon atom bearing one of the hydroxy groups in the 1,3-diols (1—4). A higher temperature results in higher yields of the salts (5, 6), even with a shorter reaction time. In the syntheses starting from the corresponding primary monobenzoates as intermediates, the yields of the salts (5, 6) are comparable to those with the 1,3-diols (1, 2) as starting materials.

Table I

Methods	Ratio of reagents	Yield of 2-phenyl-1,3-dioxan-2-ylum salt, % (reaction time)			
		5	6	7	8
1	1,3-diol: BzCl: SbCl ₅ 1:2:1	12 (40 h)	70 (40 h)	80 (15 min)	95 (15 min)
2	1,3-diol: BzCl: SbCl ₅ 1:2:1	30 (1 h)	72 (3 min)	—	—
3	1,3-diol-monobenzoate: BzCl: SbCl ₅ 1:1:1	10 (1 h)	79 (3 min)	—	—

On the basis of the experimental data, the formation of the 2-phenyl-1,3-dioxan-2-ylum hexachloroantimonates (5—8) can be interpreted by the reaction sequence given in Scheme 2.

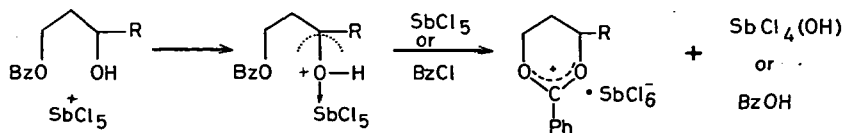


Scheme 2

The reaction begins with the interaction of the 1,3-diol and the acylating agent (A), when the faster acylation of the primary hydroxy group is to be expected [2,13]. In acylation with BzCl this is all the more characteristic [14], and the migrational ability of the Bz group is lower too [15]. The salt formation takes place with water elimination via the protonated forms of the monobenzoates (B); depending on the order of the second hydroxy group of the 1,3-diol, this can be interpreted as proceeding via a carbonium ion (route "a") in the case of 2, 3 and 4, or by a slower cyclization with an $S_{\text{N}}\text{i}$ mechanism in the case of the primary hydroxy group (1) (route "b"). This reaction pathway is supported by the experiments with 1,3-diol monobenzoates (Table I, line 3).

Thus, the larger yields and rates of formation of the salts (6—8) originating from the higher 1,3-diols (2, 4) also containing a hydroxy group can be brought into correlation with the favoured water elimination preceding the ring closure (Scheme 2, route "a").

The 1,3-dioxan-2-ylum salts (6) can be obtained in a yield of 50% from 1-benzoyloxybutanol-3 in the presence of an equimolar quantity of antimony pentachloride. On this basis a general scheme can be proposed to interpret the synthesis shown in row 3 of Table I (Scheme 3).



Scheme 3

The formation of the 2-phenyl-1,3-dioxan-2-ylum hexachloroantimonates from the corresponding 1,3-diols can be explained by the water-elimination ring-closure reaction of the intermediate monobenzoates.

Experimental

General observations. The 1,3-diols **1**, **2** and **4** were products of Fluka. **3** was prepared according to [16], and 1-benzoyloxy-propanol-3 and 1-benzoyl-oxybutanol-3 according to [17]; they were identified by chromatographic, analytical and spectroscopic methods.

The 2-phenyl-1,3-dioxan-2-ylum salts were recrystallized from CH_2Cl_2 . Melting points (m.p.) of salts are not corrected. ^1H NMR spectra ($\text{CD}_6\text{N}_5\text{O}_2$ if not otherwise stated): JEOL C—60 HL NMR spectrometer. Chemical shifts are given in ppm; abbreviations: s singlet, d doublet, dd doublet of doublets, t triplet, m multiplet; J spin-spin coupling constant in MHz. IR spectra (KBr): Unicam SP 200 IR spectrometer; ν_{max} in cm^{-1} .

Synthesis methods

1. 2.30 ml (0.02 mol) benzoyl chloride and 0.01 mol of the appropriate 1,3-diol (**1**, **2**, **3**, **4**) are added at 0°C to a solution of 1.28 ml (0.01 mol) antimony pentachloride in 5 ml chloroform, and the mixture is left to stand at room temperature. After 40 h in the case of **1** and **2**, or after 15 min in the case of **3**, and **4**, 30 ml ether is added to the mixture, and the resulting crystals are filtered off, and washed with a cold 1:2 mixture of ethyl acetate and ether, and then with ether. Yields calculated for the starting diol: **5**: 0.59 g (12%); **6**: 3.58 g (70%); **7**: 4.2 g (80%); **8**: 5.12 g (95%).

2. A solution of 0.01 mol of the appropriate 1,3-diol (**1**, **2**), in 5 ml chloroform is added to a mixture of 1.28 ml (0.01 mol) antimony pentachloride and 2.30 ml (0.02 mol) benzoyl chloride. The mixture is boiled for 60 min or for 3—5 min in the case of **1** and **2**, respectively. After cooling, 30 ml ether is added, the salt separating out is filtered off, and it is washed with cold ethyl acetate, and then with ether. Yields: **5**: 1.49 g (30%); **6**: 3.68 g (72%).

3. A solution of 1.94 g (0.01 mol) 1-benzoyloxybutanol-3, 1.28 ml (0.01 mol) antimony pentachloride and 1.15 ml (0.01 mol) benzoyl chloride in 10 ml chloroform is boiled for 3 min, then cooled and diluted with 30 ml ether. The work-up is the same as in 2. Yield: **6**: 4 g (79%) (2.55 g (50%) if the reaction is carried out without benzoyl chloride). In an analogous way, **5** can be obtained from 1-benzoyloxypropanol-3 if the reaction mixture is boiled for 60 min. Yield: **5**: 0.5 g (10%).

- 5: m.p.: 180°; ¹H NMR: 3.05 (m): 5 CH₂; 5.6 (m): 4 and 6 CH₂; 7.66—8.46 (m): aromatic protons; IR (cm⁻¹): 1600, 1590, 1550, 1510, 1450, 1440, 1380, 1290; C₁₀H₁₁O₂ SbCl₆ (497.66), Calc.: C 24.13 H 2.23, Found: C 23.70 H 2.28.
- 6: m.p.: 140°, ¹H NMR: 1.9 (d): 4 CH₃; 2.83 (m): 5 CH₂; 5.83 (m): 6 CH₂; 5.92 (m): 4 CH; 7.5—8.2 (m): aromatic protons; IR (cm⁻¹): 1600, 1590, 1540, 1510, 1470, 1450, 1390, 1350, 1280; C₁₁H₁₃O₂ SbCl₆ (511.70), Calc.: C 25.82 H 2.56, Found: C 25.75 H 2.59.
- 7: m.p.: 108°; ¹H NMR: 2.00 (s): 4 (CH₃)₂; 2.96 (t): 5 CH₂; 5.4(t): 6 CH₂; 7.5—8.3 (m): aromatic protons; IR (cm⁻¹): 1600, 1540, 1510, 1470, 1440, 1430, 1340, C₁₂H₁₅O₂ SbCl₆ (525.70), Calc.: C 27.40 H 2.87, Found: C 26.45 H 3.09.
- 8: m.p.: 111°; ¹H NMR (CD₂Cl₂): 1.9 (s): 4 (CH₃)₂; 1.83 (d): 6 CH₃; 2.75 (dd): 5 CH₂; 5.8 (m): 5 CH₂; 7.7—8.4(m): aromatic protons; IR (cm⁻¹): 1600, 1540, 1510, 1450, 1430, 1400, 1300; C₁₃H₁₇O₂ SbCl₆ (539.70), Calc.: C 28.93 H 3.14, Found: C 28.54 H 3.23.

The authors express their thanks to their colleagues in the Department of Organic Chemistry in Szeged: to Dr. Gizella Bozóki-Bartók for the elemental analyses, to Dr. György Dombi for recording the ¹H NMR spectra, and to Dr. János Kiss for the infrared spectra.

References

- [1] Meerwein, H., K. Bodenbenner, P. Borner, F. Kunert and K. Wunderlich: Liebigs Ann. **632**, 38 (1960).
- [2] Dolby, L. J., C. N. Lieske, D. R. Rosencrantz and M. J. Schwarz: J. Am. Chem. Soc. **85**, 47 (1963).
- [3] Dolby, L. J. and M. J. Schwarz: J. Org. Chem. **30**, 3581 (1965).
- [4] Kovács, Ö. K. J., Gy. Schneider and L. K. Láng, Proc. Chem. Soc.: 374 (1963).
- [5] Notheisz, F., M. Bartók and V. Rempert: Acta Phys. et Chem. Szeged **18**, 197 (1972).
- [6] Coppen, M. J., M. P. Hartshorn and D. N. Kirk: J. Chem. Soc. (C) 576 (1966).
- [7] Paulsen, H. and H. Behre: Chem. Ber. **104**, 1264 (1971).
- [8] Kovács, Ö. K. J., Gy. Schneider, L. K. Láng and J. Apjok: Tetrahedron **23**, 4181 (1967).
- [9] Zelikman, Z. I., T. P. Kosulina, V. G. Kulnevich, G. N. Dorofeyenko and Z. V. Mezheritskaya: Khim. Geterotsikl. Soed.: 169 (1976).
- [10] Samitov, Yu. Yu., Z. I. Zelikman, T. P. Kosulina and V. G. Kulnevich: Khim. Geterotsikl. Soed. **182** (1977).
- [11] Kosulina, T. P., Z. I. Zelikman and V. G. Kulnevich: Tezisi dokladov na vsesoyuznoi konferentsii po khim. karbkationa **69** (1979).
- [12] Pittman, C. V., S. P. McManus and J. W. Larsen: Chem. Ber. **72**, 352 (1972).
- [13] Nerdel, F., and T. H. Remmets: Z. Electrochem. **60**, 377 (1956).
- [14] Notheisz, F., M. Bartók and V. Rempert: Acta Phys. et Chem. Szeged **18**, 89 (1972).
- [15] Pavlova, L. V. and F. J. Rachinskii: Uspekhi Khimii **37**, 1369 (1968).
- [16] Farberov, M. I. and N. K. Shemjakina: Zh. Obschch. Khim. **26**, 2752 (1956).
- [17] McElvain, S. M. and T. P. Carney: J. Am. Chem. Soc. **68**, 2592 (1946).

ХИМИЯ 1,3-БИФУНКЦИОНАЛЬНЫХ СИСТЕМ, XXVIII. НОВЫЙ НЕПОСРЕДСТВЕННЫЙ СИНТЕЗ 1,3-ДИОКСАН-2-ИЛИЕВЫХ СОЛЕЙ ИЗ 1,3-ДИОЛОВ

Т. П. Косулина, В. Г. Кульневич, Й. Апйок и М. Барток

Гексахлоро свинцовые соли 2-фенил-1,3-диоксан-2-илия (5—8) могут быть приготовлены с хорошим выходом из 1,3-диолов (1—4) при использовании бензоилхлорида и пятихлористого свинца (схема I). Сделаны заключения относительно механизма происходящих процессов.



РЕАКЦИОННАЯ СПОСОБНОСТЬ ПОЛИМЕТИЛ-1,3-ДИОКСАЦИКЛАНОВ В РЕАКЦИИ С ОЗОНОМ

Э. М. КУРАМШИН, Л. Г. КУЛАК, С. С. ЗЛОТСКИЙ, Д. Л. РАХМАНКУЛОВ
Уфимский нефтяной институт, г. Уфа

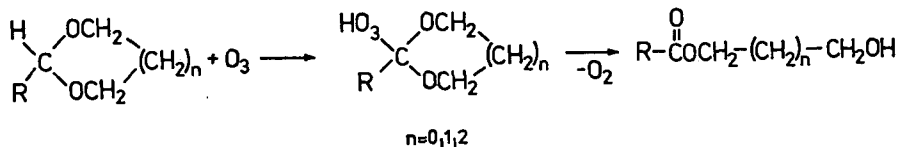
Й. ЦОМБОШ, М. БАРТОК

Кафедра органической химии университета им. Аттилы Йожефа, Сегед

(Поступило в редакцию 6 декабря 1982 г.)

При изучении кинетики реакции пяти- и шестизвенных формалей, ацеталей и кеталей с озоном установлено, что заместители при C^4 , C^5 , C^6 — атомах цикла практически невли-
яют на активность формалей, увеличивают реакционную способность ацеталей на ~ 30 — 70% ,
а кеталей — в 6 — 10 раз. Во всех случаях максимальный эффект наблюдается для 1,3-диокса-
санов. Найдено, что в пятизвенных кеталах активность третичной связи $C-H$ находящийся
в α -положении к атому кислорода более чем на порядок ниже таковой для $C-H$, смежной
с двумя гетероатомами.

Известно, что циклические ацетали под действием озона превращаются
в соответствующие моноэфиры гликолей с количественным выходом [1, 2].
Предполагается, что озонлиз ацеталей протекает по механизму 1,3-диполяр-
ного внедрения молекулы озона по ацетальной $C-H$ связи с образованием
лабильного гидротриоксида [1, 3, 4], последующий распад которого приводит
к образованию продуктов реакции [5]:



Ранее нами подробно изучено влияние природы заместителей при C^2 -
атоме цикла на реакционную способность ацеталей [6]. Найдено, что электро-
нодонорные группы увеличивают скорость реакции [4, 7], а электроноакцеп-
торные группы приводят к ее снижению [1, 4]. Продолжая эти исследования
мы изучили влияние заместителей при C^4 , C^5 , C^6 — атомах цикла на реакцион-
ную способность 1,3-диоксацикланов.

Экспериментальная часть

Синтез изученных соединений (I—XV) осуществляли по известной методике [8], взаимодействием параформальдегида (либо ацетальдегида, ацетона) с этилен-, пропиленгликолем и их производными. Физико-химические константы синтезированных соединений (I—XV) соответствовали литературным значениям [9].

Кинетику озонолиза 1,3-диоксацикланов изучали в статических условиях спектрофотометрически по расходу озона в растворе CCl_4 при 18° . Опыты проводили в кварцевой термостатируемой ячейке, помещенной в кюветную камеру спектрофотометра «Вебсман—5260». Содержание ацетала в исходной реакционной смеси $[\text{АН}]_0$ изменяли от $0,2 \cdot 10^{-3}$ до $0,1$ моль/л, начальную концентрацию озона $[\text{O}_3]_0$ от $0,4 \cdot 10^{-4}$ до $16,6 \cdot 10^{-4}$ моль/л. Растворы: (O_3 — CCl_4) и (ацеталь— CCl_4) готовили отдельно. После термостатирования эти растворы смешивали в ячейке и следили за расходом озона при $\lambda = 270$ — 280 нм. Регистрация изменения оптической плотности во времени осуществлялась автоматически.

Было установлено, что кинетические кривые для всех исследованных соединений (I—XV) имеют одинаковый вид и спрямляются в координатах: $\ln([\text{O}_3]_0/[\text{O}_3])$ — время (Рис. 1). В этих условиях озон расходуется псевдомономолекулярно с константой скорости $k' = V_{\text{O}_3}/[\text{O}_3]_0$. С увеличением концентрации ацетала в растворе константа скорости k' линейно возрастает (Рис. 2). Следовательно, начальная скорость расходуования озона V_{O_3} подчиняется уравнению второго порядка:

$$V_{\text{O}_3} = k [\text{АН}][\text{O}_3]$$

Константы скорости реакции озона с 1,3-диоксацикланами (I—XV) приведены в таблице I.

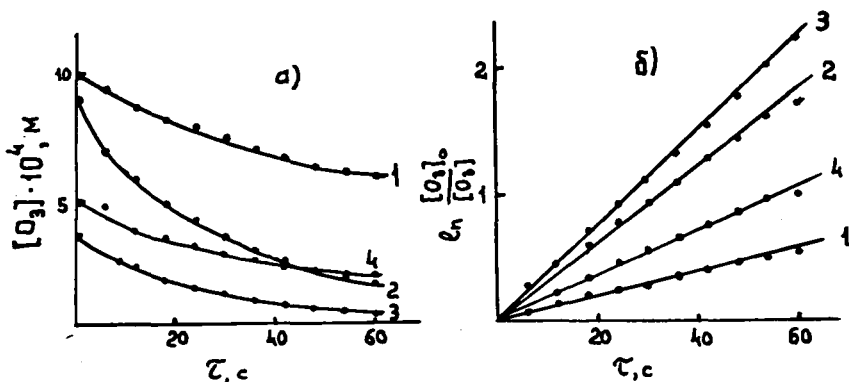


Рис. 1. Типичные кривые расходования озона в реакции с ацеталами (а) и их полулогарифмические анаморфозы (б), 18°C , CCl_4 :
 1 — 2,2,4-триметил-1,3-диоксолан ($1,0 \cdot 10^{-2}$ моль/л);
 2 — 4,4,5,5-тетраметил-1,3-диоксолан ($2,5 \cdot 10^{-3}$ моль/л);
 3 — 2,4,4,5,5-пентаметил-1,3-диоксолан ($1,0 \cdot 10^{-3}$ моль/л);
 4 — 2,4,4-триметил-1,3-диоксолан ($5,0 \cdot 10^{-4}$ моль/л).

Результаты и обсуждение

Различия в активности циклических ацеталей по отношению к озону (Табл. I) связаны с размером кольца. Пятизвенные формали (I, II), и ацетали (III—X) в 6—10 раз активнее шестизвенных аналогов (IX, X) и (XI—XIII). Наблюдаемое может быть объяснено большей напряженностью пятизвенного кольца [10]. Заместители при атомах C⁴ и C⁵ 1,3-диоксацикланового цикла не оказывают заметного влияния на константу скорости озонирования формалей (II, X). Это объясняется тем, что эти группы вследствие удаленности от реакционного центра не определяют прочности связей C²—H [11]. Производные уксусного альдегида III, V и XI, XIII в реакции с озоном значительно активнее соответствующих формалей (I, II) и (IX, X) ($k_{II}/k_I \approx 2,6$, $k_V/k_{II} \approx 3,5$; $k_{XI}/k_{IX} = 4,3$, $k_{XIII}/k_X \approx 6$), наблюдаемый эффект максимален для 1,3-диоксанов. В работах [1, 12] было показано, что при озоноллизе 1,3-диоксацикланов в переходном состоянии на ацетальном углероде возникает дефицит электронной плотности, причем стабилизация промежуточной катионоидной частицы осуществляется как неподеленными электронными парами атомов кислорода, так и алкильными заместителями, причем стабилизирующее действие алкильного заместителя максимально в случае 1,3-диоксанов. Следовательно, увеличение реакционной способности при замещении атома водорода у ацетального углерода на метильную группу связано с увеличением стабилизации промежуточной частицы.

В ряду 2-метил-1,3-диоксоланов (III—V) появление метильных заместителей при атомах C⁴ и C⁵ цикла приводит к увеличению активности молекул на 20—30%. При введении заместителей в четвертое и пятое положение цикла в 2-метил-1,3-диоксанах (XI—XIII) увеличение реакционной способности достигает ~70%. Наблюдаемое может быть объяснено конформационными особенностями рассматриваемых молекул. В работе [1] показано, что реакция озона с ацетальями имеет место только при антиперипланарном расположении атакуемой C—H связи к неподеленным парам электронов α -атомов кислорода цикла. Введение заместителей в 2-метил-1,3-диоксан приводит к закреплению конформации кресла [13] таким образом, что атакуемая C—H связь находится в благоприятной для реакции конформации [1]. Пятичленный цикл не имеет столь ярко выраженного конформационного минимума [14], поэтому введение алкильных заместителей лишь увеличивает время пребывания молекулы в благоприятной конформации.

Полное замещение атомов водорода в молекуле 1,3-диоксолана на

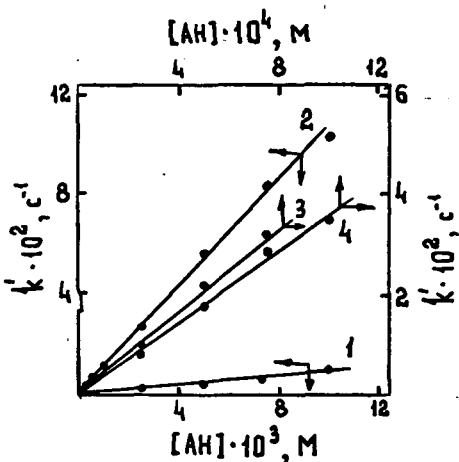


Рис. 2. Зависимость псевдомолекулярной константы скорости от начальной концентрации ацетала (CCl₄, 18 °C):
 1 — 2,2,4-триметил-1,3-диоксолан;
 2 — 4,4,5,5-тетраметил-1,3-диоксолан;
 3 — 2,4,4,5,5-пентаметил-1,3-диоксолан;
 4 — 2,4,4-триметил-1,3-диоксолан.

Таблица I

Константы скорости реакции озона с циклическими формальми (I—II, IX—X), ацетальми (III—V, XI—XIII), кетальми (VI—VIII, XIV—XV), (k) при 18 °C


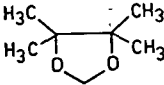
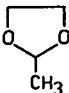
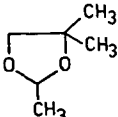
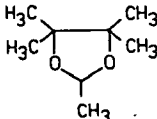
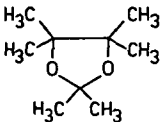
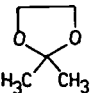
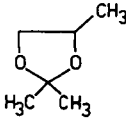
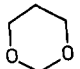
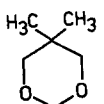
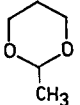
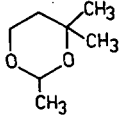
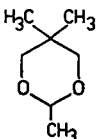
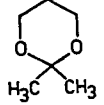
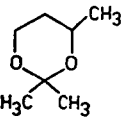
1,3-диоксациклан (ДН)	[O ₃] ₀ · 10 ⁴	[ДН] · 10 ³	k' · 10 ² , с ⁻¹	k л/моль · с
	моль/л			
1	2	3	4	5
I 	16,6	10,0	9,6	11,5
	7,1	10,0	13,0	
	7,8	7,5	12,2	
	9,1	5,0	5,0	
	5,5	2,5	3,2	
	0,9	1,0	2,0	
II 	2,7	10,0	8,8	11,7
	7,2	10,0	10,3	
	7,6	7,5	8,3	
	6,4	5,0	5,7	
	9,1	2,5	2,9	
	4,7	2,5	2,6	
	3,8	1,0	1,1	
	3,5	0,5	0,7	
	4,2	0,2	0,4	
	3,4	0,2	0,4	
III 	3,6	1,0	3,1	30,0
	4,7	0,7	2,5	
	3,3	0,5	1,4	
	3,1	0,2	0,7	
IV 	6,1	1,0	3,5	36,5
	5,6	0,8	2,9	
	5,0	0,5	1,8	
	5,0	0,2	0,8	
V 	3,7	1,0	3,7	41,0
	3,1	0,7	3,2	
	2,2	0,5	2,2	
	1,6	0,2	1,0	
	3,1	0,2	0,9	
VI 	6,2	100,0	0,1	0,01
	7,5	100,0	0,15	
	6,4	75,0	0,09	
	5,0	50,0	0,07	
	7,0	25,0	0,01	
VII 	6,4	10,0	0,13	0,13
	4,0	7,5	0,1	
	1,4	5,0	0,07	
	1,6	2,5	0,03	

Таблица 1 продолжение цлгем

1,3-диоксациклав (ДН)	[O ₃] ₀ · 10 ⁴	[ДН] · 10 ³	k' · 10 ² , с ⁻¹	k л/моль · с
	моль/л			
	2	3		
VIII 	9,9 6,2 10,6 10,8 4,9 6,0	10,0 10,0 7,5 5,0 2,5 2,5	0,9 0,6 0,5 0,4 0,2 0,2	0,8
IX 	10,0 10,0 10,0 4,6 10,0 10,0	16,0 12,0 10,0 10,0 8,0 4,0	1,5 1,0 0,9 0,9 0,7 0,4	0,9
X 	10,0 10,0 10,0 4,8 10,0 10,0	18,0 14,0 10,0 10,0 8,0 4,0	2,1 1,6 1,1 1,1 0,9 0,5	1,1
XI 	10,0 10,0 10,0 5,2 10,0 10,0	10,0 7,0 5,0 5,0 3,0 1,0	3,9 2,7 1,9 1,9 1,2 0,4	3,9
XII 	10,0 10,0 10,0 5,2 10,0 10,0	10,0 7,0 5,0 5,0 3,0 1,0	4,8 3,4 2,4 2,4 1,4 0,5	4,8
XIII 	10,0 10,0 10,0 4,8 10,0 10,0	10,0 6,0 4,0 4,0 2,0 1,0	6,6 3,9 2,7 2,6 1,3 0,7	6,6
XIV 	12,6 9,4 9,3 10,4	100,0 75,0 50,0 25,0	2,1 1,6 1,1 0,6	0,2
XV 	3,0 3,1 2,7 2,9 2,6	10,4 7,8 5,2 2,6 0,8	2,1 1,8 1,4 0,8 0,2	2,5

СН₃-группы (VI) приводит к резкому (на ~3 порядка) снижению реакционной способности 1,3-диоксациклана ($k_{VI}/k_I=10^{-3}$) и константа скорости озонирования становится близка к таковой для алифатических углеводородов (для циклогексана, при 22°, $K = 1 \cdot 10^{-2}$ л/моль · с [15]. Это связано с отсутствием в соединении VII С—Н связей, активированных атомами кислорода в α-положении.

Реакционная способность циклических кеталей (VII, VIII) и (XIV, XV) значительно уступает таковой для формалей (I, IX) и ацеталей (III, XI) и приближается к спиртам (С₂Н₅ОН, $k = 0,35$, 25 °С [16]). Отношения констант скорости озонирования кеталей и формалей диоксолановой и диоксановой структуры соответственно составляют: $k_{VII}/k_I=0,01$, $k_{XIV}/k_{IX}=0,30$, а кеталей и ацеталей — $k_{VII}/k_{III}=0,004$, $k_{XIV}/k_{XI}=0,06$ (без учета числа активных атомов водорода в молекуле). Из этого следует, что в кеталах озон преимущественно атакует углеродводородные связи, смежные с одним атомом кислорода. Поскольку прочность этих связей значительно превосходит прочность связи С²—Н, это является причиной понижения реакционной способности кеталей.

Введение метильного заместителя в четвертое положение цикла значительно повышает активность кеталей (VIII, XV) по сравнению с незамещенными аналогами (VII, XVI) ($k_{VIII}/k_{VII}=6$, $k_{XV}/k_{XIV}=10$). Однако по сравнению с 2-метил-1,3-диоксоланом (III) подобная кеталь (VIII) значительно менее активна ($k_{VIII}/k_{III}=0,026$), следовательно в пятизвенных кеталах реакционная способность третичной связи С—Н, находящейся в α-положении к атому кислорода, в ~40 раз ниже таковой для С—Н смежной с двумя атомами кислорода.

В то время как при переходе от шестизвенного ацетала (XI) к кеталу XV понижение реакционной способности крайне незначительно ($k_{XV}/k_{XI}=0,64$). Наблюдаемый эффект является неожиданным, поскольку ацетальная С—Н связь, как правило, на порядок и более активнее любой связи в 1,3-диоксациклане.

Литература

- [1] *Delongchamps, P., P. Atlani, D. Frehel, A. Malaval, C. Moreau*: Can. J. Chem. **52**, 3651 (1974).
- [2] *Брудник, Б. М., С. С. Злотский, У. Б. Имашев, Д. Л. Рахманкулов*: ЖПХ, **51**, 2125 (1978).
- [3] *Брудник, Б. М., Спирихин Л. В., Э. М. Курамшин, У. Б. Имашев, С. С. Злотский, Д. Л. Рахманкулов*: Ж. Орг. Хим. **16**, 1281 (1980).
- [4] *Taillefer, R. J., S. E. Tomas, J. Ladeau, S. Fliszar, H. Henry*: Can. J. Chem. **58**, 1138 (1980).
- [5] *Kovac, F., V. Plesnicar*: Comm. 122 (1978), J. Am. Chem. Soc. **101**, 2677 (1979).
- [6] *Брудник Б. М.*: Канд. дисс., Уфа, 1980.
- [7] *Брудник, Б. М., Э. М. Курамшин, У. Б. Имашев, С. С. Злотский, Д. Л. Рахманкулов*: Ж. Орг. Хим. **17**, 700 (1981).
- [8] *Альок, Й., М. Барток, Р. А. Караханов, Н. И. Шуйкин*: Изв. АН СССР, Сер. хим. **1968**, 2357.
- [9] *Рахманкулов Д. Л., А. М. Сыркин, Е. А. Кантор, С. С. Злотский*: Физико-химические константы кислородсодержащих гетероциклических соединений, Уфа, 1974.
- [10] *Рюхардт, Х.*: Успехи химии **47**, 2014 (1978).
- [11] *Рахманкулов, Д. Л., Р. А. Караханов, С. С. Злотский, Е. А. Кантор, У. Б. Имашев, А. М. Сыркин*: Итоги науки и техники. Технология органических веществ. Т.5. Химия и технология 1,3-диоксациклоалканов, Москва, 1979.
- [12] *Брудник, Б. М., С. С. Злотский, У. Б. Имашев, Д. Л. Рахманкулов*: Докл. АН СССР **241**, 129 (1978).

- [13] *Eliel, E. L.*: *Angew. Chem.* **84**, 779 (1972).
[14] *Willy, W. E., G. Binsth, E. L. Eliel*: *J. Am. Chem. Soc.* **92**, 5394 (1970).
[15] *Галимова Л. Г., В. Д. Комиссаров, Е. Т. Денисов*: *Изв. АН СССР, Сер. хим.* **1973**, 307.
[16] *Герчиков А. Я., В. Д. Комиссаров, Е. Т. Денисов, Г. Б. Кочемасова*: *Кинетика и катализ.* **13**, 1126 (1972).

REACTIVITY OF POLYMETHYL-1,3-DIOXACYCLOALKANES TOWARDS OZONE

E. M. Kuramshin, L. G. Kulak, S. S. Zlotskii, D. L. Rakhmankulov, J. Czombos and M. Bartók

In the reactions of five- and six-membered formals, acetals and ketals with ozone it was found that the substitution of the C(4), C(5) and C(6) atoms had practically no influence on the activity of the formals, whereas the reactivity of the acetals was increased by 30—70%, and that of the ketals by a factor of 6—10. In every case the maximum effect was obtained for the 1,3-dioxanes. It was found that in the case of the five-membered ketals, the activity of the *tert*-C—H bond in the α position to the O atom was more than one order lower than that of the C—H bond between the two hetero-atoms.



ИССЛЕДОВАНИЕ КОМПЛЕКСООБРАЗОВАНИЯ 1,3-ДИТЕТЕРОАНАЛОГОВ ЦИКЛОАЛКАНОВ МЕТОДОМ ПМР-СПЕКТРОСКОПИИ

Ф. Н. ЛАТЫПОВА, В. В. ЗОРИН, П. А. КРАСУЦКИЙ

Нефтяной институт, Уфа

Н. А. КАРАХАНОВА

Кафедра химии нефти и органического катализа университета им. М. В. Ломоносова, Москва

Й. АПЬОК, М. БАРТОК

Кафедра органической химии университета им. Агиллы Йожефа, Сегед

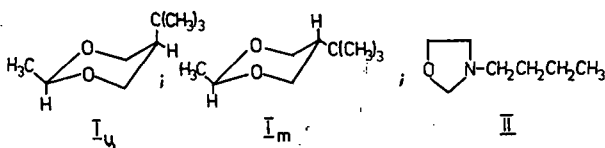
(Поступило в редакцию 6 декабря 1982 г.)

Изучено комплексообразование $\text{Eu}(\text{ДПМ})_3$ с 1,3-дигетероциклоалканами и определена связь строения с характером комплексообразования.

Комплексообразование 1,3-дигетероаналогов циклоалканов ранее изучалось методами ИК-спектроскопии [1, 2], что позволило установить строение Н-комплексов простейших циклических ацеталей. Однако однозначная информация о характере комплексообразования стереоизомерных 1,3-диоксациклов и 1,3-оксазолидинов получена не была.

В настоящей работе нами исследовалось комплексообразование индивидуальных цис- и транс-изомеров 2-метил-5-трет-бутил-1,3-диоксанов (I_ц и I_т) и 3-бутил-1,3-оксазолидина (II) методом ПМР-спектроскопии с использованием в качестве электрофильного реагента $\text{Eu}(\text{ДПМ})_3$ [3].

Соединения I_ц и I_т были получены и разделены методами, описанными в работе [4], и положения металльной и трет-бутильной групп было установлено по спектрам ПМР в соответствии с анализом, данным в работе [5].



Вещество II было получено конденсацией N-бутил-β-оксиэтил-амина с параформом [6].

Из ПМР-спектров ацеталей I_ц и I_т, зарегистрированных в CCl_4 в присутствии $\text{Eu}(\text{ДПМ})_3$, следует, что с увеличением концентрации последнего имеет место смещение всех сигналов протонов в слабое поле (Рис. 1, 2) и на-

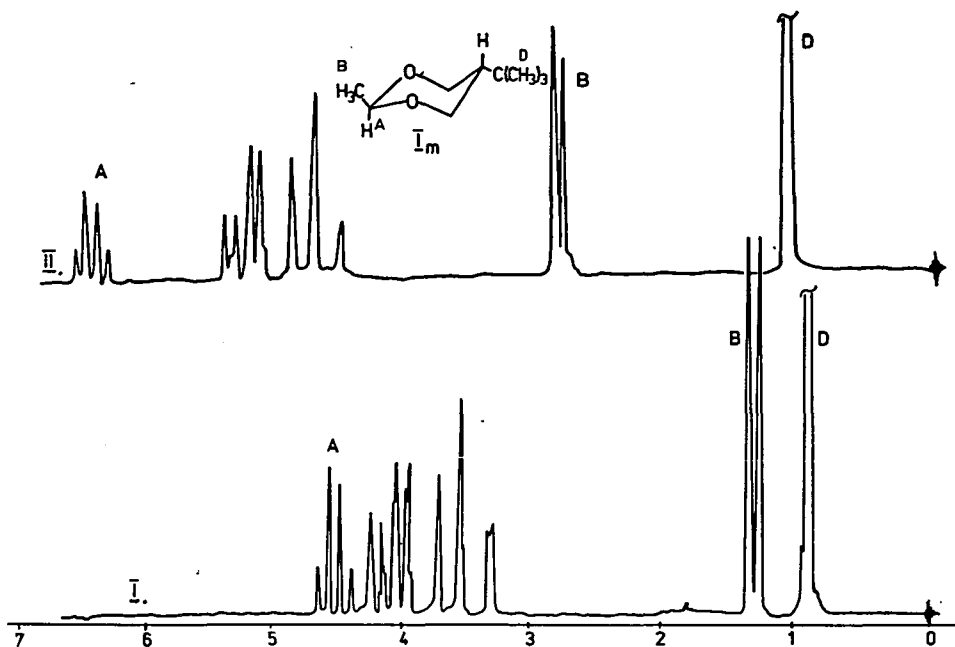


Рис. 1. I. ПМР-спектр транс-2-метил-5-т. бутилдиоксана-1,3 (CCl_4)
 II. ПМР-спектр транс-2-метил-5-т. бутилдиоксана-1,3 в присутствии $\text{Eu}(\text{ДПМ})_3$.

$$\text{Соотношение } \frac{[\text{Eu}(\text{ДПМ})_3]}{[\text{субстрат}]} = 0,15$$

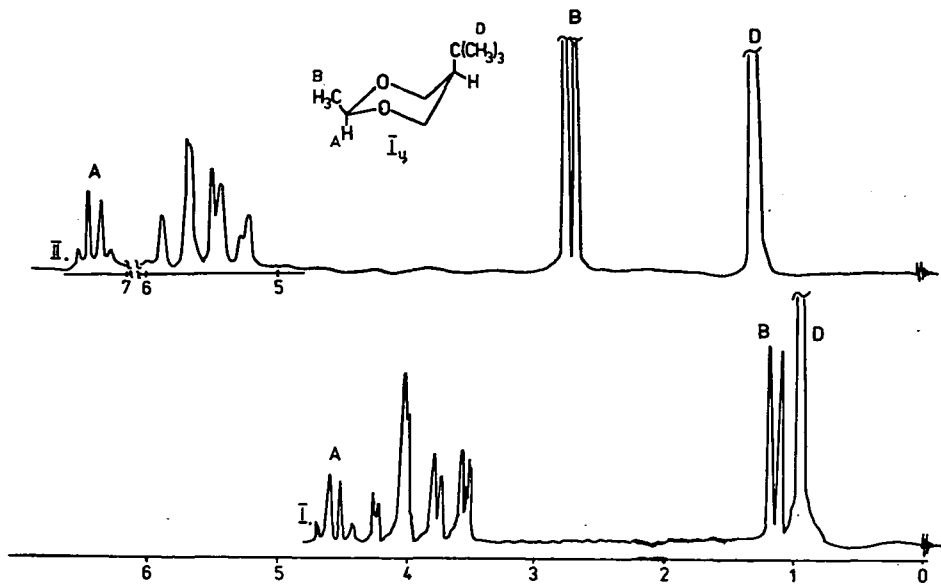
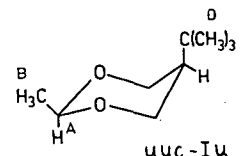
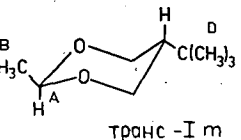


Рис. 2. I. ПМР-спектр цис-2-метил-5-т. бутилдиоксана-1,3 (CCl_4)
 II. ПМР-спектр цис-2-метил-5-т. бутилдиоксана-1,3 в присутствии $\text{Eu}(\text{ДПМ})_3$.

$$\text{Соотношения } \frac{[\text{Eu}(\text{ДПМ})_3]}{[\text{субстрат}]} = 0,15$$

Таблица I

Соединения	ЛИС, δ , м. д.		
	$2H_A$	$3H_B$	ϕH_D
 <p>цис - I_ц</p>	23,3	13,4	3,0
 <p>транс - I_т</p>	11,3	10,7	1,3

блюдается линейная зависимость химического сдвига (δ , м. д.) от соотношения $\frac{[Eu(DPM)_3]}{[субстрат]}$ (рис. 3). Из величин лантаноидных индуцированных сдвигов

(ЛИС), полученных экстраполяцией линейных участков зависимостей $\delta = f\left(\frac{[Eu(DPM)_3]}{[субстрат]}\right)$ до соотношения $\frac{[Eu(DPM)_3]}{[субстрат]} = 1$ видно, что протоны

цисизомера (I_ц) испытывают больший ЛИС, чем аналогичные группы в изомере I_т. Для метиновых групп (A_ц и A_т) и метильных групп (B_ц и B_т) ЛИС максимален (табл. I), тогда как для протонов трет-бутильного фрагмента (D_ц и D_т) ЛИС значительно меньше.

Разница в ЛИС для протонов A и D в изомерах I_ц и I_т весьма значительна, тогда как ЛИС для групп B_ц и B_т практически одинаковы. Эти результаты свидетельствуют о том, что при координации Eu(DPM)₃ с атомами кислорода, трет-бутильная группа в C⁵-аксиальном положении соединения I_ц находится значительно ближе к электрофильному центру, чем экваториальная трет-бутильная группа в изомере I_т. Существенное увеличение величины ЛИС группы A_ц от A_т, по видимому, связано с уплощением фраг-

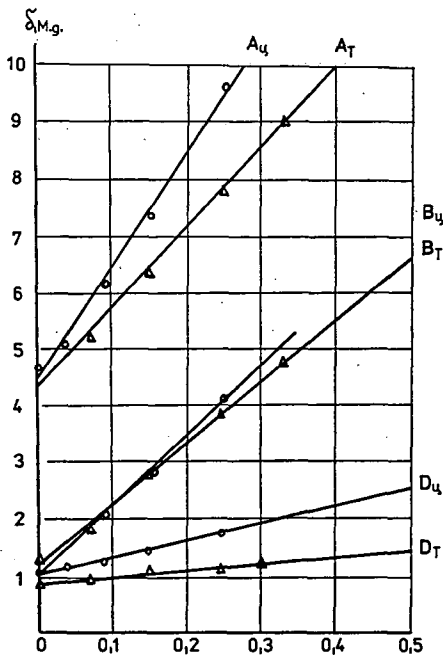


Рис. 3. Зависимость химических сдвигов протонов цис- и транс-2-метил-5-т. бутилдioxана-1,3

(δ , м. д.) от соотношения $\frac{[Eu(DPM)_3]}{[субстрат]}$

мента $O^1-C^2-O^6$ в образующемся комплексе $Eu(DPM)_3$ — цис-изомер за счет вытеснения электрофильного центра объемной трет-бутильной группой в направлении к C^2 -атому цикла. Таким образом, величины ЛИС позволяют однозначно судить о геометрии заместителей при C^5 -атоме диоксанового цикла и полезны при изучении стереохимии 2,5-дизамещенных 1,3-диоксанов.

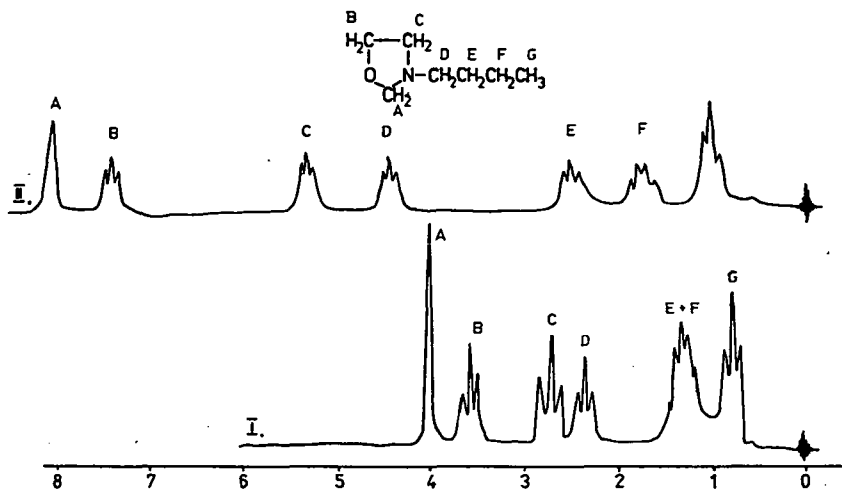


Рис. 4. I. ПМР-спектр 3-бутил-1,3-оксазациклопентана (CCl_4);
II. ПМР-спектр 3-бутил-1,3-оксазациклопентана в присутствии $Eu(DPM)_3$;

$$\text{Соотношение } \frac{[Eu(DPM)_3]}{[\text{субстрат}]} = 0,1$$

Мы исследовали природу координационного центра, в качестве которого могут выступать атомы кислорода или азота, на примере соединения II. Из анализа ПМР-спектров комплексов видно, что с увеличением концентрации $Eu(DPM)_3$ наблюдается смещение всех сигналов протонов в слабое поле (рис. 4) и хорошая линейная зависимость химического сдвига (δ , м. д.) от соотношения $\frac{[Eu(DPM)_3]}{[\text{субстрат}]}$ до величины этого соотношения $\sim 0,6$ (рис. 5). Величины ЛИС имеют наибольшие значения для протонов метиленовых групп А и В, а для

Таблица II

Соединение (I)	ЛИС, $\Delta\delta$, м. д.						
	$2H_A$	$2H_B$	$2H_C$	$2H_D$	$2H_E$	$2H_F$	$3H_G$
	43,8	42,3	31,5	26,9	13,1	6,9	3,5

остальных протонов убывают в ряду $C > D > E > F > G$ (табл. II). Это свидетельствует о том, что координационным центром для $\text{Eu}(\text{ДПМ})_3$ в соединении II является атом кислорода. Если бы координация проходила также по атому азота, это проявилось бы в существенном увеличении ЛИС протонов группы А в сравнении с В.

Экспериментальная часть

Использованная методика получения соединений (II и III) заключалась в ацетализации 2-трет-бутил-1,3-пропандиола уксусным альдегидом в присутствии пара-толуолсульфокислоты при $80-90^\circ\text{C}$ с азеотропным удалением реакционной воды. Соединение II было получено [6] взаимодействием формальдегида с N-бутил- β -оксиэтиламинном. Спектры ПМР записывали на приборе «Tesla»—BS—489.

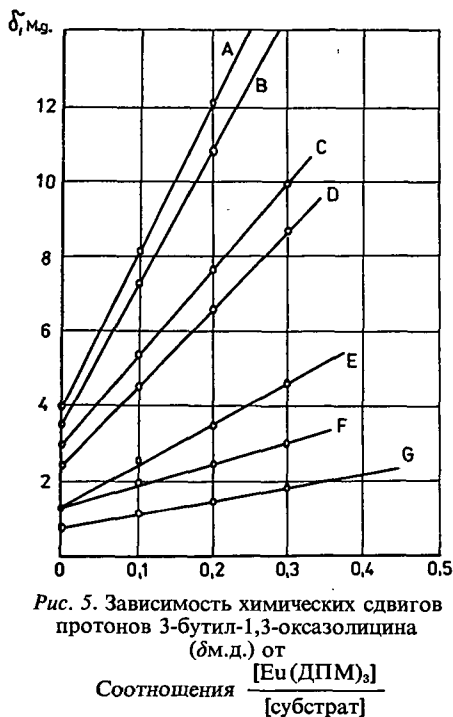


Рис. 5. Зависимость химических сдвигов протонов 3-бутил-1,3-оксазолицина (δ, м.д.) от соотношения $\frac{[\text{Eu}(\text{ДПМ})_3]}{[\text{субстрат}]}$

Литература

- [1] Латыпова, Ф. Н., Т. Ф. Ахунов, С. С. Злотский, Д. Л. Рахманкулов: Ж. прикл. хим. **50**, 223 (1977).
- [2] Ланшова, А. А.: Канд. диссерт., УНИ. Уфа, 1980.
- [3] Kime, K. A., R. E. Sievers: A Practical Guide to Uses of Lanthanide NMR Shift Reagents, *Aldrichimica Acta*, **10**, № 4, 1977.
- [4] Богатский, А. В., Ю. Ю. Самитов, З. Д. Богатская: Ж. орг. хим., **5**, 2230 (1969).
- [5] Самитов, Ю. Ю.: Атлас спектров ЯМР пространственных изомеров, **1**, Издательство Казанского университета, 1978.
- [6] Soliman, S. A., H. Abdine: *Aust. J. Chem.* **28**, 49 (1975).

EPR STUDY OF EUROPIUM COMPLEX FORMATION OF 1,3-DIHETERO ANALOGUES OF CYCLOALKANES

F. N. Latypova, V. V. Zorin, P. A. Krasutskii, N. A. Karakhanova, J. Apjok and M. Bartók

Complex formation between $\text{Eu}(\text{DPM})_3$ and 1,3-diheterocycloalkanes was investigated and the connection of the structure with the complex-formation characteristics was established.



СИНТЕЗ, СТРУКТУРА И СВОЙСТВА КАРБОКСИЛАТОВ МЕТАЛЛОВ, I. ВЛИЯНИЕ УСЛОВИЙ СИНТЕЗА БИС-(2-ЭТИЛ-ГЕКСАНОАТА) НИКЕЛЯ (II) НА ИНФРАКРАСНЫЕ СПЕКТРЫ ПРОДУКТА

О. БЕРКЕШИ и И. А. АНДОР

Кафедра общей и физической химии университета им. Аттилы Йожефа, Сегед

(Поступило в редакцию 5 октября 1982 г.)

Приготовлены соли бис-(2-этил-гексаноата) никеля (II) при разных молных соотношениях исходных соединений и разных рН среды, реакцией двойного обмена. Показаны и обсуждены происходящие изменения в ИК спектрах продуктов, выделенных экстракцией хлороформом, в области частот карбонильных и карбоксилатных валентных колебаний.

Интерес исследователей к изучению вопросов связанных со структурой и свойствами карбоксилатных соединений в последние годы все более расширяется. Это может объясняться, в первую очередь, возрастающим вниманием к соединениям металлов с биологически активными веществами [1—5], а также повышением роли экстракционных процессов в промышленности при выделении ряда важных элементов из разбавленных растворов [6—9]. В связи с этим, теоретическими вопросами структуры карбоксилатов и их экспериментальным изучением занимается широкий круг исследователей [10—17]. Детальное изложение основных положений о стереохимии карбоксилатов переходных металлов находим в обзорной статье Порай-Кошиц [18].

К изучению структуры карбоксилатов очень широко привлекается метод ИК спектроскопии [19]. Обзор работ, описывающих первоначальные данные по спектрам карбоксилатов находим в статье Шевченко [20]. Вопросы связи структуры и ИК спектров карбоксилатов подробно рассмотрены в монографиях Накамото [21, 22]. Однако, до настоящего времени основные корреляции между структурой, составом и ИК спектрами карбоксилатов различных металлов являются спорными [23]. Основной причиной разногласий является весьма сильный разброс данных разных авторов по основным характеристическим колебаниям карбоксилатов для одних и тех же соединений, в связи с чем возникает сомнение относительно идентичности исследованных образцов. Причиной литературных разногласий может служить также разная интерпретация спектров и оценка характеристических частот при наличии, как это в большинстве случаев наблюдается в спектрах, расщепления полос и появления плеч на полосах. Ранее нами было отмечено, что поглощение в ИК спектре в области $1620-1500\text{ см}^{-1}$, найденное для лаурата кальция, должно рассматриваться не только как соответствующее асимметричным валентным колебаниям карбоксилатной группы ($\nu_{as}\text{CO}_2^-$), но как серия полос, характерная для структуры карбоксилатов металлов [24]. Проведенное нами ранее изучение

чество прибавляемой щелочи увеличили до выпадения осадка $\text{Ni}(\text{OH})_2$. Расход $5,0 \cdot 10^{-2}$ М раствора NaOH составлял 6 cm^3 на 10 cm^3 исходной смеси (после экстракции получен продукт — С).

К приготовленной аналогично предыдущему исходной смеси добавили $0,1 \text{ cm}^3$ 25%-ного раствора NH_4OH . При этом только незначительная часть $\text{Ni}(\text{OH})_2$ перешла в аммиачный комплекс, несмотря на высокий рН среды, достигающего значения 13 (выделенный экстракцией продукт — D).

Экспериментальные данные

Поскольку ИК спектры снимали на двухлучевом приборе (в кювете сравнения помещался хлороформ), основные, представляющие для наших целей интерес, области спектра ($4000\text{—}2500$ и $1800\text{—}1200 \text{ cm}^{-1}$) были пригодны для проведения исследования [26].

На *рис. 1*, для уточнения отнесения полос поглощения, представлены ИК спектры 2-этил-гексановой кислоты и ее натриевой соли в области волновых чисел $1800\text{—}1200 \text{ cm}^{-1}$. Как видно из рисунка, в данной области волновых чисел в спектре НОкт в растворе хлороформа, выделяется характеристическая полоса при 1715 cm^{-1} , соответствующая валентному колебанию карбонила ($\nu \text{ C}=\text{O}$) в димеризованных карбоновых кислотах. Обнаруживается также слабая гибридная полоса деформационного колебания гидроксила и валентного колебания связи $\text{C}-\text{O}$ в ассоциированных кислотах при 1415 cm^{-1} . Остальные полосы соответствуют колебаниям метильных и метиленовых групп.

При образовании NaOkt совершенно четко проявляются (в хлороформовых растворах) вместо карбонильной полосы две новые, соответствующие $\nu_{\text{as}} \text{CO}_2^-$ при 1555 cm^{-1} и симметричным валентным колебаниям карбоксилатной группы ($\nu_s \text{CO}_2^-$) при 1425 cm^{-1} . Как видно, в спектре NaOkt не обнаруживаются признаки примеси свободной кислоты. Характерные для карбоксилата полосы являются сильными, острыми и нерасчлененными.

На *рис. 2* представлены спектры продуктов, полученных в серии для выяснения влияния мольных соотношений реагентов NiSO_4 и NaOkt . При этом, естественно, закономерно изменялся рН среды, поскольку исходный $0,1$ М раствор NiSO_4 имел рН 5,98, а $0,2$ М раствор NaOkt имел рН 7,35. Из представленных данных следует, что при изменении мольных соотношений, в спектрах продуктов наблюдаются также закономерные изменения. При большом избытке NiSO_4 (относительно низкий рН, кривая V) наблюдается наиболее сложный спектр: плечо при 1750 cm^{-1} на полосе, соответствующей колебаниям $\nu \text{ C}=\text{O}$ димеров кислот (1715 cm^{-1}), может быть оценено как $\nu \text{ C}=\text{O}$ для мономеров карбоновых кислот. Со стороны меньших волновых чисел также имеется плечо при 1690 cm^{-1} .

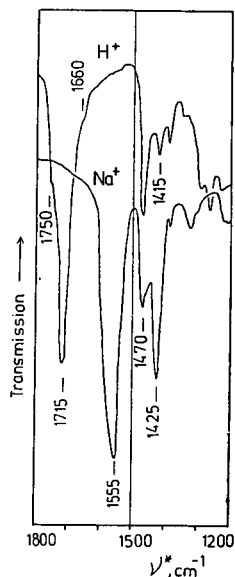


Рис. 1. ИК спектры 2-этил-гексановой кислоты (H^+) и ее натриевой соли (Na^+).

продуктов взаимодействия водных растворов хлорида берилия и калиевых мыл насыщенных жирных кислот при разных рН среды показало на необходимость детального рассмотрения и уточнения отнесения полос ИК спектров во всей области частот появления колебаний карбонильных и карбоксилатных групп [25].

Задачей данной работы являлось получение соли Ni^{2+} с 2-этил-гексановой кислотой методом реакции замещения в натриевой соли 2-этил-гексаноата, при различных молярных соотношениях исходных реагентов и рН среды; снятие ИК спектров продуктов и проведение попытки объяснения причин возникновения различий в спектрах солей в области появления полос валентных колебаний карбонильной и карбоксилатной групп.

Объекты и методы исследования

2-этил-гексановую кислоту (НОкт) применяли фирмы Merck со степенью чистоты «zur Synthese», остальные реактивы были фирмы Reanal аналитической степени чистоты.

ИК спектры снимали на спектрометре типа MOM—2000, в растворах хлороформа, в кюветах NaCl при толщинах слоя 0,1 и 0,055 мм. Чувствительность и ошибка измерений составляла не более $\pm 5 \text{ cm}^{-1}$ в определении волновых чисел максимумов полос поглощения.

Натриевую соль 2-этил-гексаноата (NaOkt) готовили нейтрализацией разбавленного водного раствора NaOH избытком кислоты. После завершения реакции основная масса избыточной кислоты HOkt отслаивается, которую отделяли в делительной воронке. Остатки кислоты извлекали экстракцией хлороформом из водного раствора соли. Разбавленный раствор натриевой соли концентрировали выпариванием и остаток сушили в вакууме при 363—373 К в течение 25 часов. Продукт хранили в эксикаторе над P_2O_5 .

Соль никель(II)-бис-(2-этил-гексаноата) (NiOkt_2) готовили сливанием 0,1 М растворов NiSO_4 (или $\text{Ni}(\text{NO}_3)_2$) и 0,2 М растворов NaOkt при молярных соотношениях реагентов, соответственно: 1:6 — I, 3:10 — II, 1:2 — III, 10:3 — IV, 6:1 — V. После завершения реакции смесь осталась гомогенной. Целевой продукт извлекался трехкратной экстракцией хлороформом.

Поскольку в проведенной серии синтезов рН среды были в слабокислой области, нами были приняты условия синтеза NiOkt_2 , соответствующие нейтральным и более высокому рН среды.

Титровали 0,1 М раствор NiSO_4 $5,0 \cdot 10^{-2}$ М раствором NaOH до появления осадка $\text{Ni}(\text{OH})_2$, расход раствора щелочи на 10 cm^3 исходного раствора составлял $2,6 \text{ cm}^3$. Полученный таким образом раствор NiSO_4 смешивали с эквивалентным количеством 0,2 М раствора NaOkt, затем производили экстракцию хлороформом (продукт — А).

Смешивали равные объемы исходных растворов NiSO_4 (0,1 М) и NaOkt (0,2 М) и затем титровали $5,0 \cdot 10^{-2}$ М раствором NaOH до появления осадка $\text{Ni}(\text{OH})_2$, расход щелочи составлял 4 cm^3 на 10 cm^3 смеси. После перемешивания, через некоторое время, произвели экстракцию как в предыдущем случае (продукт — В).

Аналогично приготовлению продукта В готовили смесь, только коли-

Полоса $\nu_{as} \text{CO}_2^-$ расщеплена, при этом интенсивность полос в дублете почти одинаковая с минимальным преобладанием полосы при 1590 cm^{-1} против полосы при 1615 cm^{-1} .

Уменьшение избытка NiSO_4 (кривые IV и III) приводит к исчезновению полос с наиболее высокими волновыми числами (1750 и 1715 cm^{-1}), остается единственная хорошо выраженная полоса при 1690 cm^{-1} . Относительная интенсивность более высокочастотной составляющей дублета $\nu_{as} \text{CO}_2^-$ постепенно уменьшается. При избытке NaOkt в реакционной смеси (кривые II и I) обнаруживается плечо на полосе $\nu_{as} \text{CO}_2^-$ около 1560 cm^{-1} . Спектральная полоса, соответствующая $\nu_s \text{CO}_2^-$ при 1420 cm^{-1} во всей серии остается без особых изменений.

Результаты проведенной аналогичной серии опытов с применением $0,1 \text{ M}$ раствора $\text{Ni}(\text{NO}_3)_2$ с $\text{pH } 6,17$ вместо NiSO_4 , представлены на *рис. 3*. Как видно из спектров полученных продуктов, явления, обнаруживающиеся при увели-

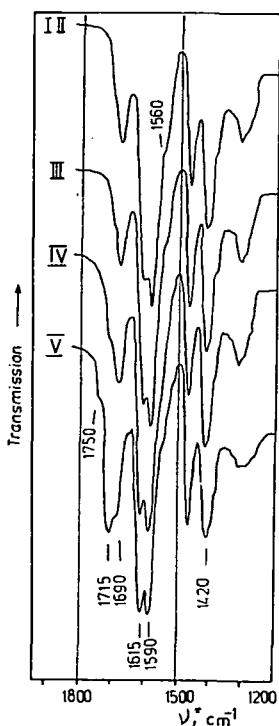


Рис. 2. ИК спектры NiOkt_2 , полученных при разных мольных соотношениях исходных реагентов NiSO_4 и NaOkt соответственно: 1:6 — I, 3:10 — II, 1:2 — III, 10:3 — IV, 6:1 — V.

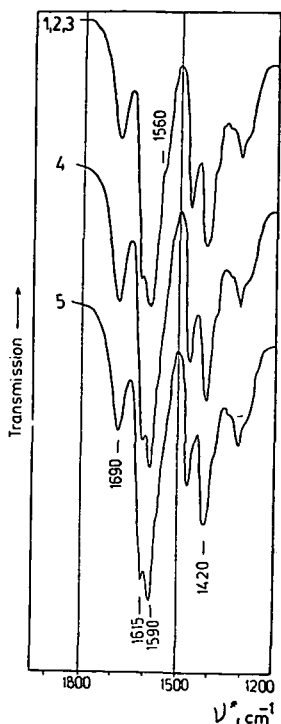


Рис. 3. ИК спектры NiOkt_2 , полученных при разных мольных соотношениях исходных реагентов $\text{Ni}(\text{NO}_3)_2$ и NaOkt соответственно: 1:6 — 1, 3:10 — 2, 1:2 — 3, 10:3 — 4, 6:1 — 5.

чении доли $\text{Ni}(\text{NO}_3)_2$ в реакционной смеси, показывают такую же закономерность, какая наблюдалась в предыдущей серии с увеличением доли NiSO_4 до эквивалентных соотношений реагентов (см. рис. 2, кривая III). Это обстоятельство указывает на определяющую роль pH реакционной среды на состав и структуру продуктов отражающихся в ИК спектрах, независимо от структуры аниона исходной соли металла.

Спектр NiOkt_2 , полученной после предварительного повышения pH среды раствора NiSO_4 до значения 7,3, не отличается принципиально от спектров представленных на рис. 2, сохраняется даже плечо, находящееся при 1715 cm^{-1} (рис. 4, кривая А).

Спектры продуктов В и С, соответствующие повышению pH реакционной среды после смешения реагентов до 7,6 и 9,9 соответственно, полностью совпадают и отличаются от аналогичного спектра (рис. 2, кривая III) только в области волновых чисел выше 3100 cm^{-1} .

Принципиально отличающийся спектр имеет продукт D, полученный в присутствии NH_4OH , повысившего pH среды до значения 13. Полосы соответствующие карбонильным колебаниям, очень слабые (рис. 4, кривая D). Полоса $\nu_{\text{as}} \text{CO}_2^-$ становится широкой без острых максимумов. Появляется хорошо выраженное поглощение при 3300 cm^{-1} , соответствующее валентным колебаниям OH группы.

С целью установления влияния щелочной отмывки продуктов на их ИК спектры была проведена также серия опытов. Экстрагированный хлороформом продукт, полученный смешением эквивалентных количеств исходных растворов, отмывался равными объемами водных растворов NaOH с концентрацией от 0,1 до 1,0 М. Спектры отмытых продуктов представлены на рис. 5. Совершенно ясно видно из данных рисунка, что интенсивность полосы при 1690 cm^{-1} постепенно уменьшается. Уменьшается также относительная интенсивность более высокочастотной составляющей дублета $\nu_{\text{as}} \text{CO}_2^-$ при 1615 cm^{-1} . Общий вид полосы становится менее острым, максимум расширенным. В области поглощений выше 3000 cm^{-1} до концентрации отмывающего раствора NaOH равной 0,6 М не произошли никакие изменения. При более высоких концентрациях NaOH (0,7—1,0 М) с возрастающей интенсивностью появляется диффузная полоса при 3300 cm^{-1} .

На рис. 6. представлены спектры экстракта, к которому добавлены различные количества HOkt .

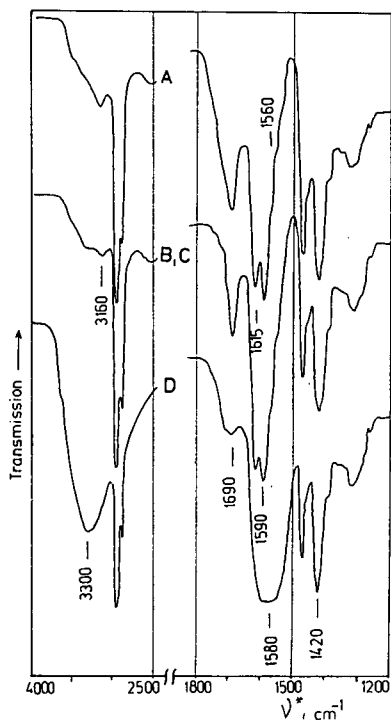


Рис. 4. ИК спектры NiOkt_2 , полученных методами описанными в тексте, при разных pH среды: 7,3 — А, 7,6 — В, 8,9 — С, 13 — D.

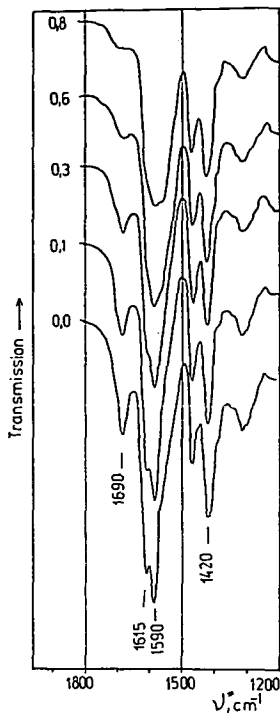


Рис. 5. ИК спектры NiOkt₂ после отмывания хлороформовых растворов водными растворами NaOH. Цифры на кривых соответствуют концентрациям NaOH в mol/dm³.

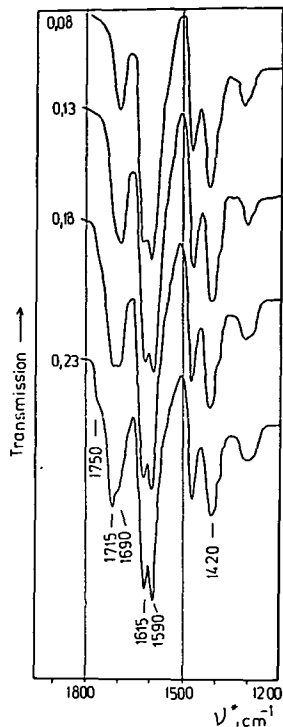


Рис. 6. ИК спектры NiOkt₂ при прибавлении разных количеств HOkt. Цифры на кривых соответствуют концентрациям кислоты в mol/dm³.

Обсуждение полученных экспериментальных результатов

Представленный на рис. 1 спектр HOkt характеризуется интенсивной острой полосой поглощения ν C=O (в цикле димеризованных карбоксиллов) на которой можно обнаружить два нерезко выраженных плеча при 1750 и 1660 cm^{-1} . Первое из них, при снятии спектров в растворах хлороформа при уменьшающихся концентрациях HOkt отделяется самостоятельной полосой, соответствующей ν C=O мономерных карбоксильных групп. Плечо при 1660 cm^{-1} обуславливается, по-видимому, наличием влаги в кислоте (деформационные колебания группы OH).

Приготовленная описанным методом NaOkt растворялась в хлороформе и в ее спектре (рис. 1) отсутствуют карбонильные полосы. Доминирующей является полоса поглощения, соответствующая ν_{as} CO₂⁻ при 1555 cm^{-1} , острая интенсивная и нерасчлененная. В спектре NaOkt ν_{s} CO₂⁻ также является характерной, поскольку по сравнению с полосой 1415 cm^{-1} соответствующей колеба-

ниям кислот, является значительно интенсивней с острым максимумом при 1525 см^{-1} . Необходимо отметить, что при попытке экстракции NaOkt из водного раствора хлороформом, в спектре экстракта не обнаруживаются полосы характерные для группы CO_2^- , но появляется полоса $\nu\text{C}=\text{O}$. Это явление объясняется высоким значением коэффициента распределения NaOkt в воде по отношению к хлороформу и гидролизом NaOkt в разбавленных водных растворах, вследствие которого экстрагируется образующаяся HOkt , что и обнаруживается в спектре.

Приготовленная при большом избытке NiSO_4 (соответственно с наиболее низким рН реакционной среды) экстрагированная хлороформом NiOkt_2 имеет, как отмечалось уже выше, наиболее сложный спектр (рис. 2, кривая V). Как было показано выше и найдено ранее и другими авторами [27], появление карбонильной полосы при 1715 см^{-1} следовало ожидать. Интересным является обнаруживающееся плечо при 1750 см^{-1} и более интенсивное плечо при 1690 см^{-1} . При увеличении доли NaOkt в реакционной смеси, что сопровождается постепенным повышением рН среды, исчезает не только плечо при 1750 см^{-1} , но происходит смена интенсивностей полос при 1715 и 1690 см^{-1} (рис. 2, кривые IV—I). Это может свидетельствовать о том, что карбонилы кислоты могут находиться в более сильной связи с NiOkt_2 , чем в циклах карбоксилатов. Продукты I—V, а также А, В и С не кристаллизовались и не удалось их выделить из растворов. При загущении образуют вязкие растворы, которые после высыхания представляют собой стекловидный прозрачный продукт зеленого цвета.

Повышение рН реакционной среды, при эквивалентных соотношениях реагентов, уменьшает интенсивность полосы при 1690 см^{-1} (рис. 4). Более того, если провести отмывку хлороформового раствора продукта равными объемами водных растворов щелочи возрастающей концентрации, также получены спектры с понижающейся интенсивностью полосы 1690 см^{-1} (рис. 5), что свидетельствует о непрочной связи карбонильных групп с NiOkt_2 .

Продукты, полученные либо отмыванием раствором щелочи, либо при высоком рН среды (продукт D) имеют отличающийся спектр от остальных образцов в области $3500\text{—}3100\text{ см}^{-1}$ (рис. 4, кривая D), когда при 3300 см^{-1} с заметной интенсивностью появляется полоса валентных колебаний OH группы. Полностью отмытый от кислоты, или полученная при высоком рН среды NiOkt_2 выделяется из раствора в виде осадка. Результаты анализа осадка комплексонометрическим титрованием с EDTA, позволяют предложить состав такого продукта, соответствующий формуле $\text{Ni}(\text{OH})\text{Okt}$ с относительной ошибкой всего 2%.

С другой стороны, добавление возрастающих количеств HOkt к экстракту, ранее полностью отмытого от кислоты раствором щелочи (до исчезновения карбонильных полос в спектре), приводит сначала к появлению полосы при 1690 см^{-1} , а затем полос при 1715 и 1750 см^{-1} (рис. 6).

Наряду с изменениями в спектрах в области около 1700 см^{-1} , такие же характерные изменения наблюдаются в виде полосы, соответствующей $\nu_{\text{as}}\text{CO}_2^-$. На рис. 1 видно, что NaOkt характеризуется полосой $\nu_{\text{as}}\text{CO}_2^-$, имеющей острый максимум при 1555 см^{-1} . Для NiOkt_2 характерен дублет с максимумами при 1615 и 1590 см^{-1} , относительная интенсивность более высокочастотной составляющей которого увеличивается с повышением мольного соотношения

$\text{NiSO}_4 \cdot \text{NaOkt}$ (рис. 2), или $\text{Ni}(\text{NO}_3)_2 \cdot \text{NaOkt}$ (рис. 3). Замечательно, что добавление кислоты к продукту с составом $\text{Ni}(\text{OH})\text{Okt}$ приводит к этому же результату. Вместе с тем, что в спектрах отмытой от остатков кислоты NiOkt_2 (рис. 5) и полученной при высоком pH среды (рис. 4, продукт D) полоса $\nu_{\text{as}} \text{CO}_2^-$ является широкой без острого максимума, дает основание утверждению, что расщепление полосы, очевидно, не является простым результатом механического резонанса карбоксилатных групп, присоединенных к центральному атому металла, а отражает разные состояния карбоксилатных групп.

Появление ОН группы в координационной сфере металла, по-видимому, упорядочивает расположение и состояние карбоксилатных групп. Введение избыточной же кислоты способствует, очевидно, образованию более сложных, но энергетически и стерически строже определенных состояний.

Тот факт, что замена сульфата на нитрат никеля меняет вид ИК спектров только в той мере, насколько изменяется pH реакционной среды (рис. 3), свидетельствует об общем значении найденных закономерностей изменений в спектрах в зависимости от условий приготовления NiOkt_2 .

Необходимо отметить, что вид и положение полосы соответствующей $\nu_s \text{CO}_2^-$ при всех принятых нами условиях, остался без существенных изменений с острым максимумом при 1420 cm^{-1} . Это обстоятельство, совместно с найденным постоянством интенсивности и положения полосы при 1590 cm^{-1} , может быть оценено как подтверждение правомерности отнесения последней полосы к колебаниям $\nu_{\text{as}} \text{CO}_2^-$.

Из рассмотрения приведенных данных следует также, что в случае синтеза NiOkt_2 реакцией двойного обмена, в зависимости от условий приготовления и очистки продуктов, не образуется индивидуальное вещество, а могут образоваться соединения разного состава: $\text{Ni}(\text{OH})\text{Okt}$, NiOkt_2 и $\text{NiOkt}_2 \cdot x\text{HOkt}$, или их смеси с разным соотношением указанных соединений в продукте. В результате этого спектры имеют ряд осложнений, которые могут затруднить точное отнесение полос поглощения к характеристическим частотам и могут быть причиной разноречивых оценок положения максимумов полос в спектрах в области частот валентных колебаний карбонильных и карбоксилатных групп.

Литература

- [1] Эйхгорн, Г. (ред.): Неорганическая биохимия, т. 1 и 2, «Мир», Москва, 1978.
- [2] Фридман, Я. Д. (ред.): Физико-химическое изучение соединений металлов с биологически активными веществами, «Илим», Фрунзе, 1977.
- [3] Шатаева, Л. К., Н. Н. Кузнецова, Г. Э. Елькин: Карбоксильные катиониты в биологии, «Наука», Ленинград, 1979.
- [4] Синицына, Т. А., В. П. Краснов и др.: Ж. общ. хим., **51**, 2592 (1981).
- [5] XXII International Conference on Coordination Chemistry, vol. 1, (Abstracts of papers) Budapest, 1982.
- [6] Золотов, Ю. А.: Экстракционное концентрирование, «Химия», Москва, 1971.
- [7] Singh, J. M., S. N. Tandon: J. Inorg. Nucl. Chem., **41**, 1205 (1979).
- [8] Горячев, А. А., Е. К. Копкова: Ж. неорг. хим., **25**, 1347 (1980).
- [9] Лобанов, Ф. И., В. П. Гладышев и др.: Ж. неорг. хим., **26**, 1347 (1981).
- [10] Melnik, M.: Coord. Chem. Rev., **36**, 1 (1981).
- [11] Gil, V. M. S., M. E. T. L. Saraiva et al.: J. Inorg. Nucl. Chem., **42**, 389 (1981).
- [12] Huyskens, P., N. Felix et al.: J. Phys. Chem., **84**, 1387 (1980).
- [13] Yousif, Y. Z., F. J. M. Al-Imarach: J. Inorg. Nucl. Chem.: **42**, 779 (1980).
- [14] Bombieri, G., F. Benetollo et al.: J. Inorg. Nucl. Chem., **42**, 1423 (1980).

- [15] Baker, L. C. W., L. Lebiada et al.: J. Amer. Chem. Soc., **102**, 3276 (1980).
[16] Амирасланов, И. Р., Б. Т. Усубалиев и др.: Ж. структ. хим., **21**, № 5, 112 (1980).
[17] Скрылев, Л. Д., И. И. Сейфуллина и др.: Ж. неорг. хим., **26**, 1501 (1981).
[18] Порай-Кошиц, М. А.: Ж. структ. хим., **21**, № 3, 146 (1980).
[19] Davies, M.: Infra-Red Spectroscopy and Molecular Structure, Elsevier Publ. Co., Amsterdam, 1963.
[20] Шевченко, Л. Л.: Успехи хим., **32**, 457 (1963).
[21] Nakamoto, K.: Infrared Spectra of Inorganic and Coordination Compounds, J. Wiley, New York, 1963.
[22] Nakamoto, K., P. J. McCarthy: Spectroscopy and Structure of Metal Chelate Compounds, J. Wiley, New York, 1968.
[23] Deacon, G. B., R. J. Phillips: Coord. Chem. Rev., **33**, 227 (1980).
[24] Андор, И. А., Я. Киш: Acta Phys. Chem. Szeged, **21**, 143 (1975).
[25] Андор, И. А., И. Древени и др.: Acta Phys. Chem. Szeged, **28**, 253 (1982).
[26] Sadtler Standard Spectra: 26 Frequently Used Spectra for the Infrared Spectroscopist, Pennsylvania.
[27] Kambe, H.: Bull. Chem. Soc. Japan, **34**, 1786 (1961).

SYNTHESIS, STRUCTURE AND PROPERTIES OF METAL CARBOXYLATES, I.
EFFECTS OF EXPERIMENTAL CONDITIONS ON THE IR SPECTRA OF COMPOUNDS
FORMED IN Ni(II)-bis(-2-ethylhexanoate) PRODUCTION

O. Berkesi and J. A. Andor

Ni(II)-bis(-2-ethylhexanoate) was prepared by methathesis, from different mole ratios of the starting materials and at different pH values. The changes in the IR spectra of the products (obtained by CHCl_3 extraction) in the range of carbonyl and carboxylate stretching vibrations were established and are discussed.



MODIFICATION OF QUARTZ SURFACE WITH AQUEOUS SOLUTIONS OF POLYELECTROLYTES AND SURFACE-ACTIVE SUBSTANCES

By

K. B. MUSABEKOV, K. I. OMAROVA, A. I. IZIMOV
Kirov Kazakh State University, Alma-Ata, U. S. S. R.

(Received 20th October, 1982)

The influence of anionic [polyacrylic (PAA), polymethacrylic (PMAA) acids] and cationic [hydrochlorides of poly-2-methyl-5-vinylpyridine (PMVP) and copolymer of 2-methyl-5-vinylpyridine with butylmethacrylate (MVP-BMA)] polyelectrolytes (PE), and also their mixtures with cationic (cetyltrimethylammonium bromide (CTAB)) and anionic (sodium dodecylsulphate (DDS)) surface-active substances (SAS) on surface properties of quartz was investigated. The greatest modification of PE and their mixtures with SAS is displayed when they are preliminary deposit on quartz surface from aqueous solutions and dried. The modification act of PE and SAS is displayed in exchanges of the contact angle of wetting with water and electrokinetic potential of quartz.

The current stage in the development of colloid chemistry is characterized by the use of high-molecular surface-active substances (HMSAS) in the processes of wetting, stabilization and flocculation of dispersed systems, *i.e.* in processes connected with their surface characteristics [1—5]. The influence of HMSAS on dispersed systems is connected with their adsorption on interphase boundaries [6], which results in changes in the surface state of the system particles, and the structure of the double electric layer (DEL) in particular. A value that is easily measured practically and characterizes the parameters of the DEL, is the electrokinetic ζ -potential. The value of the ζ -potential is used by some research workers to characterize the binding strength between macromolecules and mineral particles [1] and to find the mechanism of their interaction [7].

On the other hand, the contact angle (θ), which is a measure of the wetting occurring in three-phase systems, is determined by the correlation of the interfacial tension (σ) of the contacting phases. A change in surface tension in the presence of HMSAS on any phase boundary will influence the value of θ . By studying the wetting of solid surfaces with various liquids, we can get information about the state of the solid surface in the presence of polymers.

In our opinion, a complex study of wetting and electrokinetic characteristics of solids will make it possible to find out more peculiarities pertaining to the formation of adsorption layers of diphilic macromolecules, which determine the stabilizing and flocculating actions of the latter. Further, a study of the possibilities of regulating wetting processes with the help of HMSAS, including diphilic polyelectrolytes, is in itself of practical importance.

This paper presents the results of a systematic study of the influence of the nature molecular mass and degree of diphil character of HMSAS on the water wetting and the ζ -potential of one of the hidrophilic minerals most widely spread in nature quartz. The simple composition and low solubility make this the most convenient substance to study.

We have used the following cation-active HMSAS: hydrochlorides of poly-2-methyl-5-vinylpyridine (PMVP) with an average molecular mass (M_n) 1.9×10^4 and 3.4×10^5 , and of copolymers of 2-methyl-5-vinylpyridine (MVP) with butyl methacrylate (BMA) in initial molar ratios 9:1 (copolymer 1) and 7:3 (copolymer 2). PMVP and its copolymers were obtained by free-radical polymerization in the block at 70 °C in the presence of the dinitrile of azo-bis-isobutyric acid (DAA) in a quantity of 0.2% of the polymer weight [8]. After fractionation in the hexane-petroleum ether system, we determined the average molecular masses viscosimetrically [9]. The constants required for the calculation of M_n were taken from [8].

Anion-active polymers were polyacrylic acid (PAA) with M_n 1.7×10^4 , 5.7×10^4 , 9.9×10^4 , 1.8×10^5 and 2.7×10^5 , and polymethacrylic acid (PMAA) with M_n 1.8×10^5 , 2.7×10^5 and 5.6×10^5 . We prepared PAA by radical polymerization in 30% dioxane solution in the presence of benzoyl peroxide [10]. PMAA was also obtained by radical polymerization in a benzoyl peroxide solution. The initiator was DAA.

The molecular masses of PAA and PMAA fractionated in the dioxane-petroleum ether [11] methanol-ethyl acetate systems: acetic acid (9:1), respectively [11], were determined viscosimetrically with the help of the equation constants of Mark—Hauwink—Kuhn given in [12].

The contact angles (θ) of wetting of a polished plate (polishing class 14) of optical quartz glass K—8 made by the Lytkarinsk Optical Glass Works were measured help of a horizontal microscope with a goniometric attachment and a special movable stage [13]. The value of θ was found by the tangent method, the measurement error being $\pm 0.5^\circ$. At the same time the value of θ was calculated according to the main parameters of the adherent drop [14]. The measurement error here was not more than $\pm 0.25^\circ$. The discrepancies in the values of θ determined by the above two methods did not exceed $\pm 0.5^\circ$.

The values of θ were read five minutes after the drop was applied to the surface of the quartz plate. During this time θ diminished by 3—5° and then in the course of five hours it remained constant. Check measurements were taken every 30 minutes during five hours. Before each measurement the plates were treated with a newly-prepared chromic acid mixture, then thoroughly washed with distilled water and dried in a vacuum exsiccator over phosphorus pentoxide.

The ζ -potential was determined by the flow potential method, with the surface conductivity taken into account [15]. To make the measurement we used crystal powder ground to a particle size of 17 to 20 mcm. The quartz powder was preliminarily washed free of Fe^{3+} ions with sulphuric acid while being heated, and was then washed with distilled water and dried at 105—11 °C. Owing to the high resistance of the quartz powder diaphragm, the HMSAS solutions were prepared using a 10^{-4} M solution of KCl. Before each measurement of the ζ -potential, HMSAS solution of appropriate concentration was let through the quartz diaphragm until the electrical conductivity of the outflowing solution was equal to that of the initial solution.

1. Effects of polyelectrolytes on water wetting and electrokinetic potential of quartz

The contact angles of quartz wetted with aqueous solutions of the above-mentioned polyelectrolytes ($\theta=4-6^\circ$), in spite of their marked surface activity on the liquid-gas boundary [16], differ little from those of quartz wetted with pure water

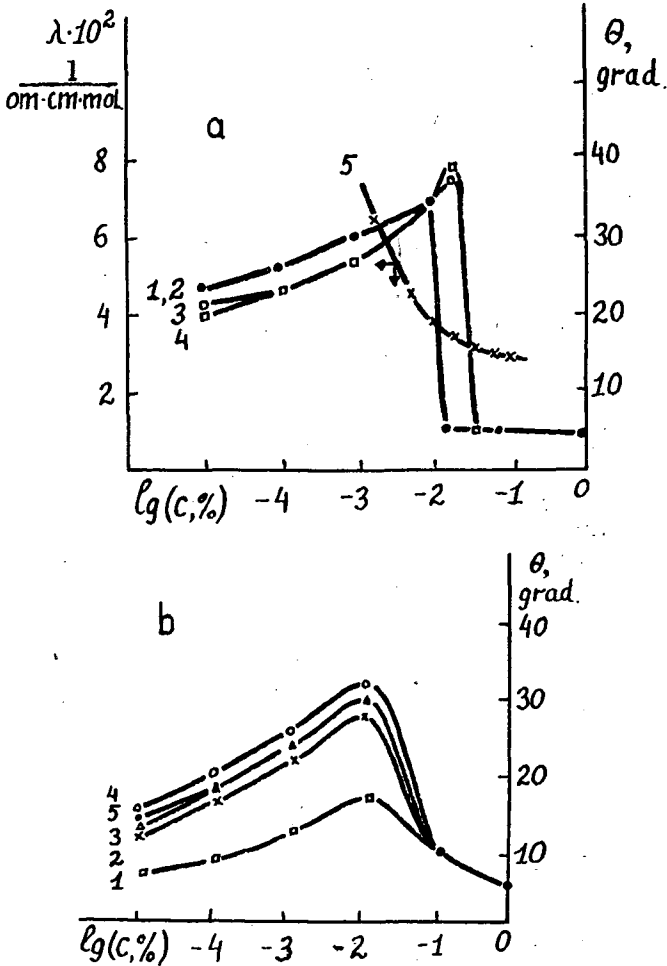


Fig. 1. Contact angles of quartz wetted with water modified by HMSAS solutions:
 1a) PMVP hydrochlorides with $M_n(190.000$ (1) and 340.000 (2), copolymers MVP:BMA=9:1 (3) and 7:3(4); and PMVP equivalent electric conductivity with $M_n=190.000$ (5);
 1b) PAA with $M_n=17.300$ (1), 180.000 (2), 270.000 (3), 513.000 (4), and PMAA with $M_n=180.000$ (5).

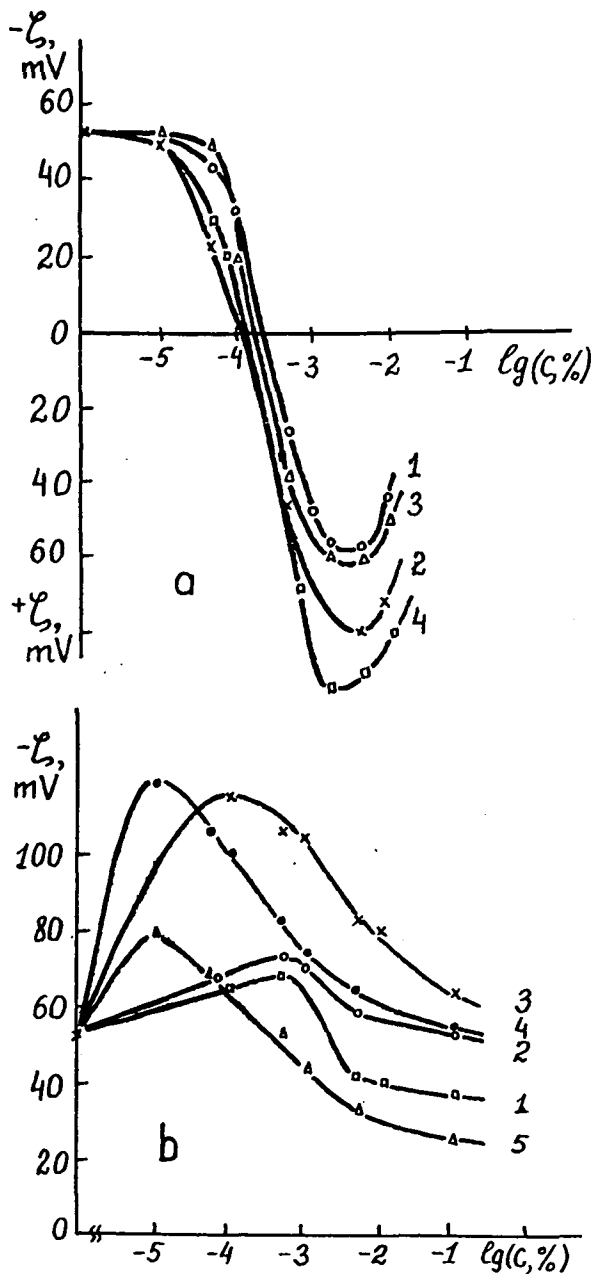


Fig. 2. Electrokinetic potential of quartz in aqueous solutions of HMSAS:
 2a) PMVP hydrochlorides with $M_n=190.000$ (1) and 340.000 (2),
 copolymers MVP:BMA=9:1 (3) and 7:3 (4);
 2b) PAA with $M_n=17.300$ (1), 57.000 (2), 99.000 (3), 180.000 (4) and 513.000 (5);

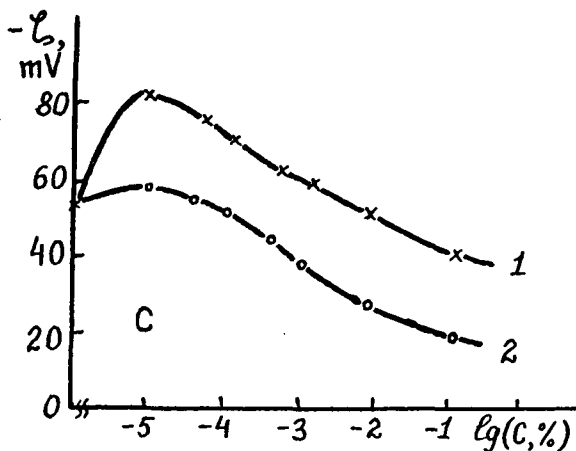


Fig. 2

2c) PMAA with $M_n = 180,000$ (1) and $560,000$ (2).

[17], except for copolymers which give a slight ($8-10^\circ$) increase of θ at high concentrations. This insignificant change in θ may be explained by the fact that the process of drop spreading on the quartz surface occurs faster than the adsorption of HMSAS. Thus, for instance, the adsorption equilibrium on the HMSAS aqueous solution air boundary becomes stable in the course of 12–24 hours owing to the low rate of diffusion of macromolecules to the interface [16]. This small increase in θ in the case of copolymers is apparently connected with their greater surface activity.

The preliminary treatment, *i.e.* keeping the quartz plates in aqueous solutions of HMSAS for 6 hours, brings about quite a different regularity. In this instance, even if the concentration of the HMSAS solutions is very low ($C \approx 10^{-5}\%$), θ noticeably changes; it rises with concentration increase, reaching its maximum at $C \approx 10^{-2}\%$ (Fig. 1).

The increase of θ along with the rise of the concentration during such a long-term contact of the quartz with HMSAS solutions may be explained by the formation of an adsorption layer of HMSAS on the quartz plate surface. The identical type of the concentration-dependence of θ for both cationic (Fig. 1a) and anionic (Fig. 1b) HMSAS suggests that in both instances the macromolecules are oriented in the adsorption layer according to the classical mechanism "similar to similar", which is accompanied by hydrophobization of the quartz surface.

The measurement of the ζ -potential of quartz in aqueous solutions of the HMSAS under study confirms the quartz adsorption of HMSAS (Figs 2, 4). Thus, solutions of PMVP and its copolymers give typical S-shaped curves with a change in the surface charge sign at a specific polymer concentration for each molecular mass. The change in the ζ -potential sign is due to the superequivalent adsorption of macrocation on the quartz surface. This kind of dependence is observed in the presence of multivalent ions, in solutions of potential-determining ions, surface-active substances when the charges of the dispersed phase particle and of the ion introduced into the solution have opposite signs [18–21].

The probable cause of adsorption of PAA and PMAA macromolecules is the formation of hydrogen bonds between the carboxylic groups of the polyelectrolyte and the silanol groups of quartz [1, 2]. However, it was found that the total surface charge of quartz is composed of the charge of the active centres, which differ in value and sign [22, 23]. Therefore, the possibility of adsorption of the HMSAS polyion on the oppositely charged centres of the quartz surface is not excluded [20]. Quartz adsorption of the PAA and PMAA polyions is accompanied by an increase in the negative charge, and therefore in the negative ζ -potential of the latter (Fig. 2) at low concentrations of polyelectrolyte. An increase in the negative values of the ζ -potential in PAA and PMAA solutions is observed in suspensions of clay minerals, too [24].

It is noteworthy that the maximum values of θ of water-wetted quartz preliminarily treated with HMSAS aqueous solutions are observed in the concentration range in which there is a break in the conductometric titration curve [25] (Fig. 1a, curve 5). It is known that high-molecular compounds, and polyelectrolytes in particular, are capable of considerable conformational transformations on ionization, these being especially noticeable in aqueous solutions [11, 26]. Hence, a concentration which brings about a break in a curve showing the dependence of different physicochemical properties on the polymer concentration is called by us a concentration of the conformational transition (CCT), on the analogy of the critical concentration of micelle formation (CCM) of hemicolloid SAS. Proceeding from this, the extremal dependence θ *v.s.* $\log C$ can be explained, with the different characters of the polymer adsorption layer formation on the quartz surface above and below the CCT taken into account. At concentrations of HMSAS lower than the CCT, when the intermolecular hydrophobic interactions are comparatively weak, the macromolecules are of less compact conformation. It may be admitted that such macromolecules, when moving to the adsorbent surface, are able to develop due to the adsorption forces. (The possibility of macromolecular coil deformation in the adsorption layers is discussed in the literature [27].) As a result of this, a proportion of the hydrophobic groups become "uncovered", which leads to hydrophobization of the quartz surface, manifested in an increase in θ .

In the concentration range higher than the CCT the adsorption layer is formed of more compacted macromolecule coils. Apparently, the great compactness of the macromolecule segments in the adsorption layer makes it difficult for the segments to differentiate according to the polarity, as a result of which the HMSAS adsorption layer on the quartz surface remains hydrophilic.

Further, when the concentration of the HMSAS under study increases, the pH of their solutions falls and approaches 2 in the concentration range $\sim 10^{-1}$ –1%, which corresponds to the isoelectric point (IEP) of quartz [28]. It is known that at the IEP of quartz the wettability of solids becomes worse (for quartz at the IEP $\theta=40^\circ$) [28–30]. However, despite the fact that the pH approaches the IEP of quartz, as Fig. 1 shows, concentrations higher than 10^{-2} % give an abrupt decrease in θ , which is confirmation of the possible adsorption of macromolecules in the form of compact coils.

It is interesting to compare the influence of the above-mentioned polyelectrolytes on the quartz surface properties with the action of polyethylenimine (PEI), which is known [31] to be characterized by insignificant intermolecular interactions and weakly expressed conformational transitions. The interest in PEI is due to the wide range of

its practical uses. In the case of PEI* the concentration-dependence of the contact angle is of an extremal kind (Fig. 3). A change in the value of θ as the concentration grows is linked with the quartz surface adsorption of PEI. Quartz adsorption of PEI is insignificant (0.2—3.5 mmole/g), which is apparently connected with the small specific surface of quartz (0.12 m²/g). The adsorption was determined by the spectrophotometric method and confirmed by IR-spectrometry. Thus, the IR-spectra of

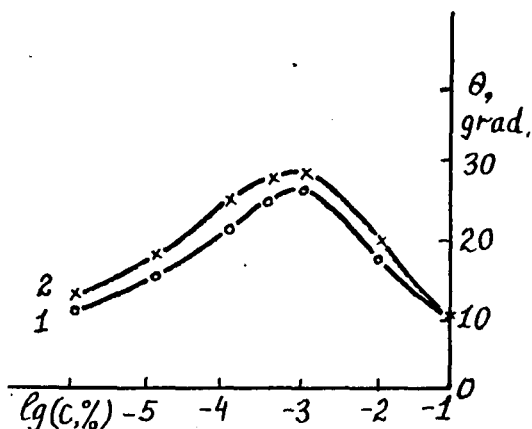


Fig. 3. Contact angles of quartz wetted with water modified by PEI solutions with $M_n = 30,000$ (1) and $100,000$ (2).

quartz surface owing to the dissociation of silanol groups when the pH of the PEI solution increases with the growth of the concentration (to pH=10.2). With the increases of the solid-phase surface charge, the expected rise in polymer adsorption is probably compensated by a fall in the degree of PEI dissociation as the pH of the solution increases.

Thus, the results obtained show that the conformational state of the macromolecules in the solution considerably influences their hydrophobizing action.

The results of measurements of the ζ -potential and θ of water-wetted quartz confirm the well-known regularity about the increase in the adsorption of the polymer along with the growth of its molecular mass [32]. Thus, with an increase in M_n the maximum in the ζ vs. log C curves for anionic HMSAS (Fig. 2b, c) and a change in the charge sign of the quartz surface in PMVP solutions (Fig. 2a) are observed for lower concentrations. A noticeable influence of the polymer molecular mass reveals itself in the lower-molecular region ($M_n < 1 \cdot 10^5$). For example, the difference in the maximum values of the ζ -potential for PAA with $M_n = 1.7 \times 10^4$ and 9.9×10^4 is ~ 60 mV (Fig. 2b), while the difference in the values of θ is 15° (Fig. 1b). The values of θ for HMSAS with a molecular mass higher than 1×10^5 do not differ considerably. The value of the quartz ζ -potential decreases as both M_n and the concentration of the HMSAS solutions increase.

* Polyethylenimine was synthesized at the A. V. Topchiev Institute of Petrochemical Analysis (Moscow) by Dr. P. A. Gembitsky.

quartz samples kept in PEI solutions of various concentrations, in comparison with the spectra of pure quartz, show bands corresponding to the valency and deformational fluctuations of bonds in the CH- of CH₂-groups (2930, 2830, 1460, 1290, 1180 cm⁻¹).

Unlike PMVP, PAA and PMAA, PEI does not show abrupt decreases in θ to those of pure quartz θ . When the concentrations of PEI are higher than $10^{-3}\%$, θ decreases. In this instance the quantity of adsorbed polymer practically does not depend on the concentration ($C > 10^{-3}\%$). Therefore, the reduction in θ is apparently connected with an additional negative charge which appears on the

The fall in the ζ -potential as the concentration of HMSAS increases is apparently linked with a reduction of the ionization degree of the polyelectrolytes under study, the sliding surface shift into the liquid phase, an increase in the solution viscosity and, hence, a reduction in the mobility of the double layer antions. (In calculations of the ζ -potential, the viscosity of the solution was considered to be equal to that of water.)

The effects of an increase in the solution viscosity and the shift of the sliding surface into the liquid phase are probably the more significant, the greater the HMSAS molecular mass. Therefore, the ζ -potential values for the PAA with high M_n (Fig. 2b, curves 4, 5) are lower than those for polymers of smaller molecular masses. A similar relation was found for PMAA, too (Fig. 2c). It must also be taken into account that not only the solution viscosity but also the dielectric penetrability changes near the solid surface. All the above factors will lead to a decrease in the ζ -potential when the polymer concentration in the solution increases [33].

The hydrophilic surface adsorption of polymer macromolecules may lead to their hydrophobization. It is known that hydrophobization intensifies as the diphil-character of macromolecules increases. The hydrophobicity (m) of macromolecules of the polyelectrolytes studied, which was estimated as the number of hydrophobic (—CH_3 , =CH_2 , =CH— , =C=) groups *per* functional (hydrophilic) group, increases from PAA to PMAA and in the sequence $\text{PMVP—I} \rightarrow \text{PMVP—II} \rightarrow \text{copolymer I} \rightarrow \text{copolymer II}$. For PAA and PMAA m is equal to 2 and 3, respectively, while for PMVP and its copolymers θ is within the range 8—11. In the sequence mentioned above, on account of the greater hydrophobization of the quartz particles, a greater fall in the ζ -potential value and a rise in θ are to be expected, the concentration and molecular mass of the polymer being the same. This is the regularity for anionic HMSAS; the dependent curves ζ vs. $\log C$ (θ vs. $\log C$) for PMAA are located lower (higher) than the similar curves for PAA (Fig. 2b, curves 4, 5; Fig. 2c, curves 1, 2). In the case of PMVP and its copolymers the influence of diphil character is of a lesser extent (Fig. 2a). It follows from this that the influence of the diphil character is manifested noticeably at low values of hydrophobicity.

Thus, the investigations carried out show that it is possible to modify the surface of dispersed particles with both cationic and anionic polyelectrolytes.

2. Influence of polyelectrolyte mixtures with low-molecular surface-active substances on quartz surface electric properties

At present great attention is being paid to the interactions of macromolecules of different natures. The majority of the studies of this kind have been carried out on albumens. A study of cooperative reactions involving polyelectrolytes is of theoretical and practical interest, as the products of these reactions (intermolecular complexes) possess a number of specific features not found in the original components. The most convenient subjects providing an understanding of the specificity of inter-macromolecular reactions are polyelectrolytes. Studies of the interactions of polyelectrolytes with surface-active substances (SAS) have begun in the past few years [34, 35]. The polyelectrolyte-SAS interaction is an insufficiently well known type of macromolecular reaction; the products of such reactions can be used to regulate various colloid-chemical phase boundary processes.

We have studied the influence of mixtures of PMVP and sodium dodecyl

sulphate (NaDDS), PAA (PMAA) and cetyltrimethylammonium bromide (CTMAbr) on the wetting ability and the ζ -potential of quartz.

Each time θ and the ζ -potential were measured, the quartz plates and the powder were treated with a mixture of polyelectrolyte and SAS at a different molar ratio $n = \frac{[\text{SAS}]}{[\text{HMSAS}]}$. The value n was regulated by changing the quantity of SAS, the volume of HMSAS being kept constant. The initial concentrations of HMSAS and SAS were equal.

As pointed out in the first part of the paper, the macromolecular conformation depends on the concentration of the polyelectrolyte solution. The measurement of PMVP viscosity shows that the sharpest change in $\eta_{\text{red.}}$, and therefore that in the coil conformation, takes place when the concentration of the PMVP solution is of the order of 0.01%. It is to be expected that, depending on the polyelectrolyte solution concentrations, its interaction with the SAS and the influence of their mixtures on the quartz wetting θ will be different.

The relation θ vs. n for all the polyelectrolytes studied is maximum at a definite value of n , which depends on the nature of the polyelectrolyte (Figs. 4, 5). The addition of SAS to the polyelectrolyte intensifies the hydrophobizing action of the latter. However, the results obtained for the mixture of PMVP and NaDDS reflect the dependence of the degree of quartz surface hydrophobization on the initial concentration of the polyelectrolyte. The sharpest increase in θ is observed when the concent-

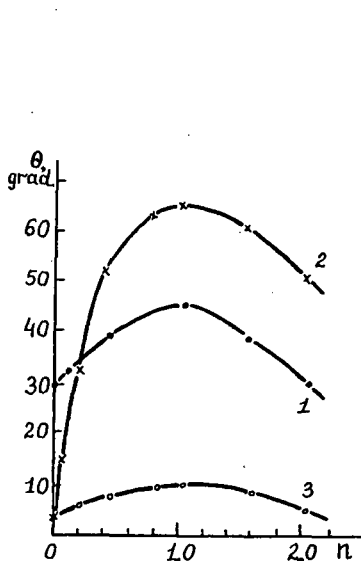


Fig. 4. Dependence of contact angles of quartz wetted with water upon the relative concentration of DDS in a mixture with PMVP with $M_n = 340,000$, $C_{\text{PMVP}} = 0.01\%$ (1), 0.155% (2) and 0.465% (3).

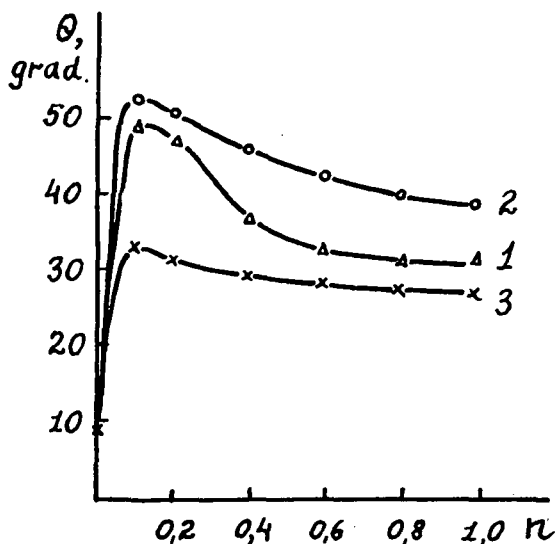


Fig. 5. Dependence of contact angles of quartz wetted with water upon the relative concentration of CTMAbr in a mixture with PAA with $M_n = 17,300$ (1) and $1,000,000$ (2), PMAA with $M_n = 1,000,000$ (3), $C_{\text{PAA}} = 0.072\%$, $C_{\text{PMAA}} = 0.086\%$.

ration of PMVP is 0.155% (curve 2, Fig. 4) and is noticeably weaker when the concentration is 0.465% (curve 3, Fig. 4, $\theta_{\max} \approx 8-10^\circ$).

The intensification of the hydrophobizing action of the polyelectrolyte in the presence of NaDDS is connected with the formation of a polyelectrolyte complex and its adsorption on the quartz surface. As a result of the interaction of PMVP and NaDDS according to the ion-exchange mechanism [35, 36], some of the ionized polyelectrolyte groups appear to be blocked by DDS^- ions, and this results in the hydrophobization of the polymer chains. In this case the macromolecules roll into coils compacted by hydrophobic interactions of non-polar radicals of NaDDS. This effect reveals itself most vividly in the $n=1$ region. With other values of n the compactization of coils of PMVP macromolecules is less clearly expressed. Proceeding from this, the change in the hydrophobizing action of PMVP with the change in its concentration in the solution (when the values of n are the same) may be explained by a change in the degree of NaDDS binding by the polyelectrolyte.

The greatest hydrophobization of the quartz surface is observed when the concentration of PMVP solutions is 0.01%. At such a concentration the PMVP macromolecules are in a more developed conformation and can therefore bind a greater amount of NaDDS, which leads to a greater hydrophobization of the polyelectrolyte chains. The quartz surface adsorption of such hydrophobized coils results in higher θ values. From this point of view the extremal dependence $\theta(n)$ is explained by the greatest compactization of coils of PMVP macromolecules, as they interact with NaDDS in the $n \approx 1$ region [35].

The possibility of adsorption of DDS^- ions on the macromolecule coil surface is confirmed by the results of measurement of the quartz ζ -potential in aqueous solutions of NaDDS and PMVP mixtures (Fig. 6, curves 1, 2). It is seen from the Figure that in a 0.155% solution of PMVP the quartz surface has a positive charge, probably conditioned by the superequivalent adsorption of the polyelectrolyte macrocation. However, when NaDDS is added, first we see a further increase in the positive values of the quartz ζ -potential, which is probably connected with the quartz surface adsorption of compacted PMVP and NaDDS complexes and a rise in the density of the positive charge. When the value of n is approximately 0.3–0.4, the ζ -potential falls and reaches the zero value when n equals 1. The fall in the ζ -potential is accompanied by a rise in the value of the quartz θ . Such a change in θ may result from the effects of two factors: a decrease in the quartz surface charge [37], and the hydrophobization of PE micelles by SAS anions. A comparison of the figures shows that the greatest value of θ corresponds to the zero value of the ζ -potential. The result obtained conforms to literature information about the maximum values of θ at the quartz IEP [28–30]. A further increase in n ($n > 1$) shows a change in the quartz surface charge, the negative values of the ζ -potential (~ 70 mV) exceeding those of quartz in a 1×10^{-4} M solution of KCl ($\sim 56-60$ mV) without PE and SAS. This may be explained proceeding from the assumption that if the mixture contains a greater amount of NaDDS, the ions of the latter are adsorbed by the PMVP coils, orienting their polar groups into the aqueous phase [34]. The compound complex formed will have an overall negative charge because of the superequivalently adsorbed DDS^- ions, and its quartz surface adsorption causes a decrease in θ .

Inversion of the ζ -potential sign and a decrease in θ are also observed in mixtures PAA and PMAA with CTMABr (Fig. 6, curves 3–5). In this instance the inter-

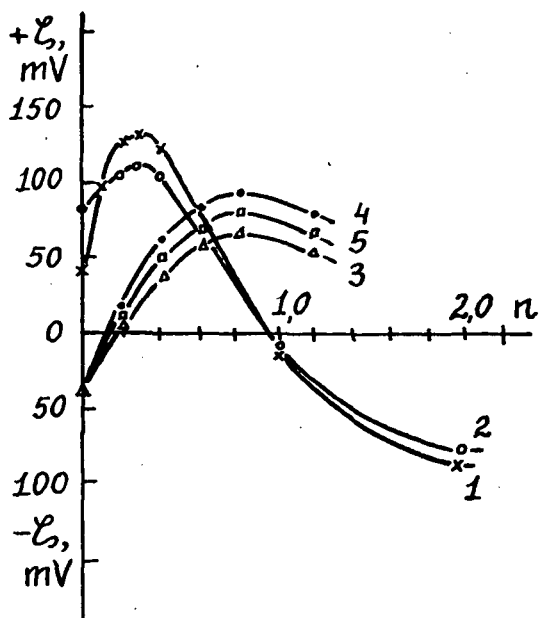


Fig. 6. Dependence of quartz electrokinetic potential upon the relative concentration of SAS in a mixture with polyelectrolytes:

1. PMVP with $M_n = 190,000 + \text{NaDDS}$ $C_{\text{PMVP}} = 0.155\%$.
2. PMVP with $M_n = 340,000 + \text{NaDDS}$ $C_{\text{PMVP}} = 0.155\%$.
3. PAA with $M_n = 17,300 + \text{CTMABr}$ $C_{\text{PAA}} = 0.072\%$.
4. PAA with $M_n = 1,000,000 + \text{CTMABr}$ $C_{\text{PAA}} = 0.072\%$.
5. PMAA with $M_n = 1,000,000 + \text{CTMABr}$ $C_{\text{PMAA}} = 0.086\%$.

action also occurs according to the ion-exchange mechanism and the maximum degree of SAS binding by the polyelectrolyte takes place when the concentration of the latter is ~ 0.01 M and $n = 0.1 - 0.2$ [36].

When the concentrations of PMVP and NaDDS are high (0.465%), the polyelectrolyte macromolecules are extremely compact, and the SAS is in the form of micelles. The interaction of compact coils of the polyelectrolyte and SAS micelles apparently leads to the formation of hydrophilic complexes, whose quartz surface adsorption does not result in the hydrophobization of the latter (Fig. 4, curve 3).

Thus, the obtained information shows the possibility of widening the ways of regulating physicochemical properties of solid surfaces with the help of polyelectrolyte complexes of SAS.

References

- [1] Kuzkin, S. F., V. P. Nebera: Sinteticheskie flokulyanty v protsesakh obezvozhivania, M. Gostekhizdat, 1963.
- [2] Baran, A. A., Ya. Ya. Vasko, B. V. Deryagin, N. M. Kudryavtseva, O. D. Kurilenko: Kolloidn. Zh. 38, 8 (1976).
- [3] Baran, A. A., I. M. Solomentseva, I. I. Kocherga, O. D. Kurilenko: Kolloidn. Zh. 38, 16 (1976).

- [4] *Baran, A. A., I. M. Solomentseva, I. I. Kocherga*: Kolloidn. Zh. 38, 26 (1976).
 [5] *Van Voorst, V. F.*: Ing. Techn. 49, 488 (1977).
 [6] *Akhmedov, K. S. et al.*: Vodorastvorimye polimery i ikh vzaimodeistvie s dispersnymi sistemami, Tashkent, FAN, 1969.
 [7] *Ovcharenko, F. D., K. S. Akhmedov, G. G. Boiko, O. L. Alekseev*: Kolloidn. Zh. 36, 995 (1974).
 [8] *Garbuglio, C., L. Crescentini, A. Myla, G. B. Gechele*: Macromol. Chem. 97, 97 (1966).
 [9] *Rafikov, S. F., V. P. Budtov, Yu. B. Monakov*: Vvedenie v fiziko-khimiya rastvorov polimerov, M. Nauka, 1978.
 [10] *Bekturov, E. A., R. E. Legkunets*: Vysokomolek. soed. A12, 626 (1970).
 [11] *N'ekrasova, T. N., O. T. Ptitsyn, M. S. Shikanova*: Vysokomol. soed. A10, 1530 (1968).
 [12] *Newman, S., W. R. Krigbaum, C. Langien, P. I. Flory*: J. Polymer Sci. 14, 451 (1954).
 [13] *Abramzon, A. A., N. A. Golovina, L. P. Zaichenko, B. M. Kaleva, T. M. Cherepanova*: Kolloidn. Zh. 40, 114 (1978).
 [14] *Zimon, A. D.*: Adgeziya zhidkosti i smachivanie, M. Khimiya, 1974.
 [15] *Grigorov, O. N., I. F. Karpova, Z. P. Kozmina, K. P. Tikhomolova, D. A. Fridrichsberg, Yu. M. Chernoberezhsky*: Rukovodstvo k prakticheskim rabotam po kolloidnoi khimii, M.-L. Khimiya, 1964.
 [16] *Aidarova, S. B., K. B. Musabekov*: Kolloidn. Zh. 41, 117 (1979).
 [17] *Voyutsky, S. S.*: Kurs kolloidnoi khimii, M. Khimiya, 1975.
 [18] *Grigorov, O. N.*: Elektrokineticheskie yavleniya, L., 1973.
 [19] *Watanabe, A., Fsuji F., Sh. Ueda*: J. Electrochem. Soc. Japan 29, 236 (1961).
 [20] *Sidorova, M. P., N. A. Kibirova, I. B. Dmitrieva*: Kolloidn. Zh. 41, 277 (1979).
 [21] *Sidorova, M. P., D. A. Fridrichsberg, N. A. Kibirova*: Vestnik LGU, No. 10. 121 (1972).
 [22] *Distler, G. I.*: Izv. Akad. Nauk SSSR, 36, 1846 (1972).
 [23] *Destler, G. I.*: Elektronnaya mikroskopiya poverkhnostnykh yavlenii. V kn.: Issledovaniya v oblasti poverkhnostnykh sil, M. Nauka, 1967. p. 84.
 [24] *Musabekov, K. B., K. I. Omarova, A. I. Isimov*: Kolloidn. Zh. 41, 145 (1979).
 [25] *Tanchuk, Yu. V., G. S. Pop*: Kolloidn. Zh. 40, 1209 (1978).
 [26] *Slusarev, I. T.*: Visokomol. soed. B13, 876 (1971).
 [27] *Aidarova, S. B., K. B. Musabekov*: Izv. Akad. Nauk. Kaz. SSR, ser. Khimiya 81 (1980).
 [28] *Gribanova, E. V., L. I. Molchanova, O. N. Grigorov, V. I. Popova*: Kolloidn. Zh. 38, 557 (1976).
 [29] *Goretskaya, A. V., B. N. Kabanov*: Zh. fiz. khimii 4, 529 (1933).
 [30] *Talmud, D. L., N. M. Lubman*: Zh. fiz. khimii 1, 411 (1930).
 [31] *Gembitsky, P. A., D. S. Zhuk, V. A. Kargin*: Polietilenimin, M. Nauka, 1971.
 [32] *Lipatov, Yu. S., L. M. Sergeeva*: Adsorbtsiya polimerov, Kiev, Naukova dumka, 1972.
 [33] *Eremenko, B. V., B. E. Platonov, I. A. Uskov, I. N. Lubchenko*: Kolloidn. Zh. 36, 240 (1974).
 [34] *Feldstein, M. M., A. B. Zezin*: Molek. Biol. 8, 142 (1974).
 [35] *Musabekov, K. B., R. E. Legkunets, B. A. Jubanov, Zh. A. Abilov*: Khimiya monomerov i polimerov, Alma-Ata, 1980, p. 104.
 [36] *Musabekov, K. B., Zh. A. Abilov, G. V. Samsonov*: Kolloidn. Zh. 40, 694 (1978).
 [37] *Pshenitsyn, V. I., A. I. Rusanov*: Kolloidn. Zh. 41, 201 (1979).

МОДИФИЦИРОВАНИЕ ПОВЕРХНОСТИ КВАРЦА ВОДНЫМИ РАСТВОРАМИ ПОЛИЭЛЕКТРОЛИТОВ И ПОВЕРХНОСТНО-АКТИВНЫХ ВЕЩЕСТВ

К. Б. Мусабеков, К. И. Омарова, А. И. Изимов

Изучено влияние анионных [полиакриловая (ПАК), полиметакриловая (ПМАК) кислоты] и катионных [гидрохлориды поли-2-метил-5-винилпиридина и сополимера — 2-метил-5-винилпиридина с бутилметакрилатом (МВП-БМА)] полиэлектролитов (ПЭ), а также их смесей с катионным [цетилтриметиламмоний бромистый (ЦТАБ)] и анионным (додецилсульфат натрия (ДДС) поверхностно-активными веществами (ПАВ)] на поверхностные свойства кварца. Наибольшее модифицирующее действие ПЭ и их смесей с ПАВ проявляется тогда, когда они предварительно наносятся на поверхность кварца из водного раствора и сушатся. Модифицирующее действие ПЭ и ПАВ проявляется в изменениях краевого угла смачивания водой и электрокинетического потенциала кварца.

Information for Contributors

1. Manuscripts should be submitted to Prof. Pál Fejes, Institute of Applied Chemistry, József Attila University, Szeged, Rerrich tér 1, Hungary, H-6720.
2. The manuscripts must not exceed in any case 32 pages (Figures, legends, Tables and Summary included). Manuscripts should be submitted in duplicate.
3. The format of the text: A/4, double spaced, 25 lines per page and 50 characters per line. Title: all capital characters; underlined twice. Subtitle(s) should be written in new line(s) in normal writing, underlined also twice, first characters: capital. (See the following example).

STEREOCHEMICAL STUDIES

Studies on Cyclic-2-Hydroxycarboxylic Acids

By

PÁL KISS

Research Institute for Industrial Chemistry, Budapest
(Received.....)

4. After these comes the summary, which is followed by the text proper. If the parts of the paper are separated by secondary titles like: Introduction, Experimental etc., the following rule holds: secondary titles of equal rank are to be written in new lines, the first word with capital letter, otherwise running text underlined once.

Example:

Introduction

Experimental part

5. The names of the authors in the running text are written in capital letters. Exceptions are the names in connection with scientific instruments, etc. where only the first letter should be capital.
6. Citations in the text with reference to selected literature at the end of the paper are to be made with squared brackets, like: [5], [4, 9], [4—9].
7. To make printing easier, mathematical formulas are to be simplified as much as possible. Reference to mathematical equations is made by numbers in parenthesis, like: (16).
8. Tables should be typen on separate pages. Please supply numbers and titles for all tables (Numbering occurs with Roman numerals: Table I).

Throughout the whole text the IUPAC nomenclature should be used.

Insert of Tables in the text will be indicated at the appropriate place of the margin, like this: Table I.

9. Figures must be drawn clearly with Chinese ink on oily drawing paper, the thickness of lines as well as size of letters and symbols should be selected with care, the minimum size is nearly 0.3 cm.

The maximum width of Figures is 24 cm, however, Figures of width equal or less than 12 cm are preferred.

Please, use upwright on the Figures.

In the case of real numbers points are used instead of commas.

The place of Figures in the text is indicated on the margin like this: Figure 13.

Please supply legends for all figures and compile these on separate sheets. Indicate only the number of the Figures in the original drawing, for this purpose use blue pencil.

0. Literature will be given under the heading References, like this: (on a separate sheet at the end of the manuscript)

[1] Allinger, N. L., M. T. Tribble: J. Phys. Chem. 33, 1565 (1976).

[2] Abraham, J. K., H. S. Hoover: Principles of Competitive Oxidation. Mc Graw-Hill, New York, 1977, p. 133.

INDEX

<i>G. Papp and F. Beleznay</i> : Changing in the Density of States Caused by Vacancy in GaP and InP	1
<i>Zs. Bor, S. Szatmári, G. Szabó and B. Rácz</i> : Distributed Feedback Dye Laser Tuning by Divergent Pumping Beams	2
<i>B. Németh, I. Sánta and L. Kozma</i> : Fluorescence Nonlinearity of Water Dissolved Fluorescein under the Action of Laser Radiation of High Power Density	3
<i>L. Szivoczka</i> : Arrhenius Parameters for the Reaction $iso-C_3H_7 + H_2 = C_3H_8 + H$	4
<i>I. Bárdi and T. Bérces</i> : Thermal Decomposition of Propane in a Recirculation System, III. Investigations in the Presence of Olefin-absorber	5
<i>I. Seres, M. Berkes and G. Ács</i> : Rapid Method for Determination of <i>i</i> -Propanol in Petroleum Sulphonate Suspensions. (in Russian)	5
<i>T. P. Kosulina, V. G. Kulnevich, J. Apjok and M. Bartók</i> : The Chemistry of 1,3-Bifunctional Systems, XXVIII. A New Direct Synthesis of 1,3-Dioxan-2-Ylium Salts from 1,3-Diols	6
<i>E. M. Kuramshin, L. G. Kulak, S. S. Zlotskii, D. L. Rakhmankulov, J. Czombos and M. Bartók</i> : Reactivity of Polymethyl-1,3-Dioxacycloalkanes Towards Ozone. (in Russian)	7
<i>F. N. Latypova, V. V. Zorin, P. A. Krasutskii, N. A. Karakhanova, J. Apjok and M. Bartók</i> : EPR Study of Europium Complex Formation of 1,3-Dihetero Analogues of Cycloalkanes. (in Russian)	7
<i>O. Berkesi and J. Andor</i> : Synthesis, Structure and Properties of Metal Carboxylates, I. Effects of Experimental Conditions on the IR Spectra of Compounds Formed in Ni(II)-bis(2-ethylhexanoate) Production. (in Russian)	8
<i>K. B. Musabekov, K. I. Omarova and A. I. Izimov</i> : Modification of Quartz Surface with Aqueous Solutions of Polyelectrolytes and Surface-Active Substances	8

A kiadásért felelős: Dr. Tandori Károly
1983

A kézirat nyomdába érkezett 1982 december 10. Megjelenés 1983. november
Páldányszám: 550. Ábrák száma: 56. Terjedeleme: 8,92 (A/5) ív
Készült monószedéssel, íves magasnyomással, az MNOSZ 5601—50/A szabványok szerint
82-5388 — Szegedi Nyomda — F. v.: Dobó József igazgató